



Microheater: material, design, fabrication, temperature control, and applications—a role in COVID-19

Z. E. Jeroish¹ · K. S. Bhuvaneshwari² · Fahmi Samsuri¹ · Vigneswaran Narayanamurthy³ 

Accepted: 29 September 2021

© The Author(s), under exclusive licence to Springer Science+Business Media, LLC, part of Springer Nature 2021

Abstract

Heating plays a vital role in science, engineering, mining, and space, where heating can be achieved via electrical, induction, infrared, or microwave radiation. For fast switching and continuous applications, hotplate or Peltier elements can be employed. However, due to bulkiness, they are ineffective for portable applications or operation at remote locations. Miniaturization of heaters reduces power consumption and bulkiness, enhances the thermal response, and integrates with several sensors or microfluidic chips. The microheater has a thickness of ~ 100 nm to ~ 100 μm and offers a temperature range up to 1900°C with precise control. In recent years, due to the escalating demand for flexible electronics, thin-film microheaters have emerged as an imperative research area. This review provides an overview of recent advancements in microheater as well as analyses different microheater designs, materials, fabrication, and temperature control. In addition, the applications of microheaters in gas sensing, biological, and electrical and mechanical sectors are emphasized. Moreover, the maximum temperature, voltage, power consumption, response time, and heating rate of each microheater are tabulated. Finally, we addressed the specific key considerations for designing and fabricating a microheater as well as the importance of microheater integration in COVID-19 diagnostic kits. This review thereby provides general guidelines to researchers to integrate microheater in micro-electromechanical systems (MEMS), which may pave the way for developing rapid and large-scale SARS-CoV-2 diagnostic kits in resource-constrained clinical or home-based environments.

Keywords Heater · Microheater · Micro hot plate · Temperature control · Thin-film heater · Gas sensor

1 Introduction

James Prescott Joule established the first research on resistive heating in 1841. The proposed method was not validated until Michael Faraday submitted his findings in 1849 and further led to acknowledgement in the Royal Society, London (Joule 1841). The overarching goal of the heaters

is to set up a suitable heating environment for the device with precise temperature controlling process. Heaters put forth several applications in the field of science, engineering, mining as well as in space. Though convenient supporting facilities accompany heaters, the conversion rate and heater size do not meet expectations (Li et al. 2018). Additionally, sensors, MEMS, wearable electronics, and point-of-care (POC) DNA amplification devices enhance the requirement of a miniaturized heater. Moreover, the downscaling of heaters results in reduced thermal mass and power consumption, which allows faster response times, higher temperatures, and engenders battery-driven technology (Spruit et al. 2017).

A microheater is a miniaturized heating system that generates heat through Joule heating, ultrasonic, or radiative heating. The temperature of the microheater depends upon multiple physics, including electrical, mechanical, and thermal, as well as material properties and geometric designs (VanHorn and Zhou 2016). The resistive microheater filament has a thickness of ~ 100 nm to ~ 100 μm. In the early times, metallic microheaters are widely utilized. However,

✉ Fahmi Samsuri
fahmi@ump.edu.my

✉ Vigneswaran Narayanamurthy
vigneswaran@utem.edu.my

¹ College of Engineering, Universiti Malaysia Pahang, 26300 Gambang, Pahang, Malaysia

² Faculty of Electronics and Computer Engineering, Universiti Teknikal Malaysia Melaka, Hang Tuah Jaya, 76100 Durian Tunggal, Melaka, Malaysia

³ Fakulti Teknologi Kejuruteraan Elektrik Dan Elektronik, Universiti Teknikal Malaysia Melaka, Hang Tuah Jaya, 76100 Durian Tunggal, Melaka, Malaysia

in high-temperature applications, microheaters need to be supported or enclosed with very high thermal-resistant ceramic materials (VanHorn and Zhou 2016). Thus, the microheater heating materials changed from metallic to metal-ceramic brittle materials. The microheater possesses the characteristics of low power consumption, fast thermal response, good heat confinement, good mechanical stability, and good fabrication yield. The integration of microheaters in microdevices possesses several applications such as gas sensors, actuators, biomedical testing devices, electron microscopes (Zheng et al. 2017), pressure anvil cells (Weir et al. 2009), and enhancing fiber heaters (Kalachev et al. 2005; Nicolau et al. 2005). Other potential uses include fuel cell heat sources (Ramousse et al. 2009), electronics and substrate heating (Zhang et al. 2010), RF applications (Liu et al. 2006; Yeh and Yang 2020), micro tube-heaters for small volume gas heating, high power micro-furnace with optional tube extension, fiber optics (Liu et al. 2017; Russo et al. 1984), ideal for long aspect ratio/very small diameter pieces, igniters (Zhang et al. 2016), microplate heaters, material testing and characterization, thermal property measurements, SEM/TEM/AFM, gas/vapour heaters/converters, and thin-film preparation (Kalachev et al. 2005). Microheaters are also employed in micro-ignition for micro propulsion systems and micro explosive boiling sensors. Furthermore, microheaters are widely implemented in 2D and 3D printing systems such as inkjet printing, thermal printing, point-of-sale (POS) printer, and selective heat sintering (SHS). The uniform temperature distribution in the heating area and the short response time is crucial while integrating with ultrasensitive temperature-dependent devices and measurements (Yu et al. 2017).

In recent years, there is emerging research in the miniaturization and portability of devices in all industries. As such leads to the demand for the integration of microheaters in most of the MEMS and microfluidic devices. However, there are only a few reviews focused on technological advancements (Bhattacharyya 2014) and the importance of microheater in gas sensors (Li et al. 2018) and biological sectors (Jain and Goodson 2011). To the best of our knowledge,

the different fabrication approaches, temperature control modules, and various applications of microheater are not reviewed yet. Hence, this review aims to provide a comprehensive overview of microheater to develop novel efficient microheaters in the future. This review article intended to focus on the material, design and fabrication, temperature control, and applications of microheater. The shortcomings of current microheater technologies are summarised and suggested some ideal requirements. We hope this review will provide general knowledge to researchers who are interested in developing microheaters in any sector, as well as gives a better picture on the potential of using the microheaters in COVID-19 detection for battling the current pandemic.

2 Heating mechanisms

Generally, the heating system is classified into two categories: external and internal heating system. The internal heating system incorporates heating elements inside the microchannel or chamber to control the temperature of the fluids (Chon and Li 2014), where the heating elements are manufactured via microfabricating process to fit in the microscaled channel (Srinivasan et al. 1997). Additionally, the conductive ionic liquid facilitates internal heating when an AC current flows through the conductive liquid held in the co-running channels of microfluidic devices, as shown in Fig. 1a. Joule heating is generated that transfers the heat in the conductive liquid to the medium. Otherwise, the heating can be achieved via exothermic or endothermic reactions and chemical or physical processes by the exothermic dissolution of H_2SO_4 in water, as shown in Fig. 1b (Guijt et al. 2003).

In an external heating system, the working fluids are heated in a microchannel with discrete heating elements. Based on heat transfer methods, the external heating methods are further divided into contact and non-contact heating techniques. Contact type heating involves the heating elements that are either clamped or glued on the surface of the channel for transferring heat into the working fluids through conduction, as depicted in Fig. 2(i). Heat is generated when electricity flows in the

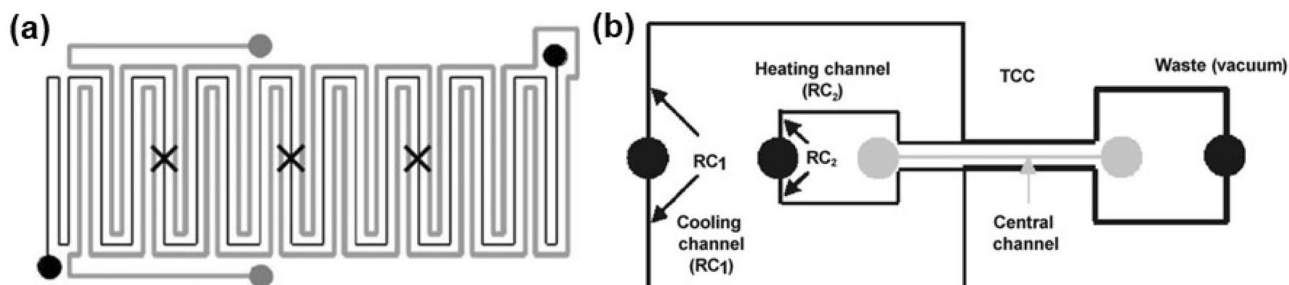
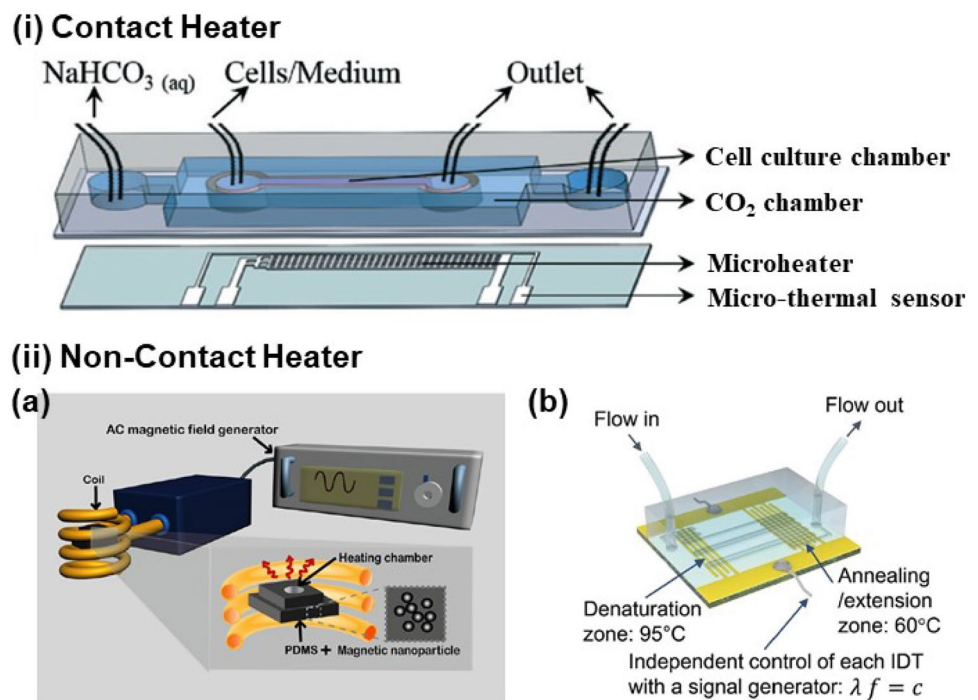


Fig. 1 Internal heating systems. **(a)** Microfluidic device incorporated with co-running heating channels (grey) and working sample (black) (de Mello et al. 2004), **(b)** Endothermic/exothermic heater (Guijt et al. 2003) Reprinted with permission from RSC

Fig. 2 External heating systems. (i) Contact heater (Yu et al. 2014) Reprinted with permission from RSC (ii) Non-contact heaters. (a) Schematic drawing of induction heating based on the magnetic nanoparticle-embedded PDMS (MNP-PDMS) chip (Kim et al. 2010) Reprinted with permission from IOP, (b) PDMS chip bonded on LiNbO₃ piezoelectric substrate (Ha et al. 2015) Reprinted with permission from Nature



high-resistance material as in an electric heater. On the other hand, the non-contact heating type allows the transfer of heat to the materials through ultrasonic or radiative heating. Thus engenders the advancement of wireless heating. The wireless microheaters forgo complicated electrical elements and wirings in the microheater. Poly dimethyl siloxane (PDMS) embedded magnetic nanoparticles generate heat under an AC magnetic field to produce a magnetic field, as depicted in Fig. 2 (ii) (a). The heat can be controlled by altering the magnetic particle and the magnetic field intensity. However, the unwanted local aggregation of particles can cause experimental errors (Kim et al. 2010). Similarly, Yeh et al. developed a wirelessly activated microheater temperature regulator for endo hyperthermia treatment of restenosis. The microheater uses an L-C tank circuit for achieving a wireless resonant RF heating capability. The microheater was integrated with a temperature regulator and an acrylate-based composite circuit breaker to prevent the device from overheating (Huang et al. 2020). Later, a fast, accurate, conductive, and transparent heating system comprised of PDMS microchannels was bonded onto a regularly spaced interdigital transducers patterned LiNbO₃ piezoelectric substrate as shown in Fig. 2 (ii) (b). The heat dissipation occurs via vibration damping of PDMS induced by piezo-actuated surface acoustic waves (Ha et al. 2015).

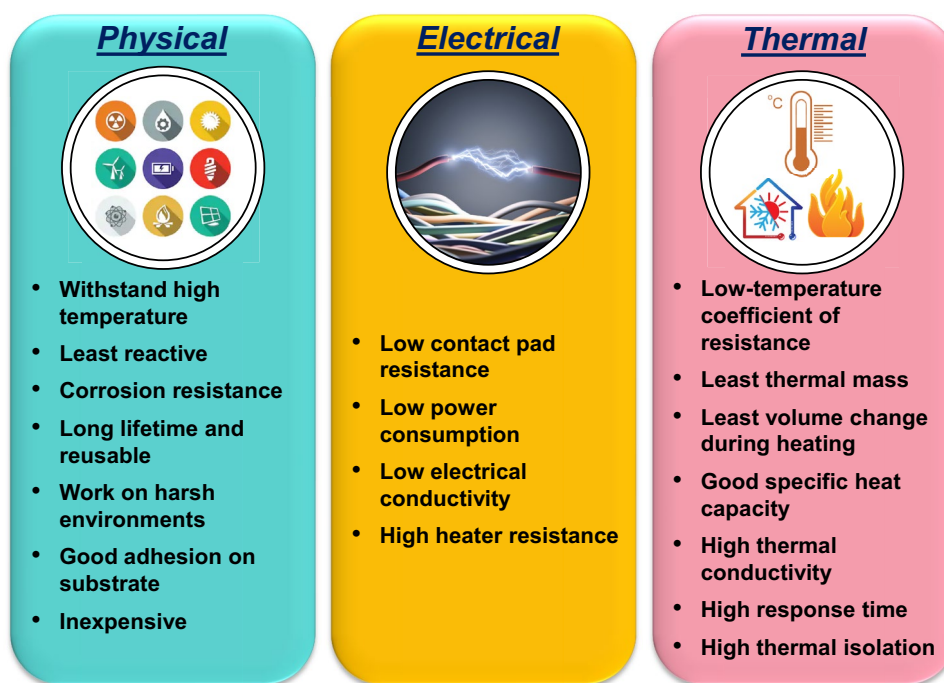
3 Material

In early times, metal blocks have been widely utilized as a heating element. Simultaneously, the requirement of a large volume of a metal layer made it expensive and bulky. Moreover, metal blocks consume enormous power, and space which reduces the portability and integrity of the heater in several applications. These drawbacks of heating elements are addressed with the emergence of micro and nanotechnology. However, several factors need to be optimised while designing efficient microheaters. First of all, the heating element is selected based on the operating temperature range for the respective applications and should possess good homogeneity on the active surface (Abdeslam et al. 2020). Furthermore, the material should be easy to fabricate and have sufficient width and thickness to manage the generated heat. The ideal characteristics of a microheater are illustrated in Fig. 3.

3.1 Materials for microheater

Microheaters are generally made of Platinum (Pt), Gold (Au), Silver (Ag), Nichrome (NiCr), Nickel (Ni), Tungsten (W), Titanium (Ti), Aluminium (Al), Copper (Cu),

Fig. 3 Ideal characteristics of a good microheater



graphene (Wang et al. 2020a), and carbon nanotubes (CNT). Moreover, Titanium nitride (TiN), Gallium nitride (GaN), Gallium arsenide (GaAs), DilverP1 (alloy of Ni, Co, Fe), Polysilicon (Poly-Si), and many metal alloys, etc. were also available as heating elements. In contrast, it is mandatory to choose an appropriate material with maximum resistivity for a microheater based on applications (Sri Surya Srikanth et al. 2019). The electrical resistivity of the heating element should be high in comparison to the contact pads so that efficient Joule heating occurs at the heater resistor, and the unwanted heat in the contact pads can be reduced. For instance, in the work of Guan et al., as depicted in Fig. 4a, the electrical resistivity of Ag in the contact pad is much smaller than that of the Ti heater resistor, and the thermal conductance of Ag is 20 times higher than that of Ti, leading to the enormous heating in the Ti resistor (Guan and Puers 2010). The high resistivity nature of the Ti element leads to high electrical resistance for the microheater and the sensor to generate maximum heat and sensing temperature, respectively, which plays a mighty role in the long term reliability of the microheater device and the temperature sensor (Javed et al. 2012).

The most commonly used materials for microheater are Pt, Au, Ag, Ti, W, and NiCr. Pt is an ideal material for heater and sensor since it has lower density, high electrical conductivity, good specific heat capacity, low power consumption, and high heating and temperature sensing rates with resistance varies linearly with temperature. It also possesses the characteristics of malleable, ductile, dense, precious, and least reactive metal (Abdeslam et al.

2020). However, Pt cannot be deposited effectively on the glass substrate. Hence, Cr or Ti was deposited as an adhesion layer before Pt deposition. Cr has good adhesion characteristics on glass and possesses a high-temperature coefficient of resistance of about $4 \times 10^{-3} \text{ }^\circ\text{C}^{-1}$, which guarantees a good sensitivity for resistance temperature sensor devices. The bottom Cr layer on the glass should be kept at a minimum thickness to avoid thermomechanical mismatch (Scorzoni et al. 2015). In addition to that, CrN was also used as intermediate material between Pt and silicon oxide to improve the adhesion, strength, and corrosion resistance of the structure. The pair of Cr–CrN and CrN–Pt, as shown in Fig. 4b, have similar thermal expansion coefficients that lead to good thermal stress resistance (Chang and Hsihe 2016). Lekshmi et al. analyzed the Pt, W, and Ti microheaters based on the power consumption and temperature for the applied voltage. The Pt microheater had shown a better trade-off between temperature and power consumption. In contrast, W results in high power consumption for generating high-temperature, and Ti possesses low power consumption but provides only low temperatures (Lekshmi et al. 2018). Whereas, in comparison with Pt, Au, Ag, and NiCr materials as heating elements, NiCr is promoted as a more suitable material because of its higher electrical resistivity ($1 - 1.5 \times 10^{-6} \text{ } \Omega\text{m}$), high thermal conductivity ($11.3 \text{ Wm}^{-1} \text{ K}^{-1}$), low-temperature coefficient of resistance (TCR), high-temperature stability, high resistance to oxidation and do not require any additional adhesive layer, which makes the sensor and heater cost-effective. (Rajput et al. 2018; Tiwari et al. 2018b).

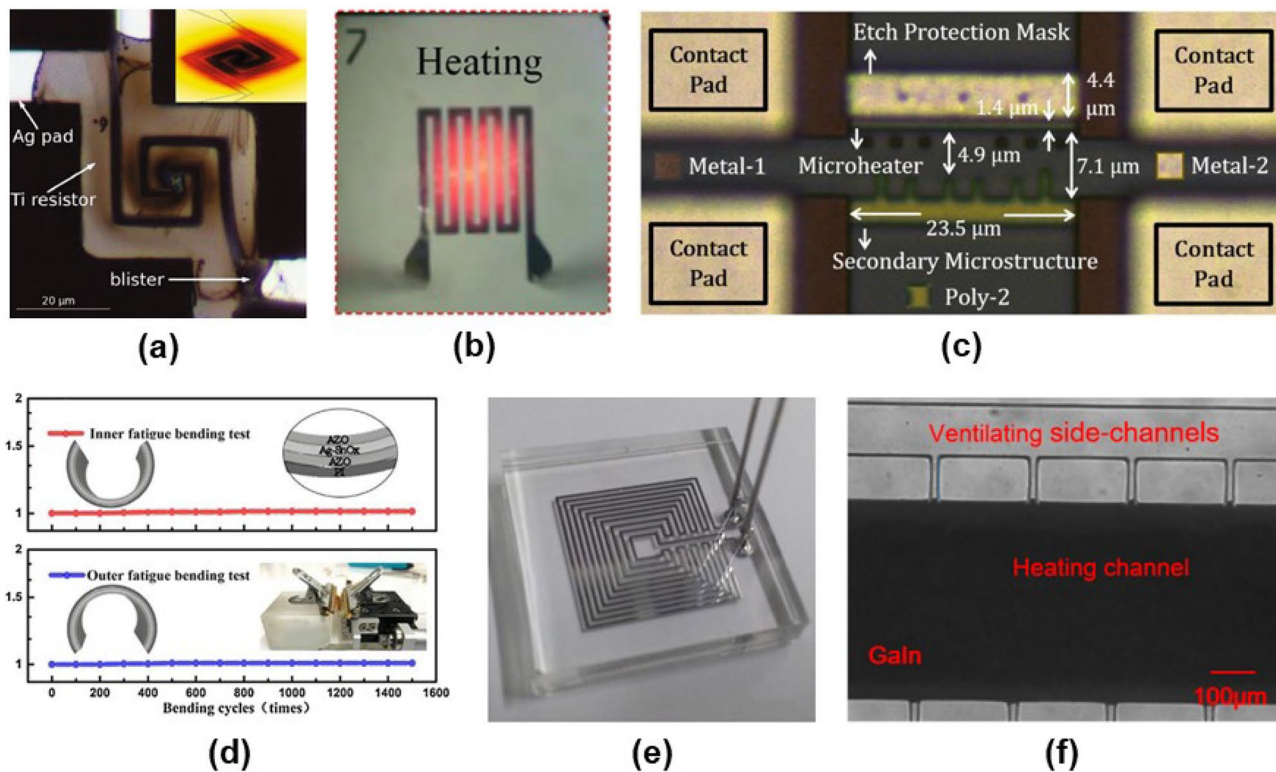


Fig. 4 Different microheater utilized by researchers (a) Ti/Ag microheater heating up to failure (Guan and Puers 2010) Reprinted with permission from Elsevier, (b) Cr–CrN, and CrN–Pt based microheater (Chang and Hsihe 2016) Reprinted with permission from Elsevier, (c) Optical micrograph of CNT growth structures in AMS 350 nm process (Roy et al. 2019) Reprinted with permission from

MDPI, (d) Change in sheet resistance of AZO/Ag-SnO_x/AZO thin film as a function of bending cycles (Wang et al. 2020b) Reprinted with permission from Elsevier, (e) liquid metal-based microheaters (Jinsol and Jungchul 2014) Reprinted with permission from IEE, (f) Liquid microheater with parallel ventilating side-channels to trap the air (Zhang et al. 2020) Reprinted with permission from MDPI

Other than the most used materials, polysilicon, CNT, Al, Cu, ITO, and AZO/Ag-SnO_x/AZO are other materials for developing microheaters. In CMOS technology, polysilicon is the most suitable microheater material. However, the simulation of square gridded-type design revealed that the polysilicon heating material generates lower temperatures than the Pt microheater for similar applied potential (Das and Kakoty 2015). The efficient metal microheaters for CNT synthesis applications can be fabricated via Al or Cu alloyed with Ni, as depicted in Fig. 4c. However, fabricating tri-nickel aluminide alloy may be more complicated than cupronickel alloy due to the native oxide layer on the Al. Hence, cupronickel was preferred over tri-Nickel Aluminide (Roy et al. 2019). Because of good linearity, low cost, and chemical stability, Al microheaters were employed for low-temperature applications (Phatthanakun et al. 2012). Li et al. developed an Al/Ti microheater to guarantee long-life reliability and high heating temperature. In contrast, Al cannot cling to a smooth surface like glass or silicon wafer. Hence, Ti can be applied as an adhesion layer (Li et al. 2017). Nieto et al., on the other hand, utilized PVD and laser ablation to fabricate the Al heater directly on a

soda-lime glass substrate. However, before starting the PVD, the glass substrate had to go through a six-step cleaning process to enhance adhesion. (Nieto et al. 2017). When exposed to the atmosphere, the surface of Al will oxidise, which can influence the experimental effects. As a result, it should be employed in space either as a propellant with no oxidants or encapsulated with other layers to avoid oxidation. (Li et al. 2017). In microfluidics, the COMSOL simulation of the Al microheater depicted the heater was 8.25 times larger than that of the reaction chamber area. Hence, the heater size and dimension must be optimized to reduce the power consumption without interfering the temperature uniformity (Matviykov et al. 2018). The use of Indium Tin Oxide (ITO) glass, a conductive transparent material that generates heat because of its electrical resistance when an electric current passes through it (Lin et al. 2011). Due to the transparency nature of ITO, cells can be visible; however, it lags the reusability (Lin et al. 2007). AZO/Ag-SnO_x/AZO thin film is also transparent and possesses high thermal durability, good damp-heat stability, excellent scratch resistance, and mechanical flexibility with no deterioration for 10,000 times of scratching and 1500 times of bending, as shown

in Fig. 4d. Moreover, it retains high response time, good cycle performance, and very high saturating temperature compared to ITO heaters (Wang et al. 2020b).

Apart from all these solid material heaters, liquid metal-based microheaters are available. Liquid metal-based microheater will break due to the development of voids when the temperature exceeds 100 °C. Void occurs mainly due to the air trapped in the liquid–metal heating channel and the formation of liquid metal oxides. Hence, Jinsol et al. fabricated liquid metal-based microheater on PDMS sheets and oxidized silicon wafers, as depicted in Fig. 4e. The performance investigation on non-pressurized and pressurized electrical contacts revealed that the void formation was noted in non-pressurized contact, which drastically increases electrical resistance and affects the performance and life span of the microheater (Jinsol and Jungchul 2014). Though pressurized contact eliminates the issue, it increases complexity and power consumption. Later, Zhang et al. designed two parallel ventilating side-channels to trap the air, as shown in Fig. 4f and circumvent the pressurized contact. This results in the formation of a protective layer of Eutectic Gallium Indium (EGaIn) oxides, which enhances the mechanical stability with higher working temperatures (Zhang et al. 2020). The physical, mechanical, optical, and thermal characteristics of various microheater materials so far discussed are tabulated in Table 1. Different colours are provided to distinguish the best (green), good (blue), and average (orange) performance material for microheater. Grey coloured materials are mainly utilised as adhesion material for Pt and Au, but Cr and Ti can also be implemented as microheater material with moderate heating efficiency.

3.2 Substrates for microheater

In a microheater chip, the substrate, which touches the ground, should possess low thermal conductivity, and the substrate acting as an intermediate layer between the heater and the heat transfer medium should have high thermal conductivity for significant heat transfers to the required medium. The various substrate so far investigated by various researchers are grouped as shown in Fig. 5. Based on the desired application and analysis, rigid, flexible, transparent, or non-transparent material will be selected as the suitable substrate material. Moreover, the stability and reliability of the microheater were also enhanced while selecting a suitable substrate. Some of the microheaters fabricated on different substrates are depicted in Fig. 6.

3.2.1 Rigid substrate

Rigid substrates have permanent shape and structure and possess high stiffness. One such substrate is sapphire, an electrical insulator with good heat sinking characteristics

and provides reasonably high thermal conductivity (Xu et al. 2016). Sapphire wafer substrate was employed for non-contact measurement of temperature distribution since it possesses good penetration of IR radiation. The poor adhesion between the sapphire substrate and the Au thin-film was eliminated via thermal annealing at 400 °C (Son et al. 2015). The microheater on the Si wafer provides better thermal uniformity compared to the PDMS sheet. Moreover, microheaters with PDMS substrate consumes high power to reach the same maximum temperature on Si wafer and can be applied on non-flat surfaces due to their flexibility and deformability (Jinsol and Jungchul 2014). The use of Pyrex-7740 glass and silica glass as base substrate possess lower thermal conductivity and higher electrical resistivity than silicon, which leads to heat confinement and engenders low power consumption (Guan and Puers 2010; Zhang et al. 2007). The comparison of different substrates suggests that at 320mW power, the microheater on silicon and alumina generates only minimal temperature, whereas the microheater on glass achieved nearly 300 °C (Prajesh et al. 2019). All these studies reveal that the substrate has a vital role in providing the desired temperature by limiting heat loss.

3.2.2 Flexible substrate

In the field of microtechnology, flexible substrates find abundant applications. Researchers are recently interested in using flexible materials in biosensors, fluidic interconnections, medical implantable, and wearable electronic devices for biomedical applications (Engel et al. 2003). Flexible circuits were manufactured predominantly using polyimide or polyester due to reduced size, weight, assembly time and cost, and improved heat dissipation capability. So, Shen et al. mounted a resistive meander copper wire between two polyimide films to form a film heater for polymerase chain reaction (PCR). The use of flexible polyimide membrane as substrate reduced the thermal mass and heat loss and providing a faster thermal response (Shen et al. 2005). When a certain amount of heating power was applied to the polyimide heater, the temperature was quickly redistributed over the suspended polyimide membrane. The suspended polyimide membrane provides a milli-second scale response time due to its small thermal mass (Yu et al. 2017). DuPont Kapton RS flexible heaters provide fast response time, puncture-resistant, and more durable than other heater technologies due to their polyimide composition (Rapolu et al. 2018). Polyethylene terephthalate (PET) sheets were also be utilized as a substrate for flexible heaters due to their poor thermal conductivity and high electrical resistivity to achieve excellent heat confinement. The microheaters can be fabricated via screen printing and do not necessitate any cleanroom facility or etching process maximum operating temperature of about 100 °C (Tiwari et al. 2018a).

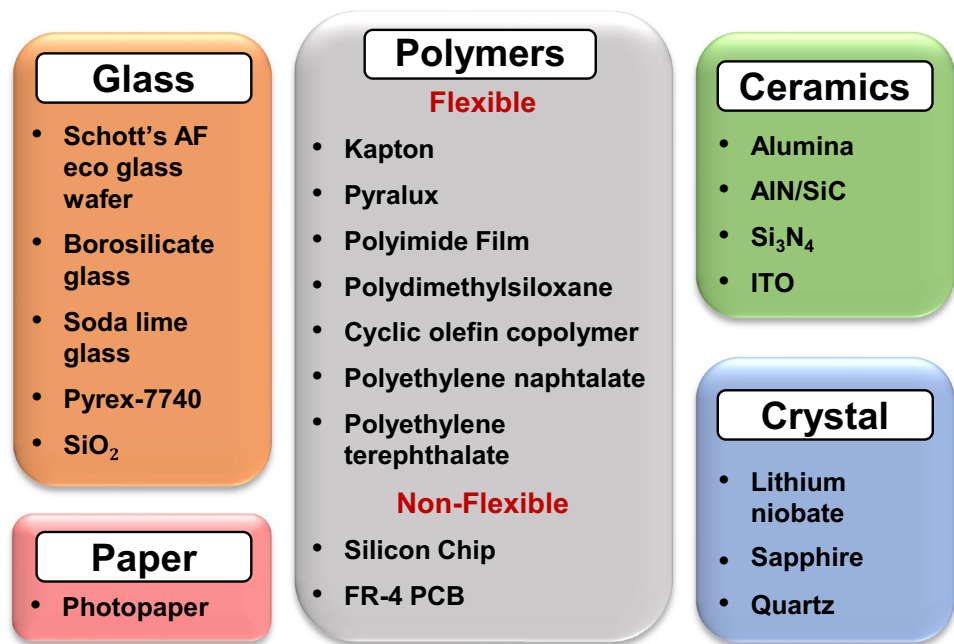
Table 1 Physical, mechanical, optical, and thermal characteristics of various microheater elements (2008; 2020; Mammama et al. 2012; Alam and Cameron 2000; Aperam 2012; AZoM 2004a, b, 2013a, b; Batzill and Diebold 2005; Becker et al. 1982; Collins and Avouris 2000; Dai et al. 2018; Deligoz et al. 2020; Dickey et al. 2008; Elements 2020; Fox 2010; Giancoli 2009; Griffiths 1999; Han et al. 2005; Hone et al. 2002; Igasaki et al. 1978; Inc.; Landon et al. 2015; Marian K. Kazimierzuk 2016; Matula 1979; Nave; Nowak et al. 1999; Pardy et al. 2017; Peng et al. 2008; Pflüger et al. 1984; Roy et al. 2010; Sánchez-Portal et al. 1999; Serway 1998; Taki et al. 2018; Thewlis and Davey 1954; Thuau et al. 2011; Trinh et al. 2018; Tsuchiya et al. 2018; Turkes et al. 1980; Ueno et al. 2017; Wang et al. 2018; Wang and Weng 2018; Wang et al. 2017; Yu et al. 2000; Yu and Kaviany 2014)

	Materials	Physical Properties			Mechanical Properties			
		Density (g/cc)	Molecular weight (g/mol)	Young's Modulus (GPa)	Poisson's Ratio	Yield Strength (MPa)	Tensile Strength (MPa)	
A	Ag	10.491	107.8682	76	0.37	55	140	
↓	Al	2.6989	26.981	68	0.36	11	193	
Z	Au	19.32	196.966	77.2	0.42	205	120	
	CNT	1.3	12.01	270–950	0.11 to 0.19	-	11–63 GPa	
	Cr	7.19	51.996	279	0.21	250	282	
	CrN	5.9	66.003	200	0.2	-	-	
	Cu	8.93	63.546	110	0.343	33.3	210	
	DilverP1 alloy	8.25	-	139	0.3	680	700	
	EGaIn	6.25	184.54	-	-	-	-	
	ITO	6.8	118.71	116	0.35	-	0.022	
	Ni	8.88	58.693	207	0.31	59	317	
	NiCr	8.4	110.689	220	0.325	344.73	2300	
	Pt	21.45	195.084	-	0.39	180	165	
	PTC polymer	1673	-	-	-	-	-	
	Si nanowire	2.329	28.085	112.4	0.28	-	2.6–4.1 GPa	
	SiC	3.1	40.11	410	0.37	21 GPa	1625	
	Sn	7.29	118.71	44.3	0.33	11	220	
	SnO ₂	6.85	150.71	280.59	0.3644	-	-	
	Ta ₂ O ₅	8.2	441.893	62.7	0.2	-	-	
	Ti	4.5	47.867	116	0.34	140	220	
	W	19.3	183.84	400	0.28	750	980	
Electrical Properties		Optical constants at 0.7 μm			Thermal Properties			
Resistivity at 20 °C (ohm m)	Electrical Conductivity (S/m)	Temperature Coefficient	Refractive Index	Relative Permittivity	Thermal Expansion Coefficient at 20 °C × 10 ⁻⁶ (°C ⁻¹)	Specific Heat (J/ Kg K)	Thermal Conductivity (W/ mK)	Melting Point (°C)
1.59 × 10 ⁻⁸	6.30 × 10 ⁷	0.0038	0.041	0.39381	18	234	419	961.93
2.65 × 10 ⁻⁸	3.77 × 10 ⁷	0.0039	1.9214	31.288	23.1	900	210	660.37
2.44 × 10 ⁻⁸	4.11 × 10 ⁷	0.0034	0.131	1.0643	14	128	301	1064.43
1 × 10 ⁻⁶	10 ⁶ to 10 ⁷	-	-	-	15.4	600	210	3550
12.5 × 10 ⁻⁸	7.9 × 10 ⁶	5.10 × 10 ⁶	3.0536	20.676	4.9	461	93.9	2180

Table 1 (continued)

Electrical Properties			Optical constants at 0.7 μm			Thermal Properties			
Resistivity at 20 °C (ohm m)	Electrical Conductivity (S/m)	Temperature Coefficient	Refractive Index	Relative Permittivity	Thermal Expansion Coefficient at 20 °C $\times 10^{-6}$ (°C ⁻¹)	Specific Heat (J/Kg K)	Thermal Conductivity (W/mK)	Melting Point (°C)	
300×10^{-6}	3.33×10^3	-	-	-	9.4	-	19.25	1500	
1.68×10^{-8}	5.96×10^7	0.00404	0.211	1.7552	17	385	398	1083.2	
49×10^{-8}	2.04×10^6	0.0037	-	-	4.60–5.20	500	17.5	1450	
2.9×10^{-8}	3.28×10^6	-	-	3.3	-	404	26.43	15.5 8	
1.5×10^{-5}	1.3×10^5	1364–2151 ppm°C ⁻¹	1.7136	2.9366	7.26	341	10.2	1900	
6.99×10^{-8}	1.43×10^7	0.006	2.0538	18.396	13	460	60.7	1455	
1.10×10^{-6}	6.70×10^5	0.0004	-	-	14	450	11.3	1400	
1.06×10^{-7}	9.43×10^6	0.00392	0.49745	6.8913	9	134	69.1	1769	
-	0.8	-	-	-	-	1000	0.43	-	
2.3×10^3	4.35×10^{-4}	-0.075	3.7838	0.092101	2.56	713	124	1412	
202×10^{-8}	$0.7-1.4 \times 10^2$	-	2.6195	9.7	11	670	180–250	2797	
1.09×10^{-7}	9.17×10^6	0.0045	2.16	27.432	4.7	256	60.7	231.97	
$2-4 \times 10^{-5}$	5×10^4	0.002	2.006	9.86	4	44.3 J/mol K	98	1630	
1.92×10^{-6}	5.2×10^5	-	2.1085	4.4456	3.25	-	5	1872	
4.20×10^{-7}	2.38×10^6	0.0038	2.8511	22.52	8.6	528	17	1650	
5.60×10^{-8}	1.79×10^7	0.0045	3.9015	22.049	4.5	134	163.3	3370	

Fig. 5 Classification of the various substrate for microheater so far investigated by various researchers



3.2.3 Improving stability of the microheater

The stability of the heater under ambient condition is one of the crucial factors to determine the life span, reusability, and usage of microheater in harsh environments. Hence, rigid microheaters are preferred. Additionally, the stability of certain microheaters such as, silver nanowires (AgNWs) based heaters, can be improved by coating polymethyl methacrylate (PMMA), as depicted in Fig. 7a. The PMMA protective layer reduces corrosion and oxidation of AgNW networks. The stability tests, such as the accelerating test and H₂S atmosphere treating, showed extreme stability with negligible resistance change and no significant influence on the transmittance, mechanical flexibility, and heating performance (Shi et al. 2018). Similarly, electrode oxidation during resistive heating can be prevented by coating a thin PDMS layer for rapid heat transfer and providing electric and fluid insulation (Lee et al. 2013).

One of the crucial requisites of a microheater is to attain high temperature ($> = 300$ °C) with minimal power consumption so that it can be battery powered and can integrate with a plethora of applications (Sri Surya Srikanth et al. 2019). Simultaneously, the heater without insulating layers provides higher temperatures with low power consumption, resulting in thermal stress (Deo 2016). In semiconductor and NDIR gas sensors, the microheater should provide and withstand high temperature. Poly-Si material heaters, as shown in Fig. 7c, are preferred as they have high thermal reliability and can withstand more than 400 °C. Though it suffers from oxidation upon heating, depositing a 2000 Å thick SiO₂ using plasma-enhanced chemical vapour deposition (PECVD), followed by partial etching using the buffered

oxide etchant (BOE), can prevent oxidation (Hwang et al. 2011b). Additionally, a 2 µm thick SiO₂ layer, as depicted in Fig. 7b, protects the whole structure from the environment, which elevates the long-term reliability of the device. Moreover, it enhances the mechanical support of microheaters, prevents current leakage through the silicon substrate, and provides thermal insulation from the environment (Bai et al. 2019; Jinsol and Jungchul 2014). AlN/3C-SiC materials also provide long term stability at high temperatures (Chung and Jeong 2010). The coating of the SiN layer on the glass substrate possesses good thermal conductivity and a low thermal expansion coefficient. Furthermore, SiN offers good insulation and can withstand high thermal stress (Chang and Hsihe 2016). SiO₂ and Si₃N₄ membrane offer high electrical insulation; hence, they can provide better isolation from the sensing samples (Velmathi et al. 2010). The SiO₂ and the SiN_x layer thicknesses were determined in such a way to eliminate the residual tensile or compressive stress in gas sensing (Moon et al. 2013). In some gas sensors, the Si₃N₄ substrate was employed. However, the adhesion of Pt microheater on the Si₃N₄ surface can be improved by depositing a thin layer of tantalum pentoxide (Ta₂O₅) (Yoon et al. 2012).

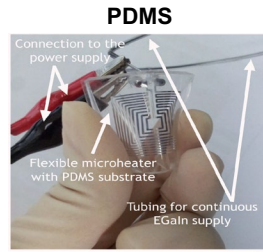
4 Microheater design

The design and material of the microheater play a critical role in enabling low power consumption, low thermal mass, effective temperature uniformity across the device, and enhanced thermal isolation from the surroundings (Velmathi et al. 2010). Similarly, the removal of a big part

Fig. 6 Different substrates employed in microheater (Jinsol and Jungchul 2014; Lin et al. 2011; Petrucci et al. 2015; Resnik et al. 2011; Son et al. 2015; Weir et al. 2009; Yeom et al. 2008; Yin et al. 2019; Yu et al. 2017) Reprinted with permission from IEEE, MDPI, Elsevier, AIP, Springer Nature, Wiley, and IOP

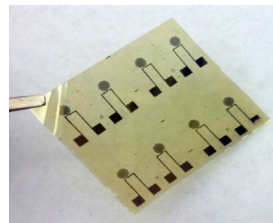
Flexible Microheater Substrates

Transparent

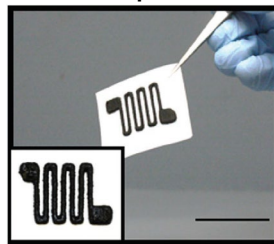


Non-transparent

PI



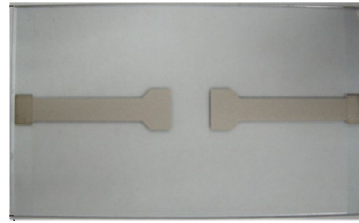
Paper



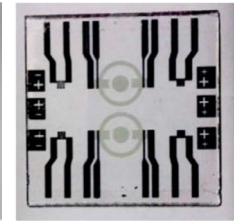
Rigid Microheater Substrates

Transparent

ITO

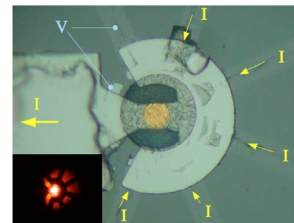


Glass

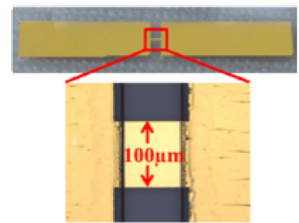


Non-transparent

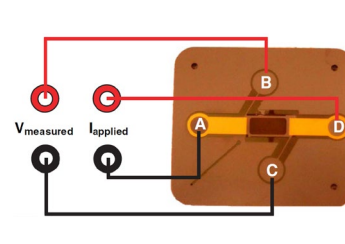
Alumina



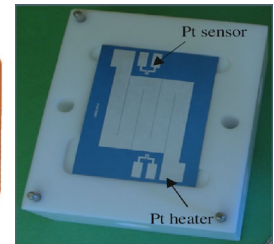
Sapphire



SOI



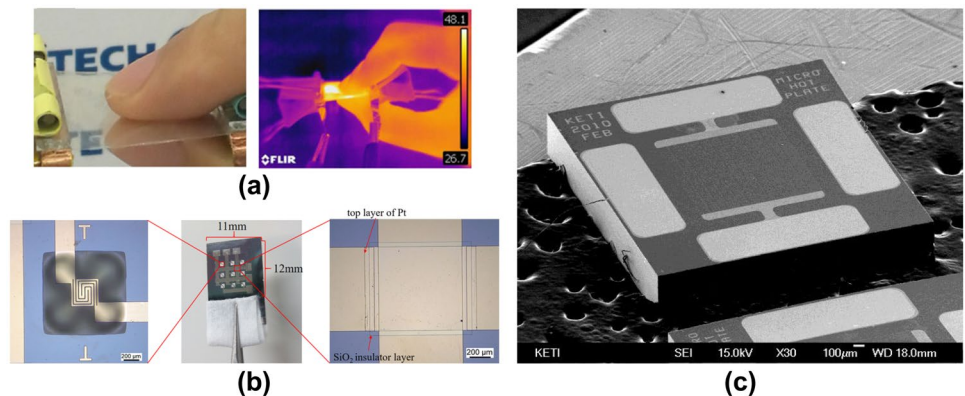
Silicon



of the thermal mass under the microheater considerably increases the thermal resistance up to 217% on a heatsink and 30% in air and decreases the thermal capacitance; thereby, the power consumption is reduced (Scorzoni et al. 2015). Additionally, the decrease in thickness of the microheater increases the resistance, which leads to a decrease in power consumption and heating temperature

(Bedoui et al. 2016). The resistance is extremely dependent on the physical dimensions of the microheater. The physical dimensions, such as the length variation of the microheater, can be exploited via experimental results and the piecewise model. Subsequently, the differential temperature change, sensitivity, and response time of the microheater were extracted through the Fabry–Perot

Fig. 7 Passive layer deposited microheaters to improve stability. (a) Silver nanowires in colourless polyimide (cPI) and PMMA (Shi et al. 2018), (b) SiO₂ deposition on Pt microheater to protect the device from the environment (Bai et al. 2019) Pictures retrieved from Springer Nature, (c) SiO₂ passivation layer was deposited to prevent oxidation of poly-Si (Hwang et al. 2011b) Reprinted with permission from MDPI



modulation technique. The results depicted that the shorter length microheaters were efficient in power consumption, heat dissipation, and performance (Kaushal and Das 2016). The resistance of the microheater is given by

$$R = \frac{\rho l}{A}$$

where R is the resistance at the same temperature at which ρ is specified, ρ is the resistivity of the material (m), l is the length of the resistor, and A is the cross-section area (width \times thickness).

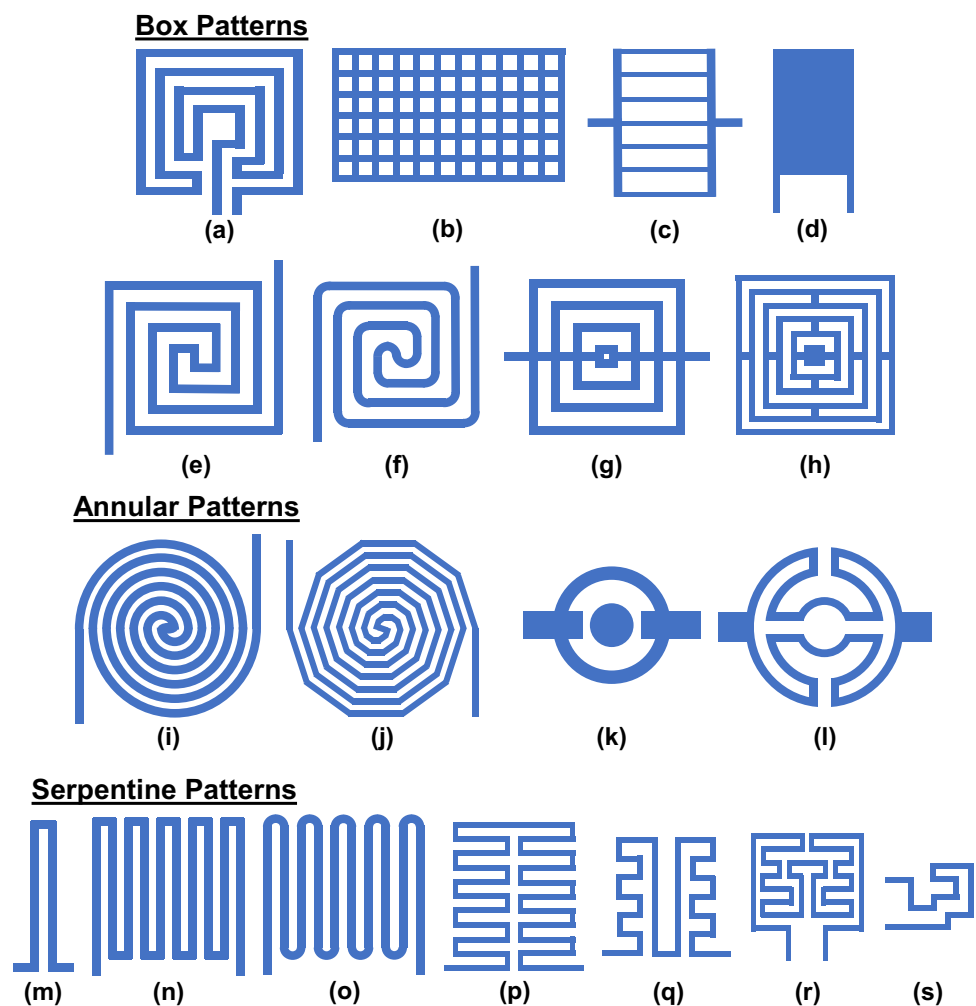
In most of the microheaters, heat is confined to the central region that decreases the thermal uniformity. For instance, the electrothermal analysis of the four-element micro hotplate array results in a more heat concentration of 706 °C at the central region, whereas the edges only possess 224 °C (Khanna et al. 2007). Hence, the uniform thermal distribution across the microheater can be achieved by maintaining lower resistance in the middle region and gradually increases towards both the extreme regions. This can be accomplished either by altering the

width of the patterns in the middle region such that more resistance at the middle region compared to the edges or altering the spacing between the heater wires. Hence the arrangement should be less closely packed at the central region, and at the edges, it should be more closely packed (Li et al. 2017). Similarly, Barman et al. varied the width and density of the meander-shaped Al microheater to provide uniform temperature distribution even in the presence of non-uniform thermal insulation (Barman et al. 2018). Thereby, Hwang et al. designed a novel microheater by optimising parallel meander structure for improved thermal uniformity and achieved over 80% of the uniform heating area; hence it has high sensitivity and selectivity in semiconductor gas sensors (Hwang et al. 2011b).

4.1 Geometry

The microheater design can vary depending on the application, from simple wire or line patterns to complex wing-shaped patterns to provide uniform thermal distribution. The various microheater designs so far investigated and

Fig. 8 Illustrative diagram of different microheater designs so far investigated by various researchers (Botau et al. 2015; Das and Kakoty 2015; Ha et al. 2015; Han and Meyyappan 2016; Hasan et al. 2016; Holt et al. 2017; Horade et al. 2016; Hwang et al. 2011a; Jinsol and Jungchul 2014; Kim et al. 2010; Lee et al. 2013; Nieto et al. 2017; Petrucci et al. 2015; Rajput et al. 2018; Roy et al. 2010; Ruiqi et al. 2011; Wu et al. 2009; Yu et al. 2017; Zhong et al. 2009). (a) Inverted C shaped, (b) Rectangular mesh pattern, (c) Lines, (d) Plate, (e) Double spiral Square, (f) Curved double spiral square, (g) Ring-shaped, (h) Square gridded, (i) Double spiral, (j) Octogen, (k) Circular, (l) Dual C, (m) Inverted U, (n) Meander, (o) Meander with rounded corners, (p) Dual meander, (q) U Dual meander, (r) Wing, (s) Hook

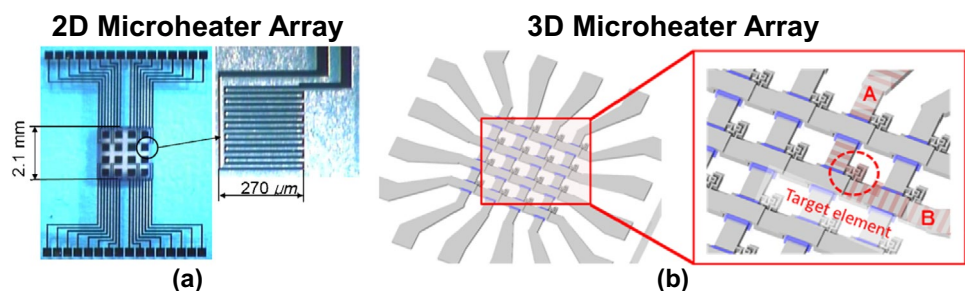


fabricated by researchers are illustrated in Fig. 8 (a) Inverted C shaped, (b) Rectangular mesh pattern, (c) Lines, (d) Plate, (e) Double spiral Square, (f) Curved double spiral square, (g) Ring-shaped, (h) Square gridded, (i) Double spiral, (j) Octogen, (k) Circular, (l) Dual C, (m) Inverted U, (n) Meander, (o) Meander with rounded corners, (p) Dual meander, (q) U Dual meander, (r) Wing, (s) Hook. The meander, fan type, and double spiral square microheaters consume low power, whereas the meander and double spiral provide better temperature distribution. Hence, Velmathi et al. designed and fabricated a double spiral square pattern resistive microheater for improving their performance at high temperatures. The spiral square model is more efficient for higher temperatures; however, it requires further improvements in achieving uniform thermal distribution (Velmathi et al. 2010). In comparison, the meander structure heater shows better thermal distribution than the spiral square model but with slightly low temperatures (Lekshmi et al. 2018; Utomo et al. 2019). Joy et al. simulated five different microheater patterns, namely single meander, double meander, fan shape, rectangle shape, and porous structure, to investigate high-temperature uniformity. The results depict the meander structure yields high uniform temperature distribution with low power consumption (Joy and Antony 2015). Yu et al. compared the temperature distribution uniformity in meander and octagon-shaped microheaters. The well-designed octagon-shaped heater on polyimide substrate has a temperature variance of $0.45\text{ }^{\circ}\text{C}$ and with a copper island at the back provides better thermal uniformity of less than $0.2\text{ }^{\circ}\text{C}$ difference. It would be much worse than meander-shaped microheaters if not properly designed. (Yu et al. 2015, 2017). Later, a rectangular mesh patterned microheater was designed and performed an electro-thermal characterization via the Finite Element Method (FEM) simulation. The simulation showed a non-uniform temperature distribution with a hot spot in the middle with a power consumption of less than 100 mW. (Botau et al. 2015). From the simulation study of Gayake et al., the edge loss can be minimized, and the temperature distribution can be improved by adapting circular geometry heaters with similar track width and gap width (Gayake et al. 2011). The circular geometry investigations provide better agreement than the meander design (Petrucci

et al. 2015). The width of the spiral tracks was modified between $12\text{ }\mu\text{m}$ and $8\text{ }\mu\text{m}$ and developed an elliptical shape hole at the centre of the spiral heater results in better thermal homogeneity at the centre and the extremities. Moreover, the current density remains stable over the entire track of the heater (Abdeslam et al. 2020). Later, the performance of a double spiral heat pad was compared with different structures, namely Peano, Hilbert, and Moore. The finite element analysis suggests that the temperature uniformity of Peano order-2 & 3, Moore order-3 & 4, Hilbert order-3 & 4 outperformed the double spiral heat-pad. Minimum metal consumption is crucial to drastically reduce the heater cost while using expensive materials. By considering these, the Peano order-2 curve provides better temperature uniformity with less metal coil length (Karnati et al. 2019). Subsequently, Tiwari et al. designed parallel heater structures with Al, Cu, Au, Nickel–Chromium, Pt, Ti, and W materials to generate uniform temperature distribution. The Model 1 with similar resistance on each parallel strip exhibits overheating in the contact pads; hence the model 2 design was reconstructed to flow minimum current through the centre and doubled as we move away from the centre (Tiwari et al. 2018b).

Moreover, in several applications, the use of a single microheater is insufficient due to the requirement of a large heating area. Hence, a microheater array is employed that comprises an array of microheaters. Initially, 2D microheaters, as depicted in Fig. 9a, were utilized. The lead wires in two-dimensional microheater arrays with few microheaters do not interfere with each other. Whereas, if several microheaters are placed, it may short-circuit or requires a large area, or results in complicated electrical connections (Jung et al. 2011). Hence, Horade et al. designed a 4×4 matrix microheater by providing insulators on the cross-over points, as shown in Fig. 9b, that put forth low-cost and can integrate with sensors, actuators, and circuits for biochemical applications (Horade et al. 2016). The 3-layer structured microheater array was designed and optimized to achieve a compact size and improved temperature uniformity. A novel two-state controlling method was adapted for selectively heating each heater unit engenders various heating patterns (Bai et al. 2019).

Fig. 9 (a) 2D 4×4 microheater array with an enlarged view of heater (Jung et al. 2011) Retrieved with permission from Elsevier, (b) 3D microheater array with lead lines are grade crossings with overpasses (Horade et al. 2016) Retrieved with permission from CCSE



5 Microheater fabrication

The implementation of the same material and fabrication technique for microheater, contact pads, and resistance temperature detectors (RTD) sensors will simplify the fabrication process, structure, and cost. Similarly, Liao et al. fabricated the heater and temperature sensing elements with the same material since it greatly simplifies the fabrication process (Liao et al. 2005). The microheaters were fabricated via flexible printed circuit board (FPCB) technology (Lee et al. 2019), complementary metal–oxide–semiconductor (CMOS) technology (Reverter et al. 2014), Nickel sulfamate bath (Nicolau et al. 2005), sputtering, electron-beam (E-beam) evaporation (Holt et al. 2018), injection molding (Zhang et al. 2020), screen printing (Tiwari et al. 2018a), aerosol/ inkjet printing (Byers et al. 2019), chemical vapour deposition (CVD) (Hwang et al. 2011b), physical vapour deposition (PVD), roll coater (Shi et al. 2018), electrohydrodynamic printing (Cao and Dong 2019), micro pen and laser sintering, surface micromachining (S. E. Moon et al. 2012), bulk micromachining (Roy et al. 2012), chemical wet etching (Yeh et al. 2013), and ultrasonic spray pyrolysis system. Some of the widely adapted methods are illustrated in Fig. 10.

5.1 Physical Vapour Deposition (PVD)

PVD is a vacuum deposition method that can deposit a thin layer on the required substrate regarding demands such as tribological behaviour improvement, optical enhancement, visual/esthetic upgrading, and many other fields (Baptista et al. 2018). The illustrative process of PVD is depicted in Fig. 11a. The deposition thickness varies from angstrom to millimetres. PVD is further classified into thermal evaporation, electron beam (e-beam) evaporation, reactive/activated reactive electron beam evaporation, sputtering, filtered cathode arc deposition, ion plating, and pulsed laser deposition. Of these, filtered cathode arc deposition, ion plating, and pulsed laser deposition were not employed in microheater fabrication since it is complex and expensive. The most commonly utilized technique is sputtering since it made undeniable progress concerning quality and increased deposition rate and met the industrial and researchers demands (Silva et al. 2002). Moreover, PVD improved the wear and corrosion resistance with ease to attain suitable thickness at a high or low rate of deposition. The PVD process was applied to deposit a thin layer of Au and Ti over the Si₃N₄ layer on a Si wafer (Ruiqi et al. 2011). While deposition of Al on a glass substrate, a six-step cleaning process is required to make the glass surface adhesive to Al (Nieto et al. 2017). However,

Fig. 10 Microheater fabrication techniques

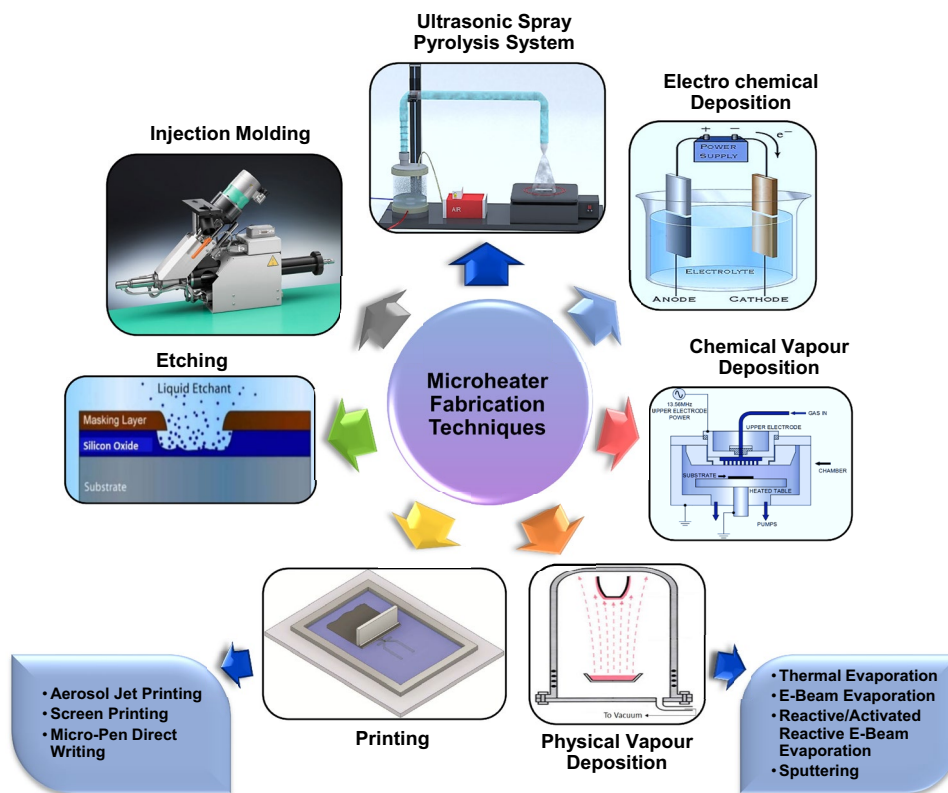
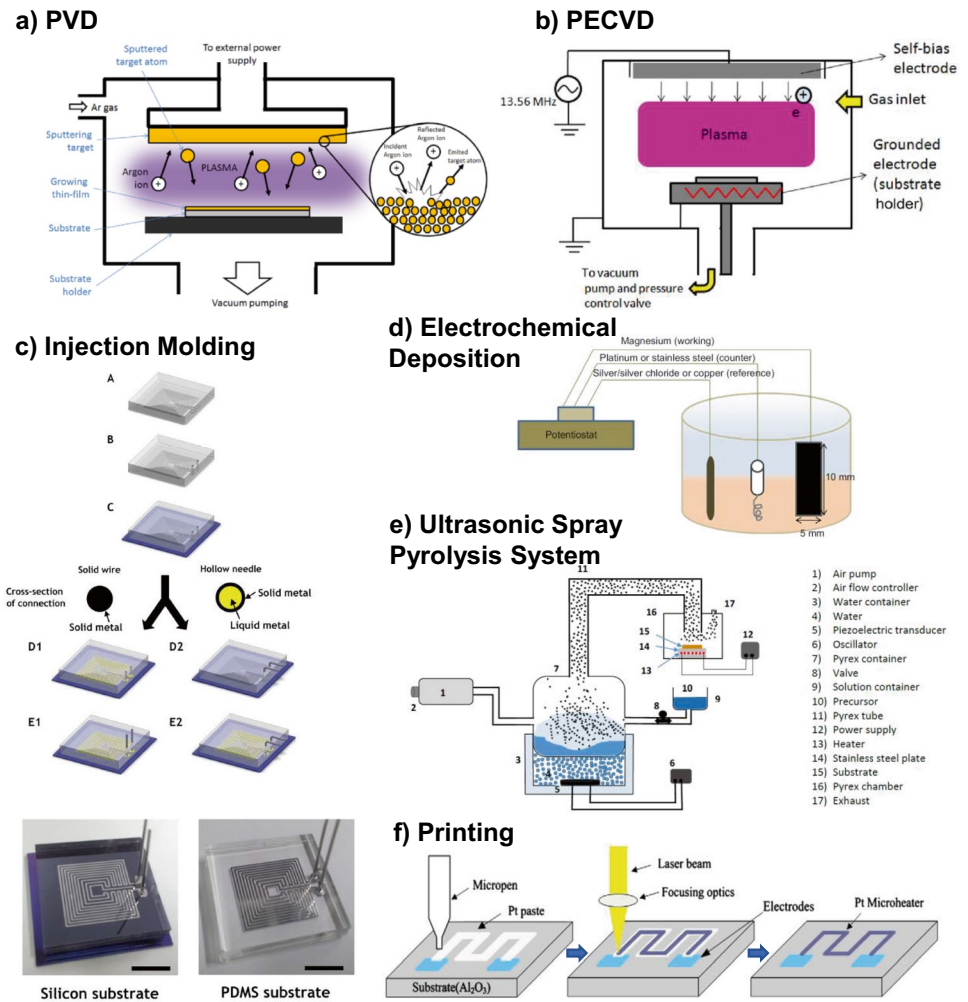


Fig. 11 Illustrations of the microheater fabrication process. **(a)** Schematic of PVD, **(b)** PECVD (Pessoa et al. 2015) Reprinted with permission from Elsevier, **(c)** Injection molding fabrication processes of liquid metal microheaters (Jinsol and Jungchul 2014) Reprinted with permission from IEEE, **(d)** Schematic of an electrochemical cell for the direct electrodeposition (Augello and Liu 2015) Reprinted with permission from Elsevier, **(e)** Illustrative of homemade spray pyrolysis system (Gharsi and Ansari 2016) Reprinted with permission from IOP, **(f)** Illustration of micro-pen direct writing and laser sintering fabrication procedure (Cai et al. 2011) Reprinted with permission from Elsevier



heterogeneous deposition may occur due to the non-uniform evaporation rate.

Thermal evaporation The thermal energy applied to the source material melts and raises the vapour pressure of the gaseous plasma in the vacuum environment tends to release or collision of atomic particles that condenses or accumulate the projected atoms on the substrate (Kiyotaka Wasa et al. 2004). In contrast, thermal evaporation has low adhesion, limited to low melting point materials and not possible to evaporate dielectric materials (Dobrzański and Pakuła 2005).

E-Beam evaporation E-Beam evaporation is purely a physical process that evaporates any material by bombarding electrons of the source material at a high vacuum to release ions or molecules for direct deposition on the target substrate materials via e-beam power. The plasma generated through the collision of atomic size released particles and gas molecules increases the adhesion of the deposited film to the

substrate through compression (Holmberg and Matthews 2009; Mattox 2010).

Reactive/activated reactive electron beam evaporation Reactive/Activated Reactive Evaporation utilizes e-beam and thermal evaporation to overcome the stoichiometry formation in certain refractory oxides and carbides during e-beam evaporation. The evaporation is done in the presence of reactive gas such as O₂, N₂, hydrocarbon. Hence, oxide layers are deposited.

Sputtering In sputtering, the source material and substrate are placed in a vacuum chamber filled with sputtering gas. By applying a high potential difference between the source and substrate, plasma is generated by the sputtering gas ionization and bombard the source material to eject atoms. The ejected atoms get deposited on the substrate. Efficient deposition occurs when the atomic weight of sputtering gas will be nearly equal to the source material. High melting point materials can be easily sputtered in low vacuum conditions.

Moreover, it provides a better adhesion than evaporation but requires high energy (Baptista et al. 2018).

5.2 Chemical Vapour Deposition (CVD)

Polysilicon is suitable for heating elements due to its high resistivity. However, it is difficult to be deposited by a simple electron beam deposition technique. Instead, it has to be deposited using a chemical vapour deposition (CVD) technique, which is expensive (Das and Kakoty 2015). CVD is the deposition of a thin film on the substrate through the reaction of chemical gas or volatile liquids under the application of external activation energy. The illustration of CVD is shown in Fig. 11b. The CVD provides access to large-area, uniform, and continuous deposition of a high-quality film with good adhesion without defects and impurities but facilitates a low deposition rate (Chen et al. 2017). Low-pressure CVD (LPCVD) implies the thin film deposition on the heated substrate under the pressure range of 0.01–1 torr at any temperature in the reactor. In PECVD, the gaseous reactant mixture at 0.1–1 torr pressure generates a glow discharge. The complex reaction between the glow discharge plasma and the substrate leads to a thin film formation on the substrate (Morosanu 1990). In CVD, there are chances of chemical hazards because using toxic, corrosive, and explosive precursor gases also difficult to deposit multi-component material (Reina et al. 2009). Moreover, CVD consumes high energy and requires a very high temperature during the deposition (Gassner et al. 2016).

5.3 Electrochemical deposition

Electrochemical deposition is the process of depositing a thin and tightly adherent coating of metal, oxide, or salt on the desired conductor substrate via simple electrolysis, as depicted in Fig. 11d. The electrolytic cell device consists of two electrodes dipped in an ionic compound electrolyte. The positive ions in the electrolyte get deposited on the desired substrate placed at the cathode while passing direct electric current. Simultaneously, negative ions migrate to the anode and transfer electrons to the electrolyte to make it neutral (Rodriguez and Tremiliosi-Filho 2013). Electrochemical deposition is a simple and powerful process of depositing nanoparticles on a graphite sheet (Liu et al. 2010). The deposition thickness depends on the deposition time, nucleation potential, concentration of the metal salt, etc. (Hsieh et al. 2012). It is a simple and low-cost deposition process with improved interfacial bonding (Augello and Liu 2015). In contrast, the electrochemical deposition leads to poor distribution and the large size of nanoparticles that are ineffective for improving the use of active

metal components. Furthermore, in electrochemical deposition, the insulator material surface cannot be deposited (Kakaei et al. 2019).

5.4 Ultrasonic spray pyrolysis system

Gharesti et al. deposited the microheater and sensing pellets using the technique called the ultrasonic spray pyrolysis system (USPS), as illustrated in Fig. 11e. The SnO₂ layer on the alumina substrate is deposited by washing the substrate with acetone, rinsed with deionized water, and dried at 150 °C. The piezoelectric transducer in a water-filled tank generates aerosol droplets by combining airflow and precursor solution of 0.1 M SnCl₂·2H₂O in absolute ethanol. The substrate is heated at 450 °C to deposit the aerosol on its surface. The investigations concluded that the non-annealed device experiences a 44% increase in resistance in the first 6 days, whereas the annealed device has stable resistance (Gharesti and Ansari 2016). In USPS, metal–organic precursors in organic solvents engender non-cracked homogeneous deposition, making organic solvents more appropriate than aqueous solvents (Rahemi Ardekani et al. 2019).

5.5 Injection molding

Wu et al. developed a novel method to fabricate the microheater without a deposition process. Subsequently, to make the microfluidic device inexpensive and disposable, PDMS can be applied as a substrate. However, due to the low surface energy of PDMS, it is not easy to pattern metal structure on PDMS. Hence, the injection molding principle was adapted to fabricate the microheater using silver paint. They fabricated the microheater inside the PDMS microchannel using a soft lithography technique. Initially, the glass substrate is coated and patterned with a SU-8 negative photoresist. Then PDMS is poured and heated to generate microgrooves on the PDMS. The PDMS cure was carefully peeled off and bonded with another PDMS layer through plasma treatment. The microchannel was then injected with silver paint as depicted in Fig. 11c and heated at three stages to evaporate the volatile organics in the silver paint and annealing the silver particles. Once heated, a thin uniform pattern of sintered silver particles forms a conductive microheater wire inside the PDMS (Wu et al. 2009). Besides, liquid metal-based flexible microheaters, such as GaIn and eutectic gallium indium based PDMS microheater chips were fabricated using injection molding (Jinsol and Jungchul 2014; Zhang et al. 2020).

5.6 Etching

Etching is a crucial process to develop the desired heater pattern. It is the process of selective removal of unwanted

material regions using suitable etching chemicals. Except for the printing process, all other methods deposit a thin uniform metal sheet over the substrate. Hence, the unwanted material structures should be removed using a suitable etchant. Substrates such as double-sided copper cladded standard PCB can be implemented for PCR applications where the electrical connections and the microheater can be fabricated on the top and the bottom sides via photolithography and Cu etching (Tserepi et al. 2013).

5.7 Printing

The printing technique circumvents the material wastage. Since this technique prints only the heater pattern, the use of etchant is eliminated. Moreover, there will be no requirement for a photoresist. Some of the printing techniques adapted for microheater fabrication are elaborated as follows.

Aerosol jet printing The sputtering deposition process involves the application of expensive and sophisticated equipment. Additionally, further modification of structures using the same manufacturing process faces difficulties. Hence, conventional silicon MEMS fabrication leads to the development of ink or aerosol jet printing. The ink is made up of suspended metal nanoparticles in the solvent, and the printed ink provides a stable microheater that can operate up to 500 °C after sintering (Vasiliev et al. 2017).

Screen printing Screen printing represents an effective way of developing stretchable electrodes on silicon thin films and large-scale production (Fasolt et al. 2017). Screen printing is the process of transferring a stencilled design onto a flat surface using a mesh screen, ink, and a squeegee. Initially, a polyester mesh stretched over a frame with a thread count of 160–200 Thread Per Inch (TPI) and uniformly coated with a mixture of emulsion and sensitizer. The coated polyester mesh is kept in a dark place for one hour to dry. Then the heater layout is printed with high-resolution on a transparency sheet. Subsequently, place the printed side

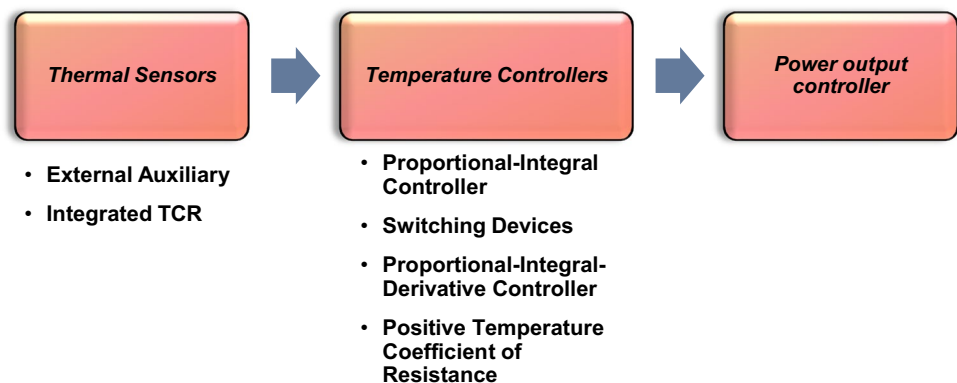
of the transparency sheet in direct contact with the screen and exposed it to ultraviolet light for 45s. After that, wash the screen with water to visualize the heater pattern. The screen is filled with metal ink and place on the substrate to print. Once printed on the substrate, the microheater chip is placed in an oven at 120 °C for 15 min (Tiwari et al. 2018a). High-temperature stable screen printing inks were utilized to fabricate high durable and low-cost microheater for microfluidic devices (Offenzeller et al. 2018). Even though the fabrication is simple for screen printing, the requirement of long production cycles, low line resolution, high heating temperatures after printing, waste of metal paste, and high costs for design alterations, especially for low-volume manufacturing, paves the way for better alternatives.

Micro-pen direct writing Micro-pen direct writing involves the combination of micro-pen and laser sintering to deposit thick-film platinum paste and pattern the deposited film, as shown in Fig. 11f. This method facilitates high efficiency and saving noble metal paste with high precision. Initially, Pt paste was directly written on the substrate using the pen head. If the paste is wet, the laser will expand and vaporizes the organic material rapidly, engenders damage to the pattern; however, if it's too dry, it is difficult to remove the un-sintered paste. Hence, the entire substrate is heated at 150 °C for 10 min with a heating rate of 3 K min⁻¹. A continuous-wave laser was then applied to deposit the pattern on the substrate, and finally, the un-sintered paste was removed by organic solvents (Cai et al. 2011).

6 Automatic temperature control module

Besides design and geometry alterations, the implementation of an efficient temperature controller impacts the uniform thermal distribution across the microheater. For instance, Zheng et al. developed 10 Ti lines and achieved constant temperature distribution through feedback control algorithms. The integral resistance feedback control

Fig. 12 Process involved in the automatic temperature control module



was designed to regulate the input voltage at each Ti line to achieve the desired resistance distribution (Zheng et al. 2017). Hence, the temperature control module is inevitable to analyze and maintain the constant temperature on the microheater surface by applying the desired voltage to the microheater coil. As depicted in Fig. 12, the automatic temperature control module comprises a temperature sensor to sense the microheater temperature, a microcontroller system programmed with a dedicated algorithm to calculate the desired voltage requirements, and a power output controller to deliver the essential voltage to the microheater. As per the thermal performance investigation, the heater can effectively heat the airflow in the microchannel without any significant increase in the chip temperature. Whereas in fluidic flow, the heater temperature decreases with the increase in flow rate (Nicolau et al. 2005). The temperature uniformity can be reached by optimizing the heating power density distribution in the heating area (Yu et al. 2017).

6.1 Thermal sensors

In the automatic temperature control module, the thermal sensor is the foremost component to sense and provide feedback to the control module to facilitate constant temperature distribution across the heater coil. Based on the requirements and portability, the thermal sensor can be inbuilt within the microheater or external.

6.1.1 External auxiliary

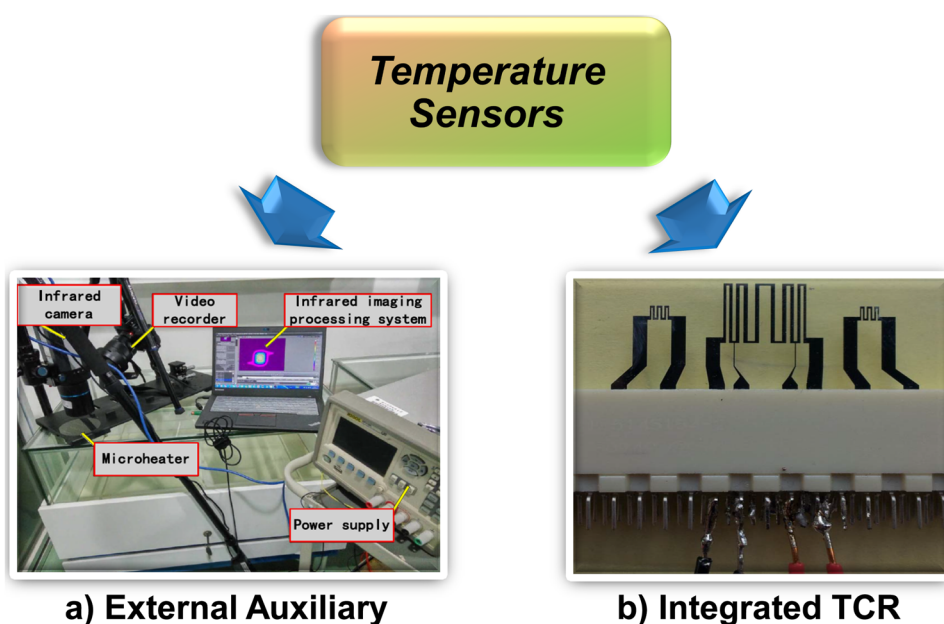
During the initial thermal sensing era, the thermal analysis was carried out via external equipment like Infra-Red (IR)

camera. Nowadays, external thermal auxiliaries are utilized mainly to calibrate TCR and analyze the heating pattern of the microheater. Furthermore, to facilitate microscopic or other online monitoring of cell culture activities and discard conventional bulky incubators, Lin et al. developed a transparent ITO microheater chip with dedicated temperature control. The thermal sensing was achieved through IR imager, and the sensed signal was sent to the temperature controller for processing (Lin et al. 2010). The auxiliaries required for external thermal sensors are shown in Fig. 13a. Similarly, Son et al. developed a novel method to measure the temperature of the microheater through an IR microscope. The investigations on different widths of microheater in atmospheric and DI water conditions revealed that there was no difference in the temperature (Son et al. 2015). These conventional temperature measurements aid a separate thermal sensor, which adds the cost and engender inaccuracy (Han and Meyyappan 2016). Furthermore, it limits portability, necessitating the need for integrated TCR.

6.1.2 Integrated TCR

The TCR reversibly shifts the resistance depending on the temperature within the working range that helps to sense the temperature of the microheater once calibrated. The fabrication cost and procedure of TCR can be reduced by using similar materials for integrated TCR and the microheater. Kang et al. fabricated Pt T-sensors and integrated them into micro gas sensors for thermal measure and control. They mainly focused on the calibration of the Pt sensor by correlating the change of electric resistance for the applied power and increase

Fig. 13 Temperature sensors adapted in microheater temperature measurement (Li et al. 2017; Scorzoni et al. 2014) Retrieved with permission from Springer Nature and IEEE



in temperature (Kang et al. 2017). SU8/Rhodamine-B thin layer (SRTL) was also sensitive to temperature and transparent material that can be coated over the microheater to measure the surface temperature distribution. This improves the indirect measurement of microfluidic channel temperature since there is no intermediate layer (Jung et al. 2011). Later, Guan et al. developed a four-point probe TCR in double spiral geometry Ag/Ti-based microheater on a glass substrate to supply Joule heating current and sense the voltage drop. This structure was capable of providing 60 °C with a low power consumption of 210 nW (Guan and Puers 2010). In addition, the power consumption characteristics and the temperature-dependent resistance of the microheater can be analyzed using the similar approach of four-wire resistance measurement (Moon et al. 2013). The 4-wire measurement, as depicted in Fig. 13b, precisely determines the voltage applied across the heater and used in the thermal time-of-flight velocity sensor of the microheater (Offenzeller et al. 2018; Petrucci et al. 2015).

Thermal sensor calibration The TCR must be calibrated after fabrication to sense the temperature by determining the resistance transition. The thermal characterization of the microheaters can be accomplished either through the measurement of the TCR or the measurement of thermal resistance and thermal time constant of the device (Scorzoni et al. 2015). The material which possesses high TCR guarantees good sensitivity for resistance temperature sensor devices. Pt is suitable for microheater and temperature sensor since it can withstand high temperatures, possesses antioxidation, lower TCR, and linear coefficient of expansion. According to Xu et al., the TCR of tungsten is constant even at high temperatures close to the melting point (Xu et al. 2016). Zhong et al. microfabricated Ti/Pt heaters with integrated

RTDs and straightforward “RTD-calibration” by inserting a thermocouple into the PCR-well (Zhong et al. 2009).

The temperature sensor is calibrated via thermistors and scaling circuitry connected to an analog-to-digital converter (ADC) of a PIC24FV16KA302 microcontroller. For instance, to determine the TCR of the nano-silver ink, four heaters were printed on photo paper and analyzed. The setup was implemented with a hotplate, multimeter, and thermometer, as illustrated in Fig. 14. The temperature of the nano-silver ink microheater was incremented 5 °C each time and kept for 15 min to heat the printed elements. The temperature and the resistance of each heater were then noted. The resistance was plotted against the temperature and compared with a linear trendline. The trendline TCR and the TCR determined for each measurement were calculated according to the equation and averaged to get the TCR of 0.003460093/ °C (du Plessis et al. 2017)

$$\alpha = \frac{\Delta R}{\Delta R_{ref} \times \Delta T}$$

where α is the linear TCR, T is the temperature of interest.

Furthermore, initially, there was a slight degradation in resistance value after each use. This may be due to the settlement of silver particles during heating and may result in decreased resistivity. However, once all the particles settle down, there will be no more resistivity changes. Hence, it is suggested to anneal the heater before the actual usage to circumvent the shift in heater resistance (Tiwari et al. 2018a).

6.2 Temperature control systems

In electric heaters, more time is required to reach higher steady-state temperatures. The ramp time can be shortened by initially driving the heater at a higher voltage. Once the specific limit reaches, the desired voltage is set to maintain the steady-state temperature (Tiwari et al. 2018a). But this technique reduces the thermal accuracy, as the resistance may vary depending on time and heat. Additionally, FEM simulation is necessary to predict the required voltage to drive the heater, and periodic temperature monitoring might be required. The usage of thermal control systems can solve this issue by using appropriate control algorithms and alters the temperature in response to resistance changes. Hence, precise temperature with rapid heating can be achieved. Some of the widely adapted microheater temperature control systems were switching systems, proportional-integral (PI) controller, proportional-integral-derivative (PID) controller. Additionally, a positive temperature coefficient of resistance can be applied to bypass external electrical devices, making POCT more portable and economical.

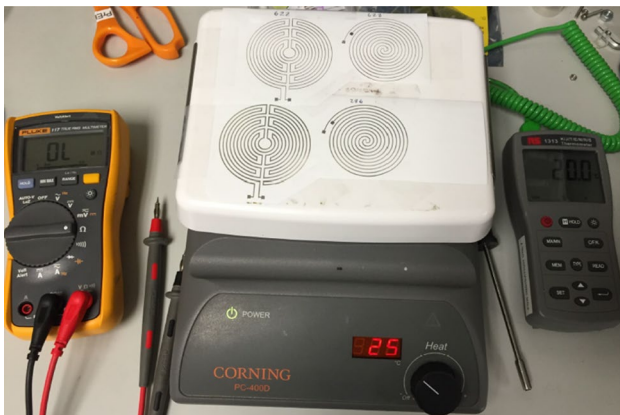


Fig. 14 Setup to determine TCR of the nano-silver ink microheater (du Plessis et al. 2017) Retrieved with permission from SPIE

6.2.1 Switching system

Closed-loop feedback control with the On/Off function was the cheapest control system and offered a rise time of 1.5s. The On/Off control initially provides maximum energy to increase the temperature of the microheater until the temperature is lower than the setpoint. If the temperature exceeds the setpoint, it shuts off the current flow. Similarly, Nie et al. used a microprocessor pulse-width-modulator (PWM) signal, as shown in Fig. 15(i)(c), for the power output control module to regulate the temperature. The power output control module turned on/off the voltage to provide the desired temperature (Nie et al. 2014). Later, Megayanti et al. designed a control system as illustrated in Fig. 15(i) (a) using AT-Mega 8535 circuit, signal conditioner, current controller, LCD, RS-232 serial communication, and microheater. The PWM method was adapted for its minimal power loss in switching devices. The switching principle was applied by controlling the output current of the transistor, resulting in high-stability temperature control with short settling and delay period (Megayanti et al. 2016). Subsequently, Jeong et al. provided a touch display module-based advanced thermal cycle controller for a dual heater using the PWM method. Hence, the PCR temperature, time, and cycle number were loaded using the touch display module for automation (Jeong et al. 2018). After, Wu et al. developed a microheater integrated with a microthermal sensor and a cooling channel for a fast cooling rate, as shown in Fig. 15(i)(b), to reduce the PCR testing time (Wu et al. 2009).

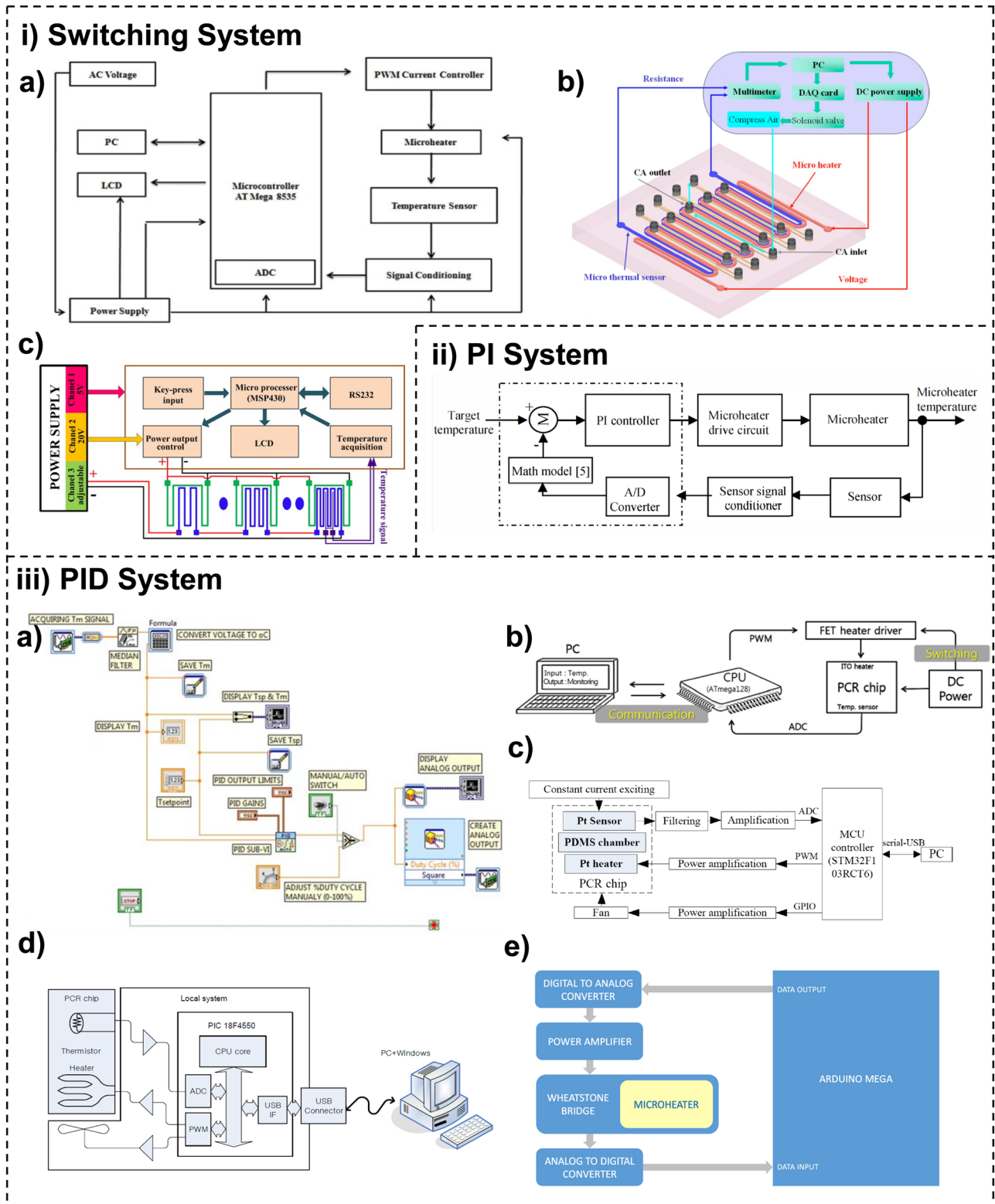
6.2.2 Proportional-Integral (PI) controller

The continuous switching of the On/Off function in the switching system leads to temperature oscillations and the generation of numerous ripples. Meanwhile, the development of the Proportional-Integral (PI) controller, as illustrated in Fig. 15(ii), forgoes the temperature oscillation by facilitating slow temperature rise while approaching the set-point, resulting in a rise time of 7.6s. Subsequently, for low-temperature applications, Phatthanakun et al. (2012) developed an aluminium microheater and a nickel thermal sensor integrated with PI closed-loop feedback temperature control kit for the rapid thermal response. The response time is 1.5s faster than ordinary PI controllers (Phatthanakun et al. 2012). The further improvements in the PI lead to the development of open-loop to closed-loop switched proportional-integral (OLCLS PI) control combines the control strategy of both open-loop and closed-loop systems. It initially behaves as an open-loop for faster rise time, and then it switched to closed-loop control. As a result, it possesses a quicker response than the PID controller and a similar disturbance handling capability as PI (Singh et al. 2018).

6.2.3 Proportional-Integral-Derivative (PID) controller

The PID controller also circumvents the ripple formation generated in the PWM method. PID controller comprises proportional, integral, and derivative action. The proportional controller produces a control action proportionate to the error, the integral action removes the steady-state error, and the derivative action is applied to decrease the peak overshoot and introduce damping (Singh et al. 2018). In the On/Off controller, the heating will only be activated if the temperature input value goes below the desired temperature setpoint value; else remains in an off state. PID controller has a similar feedback loop and wiring connections except for the latching relays, as depicted in Fig. 15(iii)(a); however, it initially retrieves the temperature data and feed into the PID sub-program, which determines the deviation error, thereby computes and control the output signal. To achieve a steady output signal in the microheater, PWM was utilized. Both the on/off and PID controllers provide good control accuracy; however, the PID controller does not require any adjustments whenever the set-point values were modified (Zainal Alam et al. 2014).

Later, Mirasoli et al. developed an electronic circuit based on (Lovecchio et al. 2015) and performed temperature control through the PID algorithm. The electronic board drives the heater by comparing the amorphous silicon (a-Si:H) diode voltage with its corresponding setpoint temperature until the setpoint was reached (Mirasoli et al. 2018). Later, Angus et al. monitored the temperatures on the heater surface, and the feedback was fed into the Arduino Uno microcontroller, in which the PID controller algorithm was programmed (Angus et al. 2015). Moreover, Han et al. controlled and monitored the real-time temperature using a microcontroller unit (MCU), as depicted in Fig. 15(iii) (b). MCU, a digital computer for automatic control of the system, forgoes the personal computer. The instructions were programmed in the microcontroller's memory to alter the voltage based on the temperature sensed on the microheater (Han et al. 2013). Similarly, Scorzoni et al. built an analog control circuit around a single operational amplifier to manage the microheater temperature accurately. Moreover, they developed a 4-terminal topology microheater for voltage delivery and sensing resistance (Scorzoni et al. 2014). Later, Moschou et al. specially designed a temperature controller board-based microcontroller to control and read the DACs and ADCs, and communicate with a personal computer (PC) where the PID control loop software was installed (Moschou et al. 2014). The user interface capability was enhanced by Hwang et al. to manage and edit directly and control the basic biochemical protocols. A local-host structure was adapted with a PIC18F4550 microcontroller, as illustrated in Fig. 15(iii)(d). The local system senses the temperature every 5 ms and calculates the output



signal through the PID controller mechanism (Hwang et al. 2015). For MAPS, it was crucial to have precise temperature control to reach 400 °C in 1 ms. Hence, Holt et al. take advantage of the PID controller circuit, a closed-loop

control based on the temperature-resistivity relationship. Arduino Mega, an 8-bit microcontroller board, calculates the resistance of the microheater and varies the power input to the microheater (Holt et al. 2017). The entire system is

◀**Fig. 15** (i) Switching temperature control. **a** Block diagram of ATmega 8535 temperature control system (Megayanti et al. 2016), **b** PDMS microfluidic chip with an integrated microheater, thermal sensor, and temperature control (Wu et al. 2009) Pictures retrieved with permission from AIP, **c** Illustration of the temperature control system and electric connections with microheater (Nie et al. 2014) Retrieved with permission from Springer Nature. (ii) Block diagram of PI closed-loop feedback control (Phatthanakun et al. 2012) Retrieved with permission from IEEE. (iii) PID temperature control. **a** Block diagram of PID temperature controller in Lab-VIEW software (Zainal Alam et al. 2014), **b** Illustration of a real-time temperature monitoring system based on MCU control (Han et al. 2013), **c** Schematic diagram of MCU (STM32F103RCT6) temperature control system (Cui et al. 2016) Pictures retrieved with permission from Springer Nature, **d** PCR Chip temperature Control System (Hwang et al. 2015) Retrieved with permission from SERSC, **e** Block diagram of the microheater control unit (Holt et al. 2017) Retrieved with permission from Springer Nature

represented in Fig. 15(iii)(e). Similarly, in the field of DNA amplification, Cui et al. generated the denaturation, annealing, and extension temperatures through Cortex-M3 ARM microcontroller temperature control system, as shown in Fig. 15(iii)(c) based on a fuzzy-PID control algorithm with PWM to regulate the heater input power (Cui et al. 2016).

6.2.4 Positive Temperature Coefficient of Resistance (PTCR)

Apart from all these control systems, self-regulating resistive heating elements were capable of maintaining their set temperatures and forgo the external regulating electronic systems, enhancing the portability in lab-on-chip (LOC) and POC applications. The purpose of a positive temperature coefficient of resistance (PTCR) material as the heating element will exhibit a rapid rise in resistance at elevated temperatures. The PTC polymer-based heating element takes 5 min to reach the set temperature of 61.5 ± 64 °C and holds up to 25 min (Pardy et al. 2017). This approach was simple, inexpensive, and did not need any control systems; however, it took a long time to achieve the desired temperature, and it was not ideal for applications requiring several thermal cycles.

7 Microheater applications

Specific reactions, sensing, and actuation occur only at elevated temperatures. For instance, in the biological sector, DNA amplification and cell culture necessitate typical temperatures at an extended period for detection and multiplication of pathogens, respectively. Similarly, in gas sensing, the semiconductor chemiresistor film was heated at a particular temperature to develop a depletion layer by adsorbing oxygen atoms to sense the reducing gas concentration. Hence,

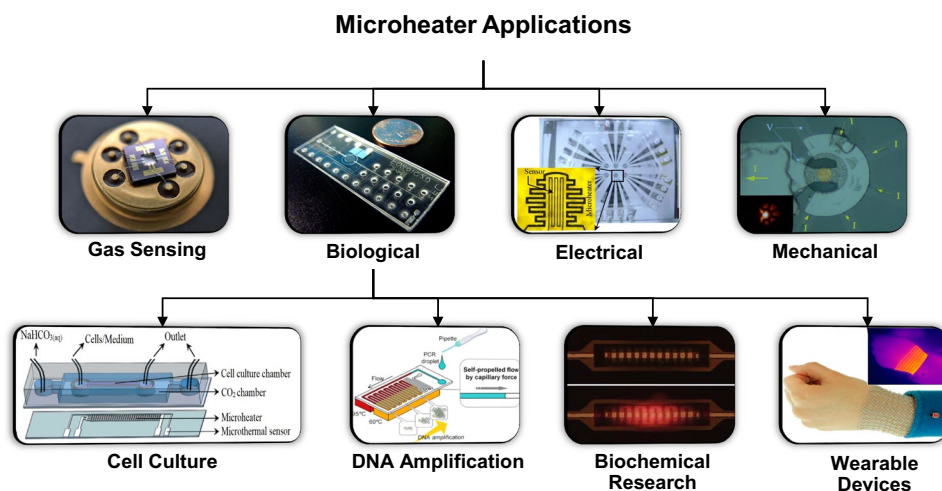
the presence of a heater in such devices is inevitable. But the integration of conventional heaters increases bulkiness and cost. Microheaters are now incorporated in several MEMS devices due to the advancement of miniaturized heaters for rapid sensing, low-power consumption, inexpensive, and compactness. Thus, the microheaters have potential applications in gas sensing, biological, electrical, and mechanical sectors, as depicted in Fig. 16.

7.1 Gas sensing

A microheater is an essential feature of a chemical gas sensor. The high sensitivity and short response time of gas sensors were achieved by operating the sensors at elevated temperatures. Hence, the integration of heaters in such devices is inevitable (Gharsi and Ansari 2016). This is due to the fact that the adsorption/desorption of the chemical gas on the sensing surface happens only at high temperatures. The metal oxide gas sensors exploit surface adsorption properties to detect the changes in the resistance as a function of varying concentrations of different gases. The sensitivity and response time of the gas sensor depends on the operating temperature of the microheater (Joy and Antony 2015). While sensing the temperature of the microheater, self-heating and interrupt-cooling may occur. The current flowing through the device to monitor the temperature may cause self-heating, which can be avoided by sensing at very low voltage with short durations. When the temperature is higher than the ambient temperature, the temperature sampling may cool down the microheater, which can be avoided by sampling as quickly as possible (Han and Meyyappan 2016). Moreover, uniform elevated temperature distribution was required for a better and smooth operation with increased stability and accuracy of the gas sensor (Das and Kakoty 2015). It was found that the multilayer heater could improve structure adhesion as well as enhances the stability, reliability, and corrosion resistance of the structure. Hence fabricated a multilayer microheater with Cr, CrN, Pt, CrN, and Cr layers as depicted in Fig. 17b. Later, Rajput et al. designed a dual meander heater to provide uniform temperature distribution to the sensor (Rajput et al. 2018). Low power consumption with an enormous heating area, high mechanical strength, and sensitivity were inevitable requirements for a high-performance microheater. Hence, Xu et al. proposed a Pt microheater on a concave-shaped dielectric membrane, as depicted in Fig. 17d, which lowers the power per active area (Xu et al. 2011). Later, introduced Pd–Pt as catalytic material to fabricate high-performance catalytic gas sensors (Xu et al. 2012).

SnO_2 was the most promising gas-sensing material. Dai et al. designed a chemiresistive thin-film gas sensor with an integrated interdigital-electrodes (IDEs) and a microheater, as shown in Fig. 17j that engenders fast response, high

Fig. 16 Potential applications of the microheater



sensitivity, low power consumption, and mass-produced potency (Dai et al. 2013). The SnO_2 nanowires network fabricated on the micro-electrodes and heater patterns suspended in a cavity, as depicted in Fig. 17a, showed selective detection to $\text{C}_2\text{H}_5\text{OH}$ (Hwang et al. 2011a). Similarly, the porous nanostructured SnO_2 layer with polycrystalline silicon (polysilicon) microheater in a thin low-stress silicon nitride (LSN) microsensor was employed for the fast and highly sensitive CO detection (Long et al. 2016). Later, Jae-Cheol et al. fabricated a sensor integrated with SiC microheater, as depicted in Fig. 17f, to detect NO in harsh environments, which was cheap and shown similar sensitivity to Pt microheater. Moreover, it can work above 15 V, whereas Pt heaters are destroyed due to combustion (Jae-Cheol and Gwi-Sang 2010). Further, Chung et al. fabricated Pt microheater and temperature sensor using 3C-SiC thin films for low power consumption and high thermal uniformity (Chung and Jeong 2010). The use of AlN/3C-SiC materials provides long-term stability at high temperatures. The SiC microheaters, as shown in Fig. 17e, have high resistance compared to polysilicon; hence high potential is required to reach the same power as of polysilicon microheater. The low power consumption, high TCR, and more stable resistance during continuous heating at 500 °C make it appropriate for highly stable catalytic gas sensing with fast response and recovery time (Harley-Trochimczyk et al. 2017). A thin layer of Si membrane over the active region of the microheater instead of a silicon plug improves the robustness and life of the device for continuous usage in coal mines (Roy et al. 2010). Later, Hwang et al. proposed a novel design to improve the temperature uniformity of the microheater using poly-Si thin film. This provides a short response time of less than 20 ms, which can replace mechanical choppers (Hwang et al. 2011b). The transfer from ceramic to thin-film gas sensors leads to the development of compactness and inerrability circuit SOI (silicon-on-insulator) substrate sensors. Hence,

Gupta et al. analyzed the temperature, current density, stress & displacement of Pt microheater on SOI substrate (Gupta and Chaudhuri 2012). The Fabry–Perot modulation technique on the microheater as depicted in Fig. 17i predicted that the higher temperature gradient in the waveguide induces thermal stress resulting in increased polarization dependencies (Kaushal and Das 2016).

Furthermore, Moon et al. developed two semi-circular Pt microheaters, as depicted in Fig. 17h, using tin oxide nano-powders for low-power-consumption and effective gas detection, with integrated monitoring systems for better thermal uniformity. The resistance of each heater electrically equal to the Wheatstone bridge (S. E. Moon et al. 2012). Later, Bai et al. fabricated a Pt microheater array, as shown in Fig. 17g, with a 3-layer structure to simplify the wire connection. Additionally, a novel two-state method was adapted to selectively heat each heating units in the array that can be applied for versatile applications (Bai et al. 2019). After that, Yoon et al. designed a highly sensitive hydrogen gas sensor, as depicted in Fig. 17c, comprised of a Pt microheater coated with SiO_2 to prevent the oxidation and hydrogen entrapment of the sensing electrodes and microheater (Yoon et al. 2012). Subsequently, Hasan et al. simulated a Pt microheater with minimal power consumption, low thermal mass, and better thermal uniformity for gas sensing applications. The analysis of voltage versus temperature, voltage versus current, voltage versus power, and temperature versus thickness of microheater shows linear results (Hasan et al. 2016). Later, Roy et al. produced a durable, low-cost Ni alloy microheater with uniform temperature distribution that can easily adapt with Si process technology for methane sensing (Roy et al. 2012). H_2S is a toxic gas emitted during the energy production process from coal and crude oil that can be detected using Electrochemical Impedance Spectroscopy (EIS) technique by reduced graphene oxide

Microheaters for Gas Sensors

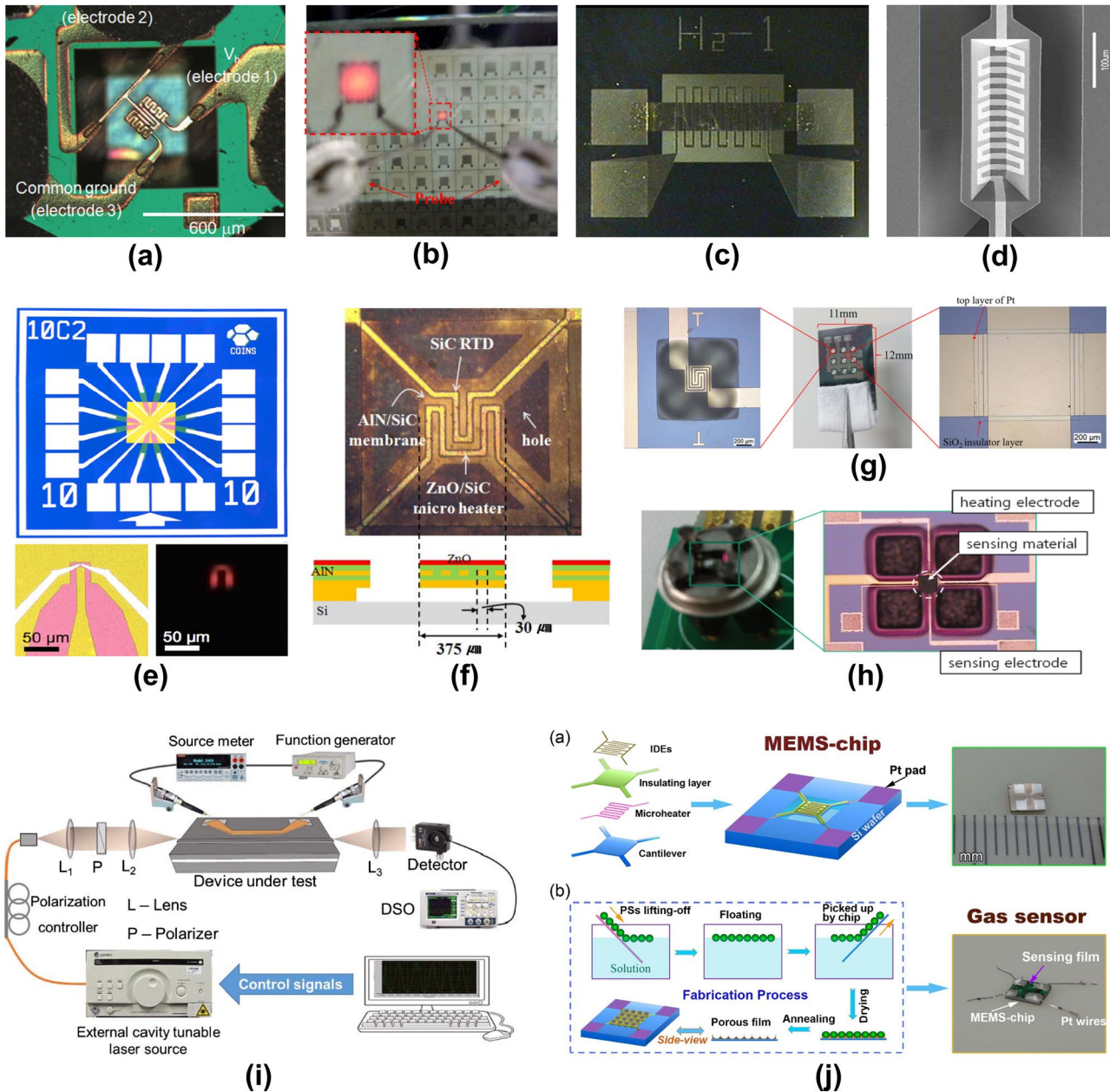


Fig. 17 Microheaters used in gas sensing. (a) optical image of the gas sensor with microheater and sensing electrode (Hwang et al. 2011a), (b) Micrographs of micro-hotplate on a glass substrate (Chang and Hsihe 2016), (c) Fabricated H₂ sensor (Yoon et al. 2012) Pictures retrieved with permission from Elsevier, (d) SEM image of the fabricated 3-D microheater (Xu et al. 2011) Retrieved with permission from IEEE, (e) Photograph of four SiC microheaters (Harley-Trochimczyk et al. 2017) Retrieved with permission from IOP, (f) NO gas sensor with integrated 3C-SiC microheater

(Jae-Cheol and Gwi-Sang 2010) Retrieved with permission from IEEE, (g) 3×3 microheater array device with three-layer structure (Bai et al. 2019) Retrieved with permission from Springer Nature, (h) Surface micromachined NO₂ gas sensor with integrated microheater (S. E. Moon et al. 2012) Retrieved with permission from Ingenta, (i) Schematic setup for testing Ti-stripe microheater (Kaushal and Das 2016) Retrieved with permission from OSA, (j) Fabricated MEMS-based porous SnO₂ film chip (Dai et al. 2013) Retrieved with permission from Springer Nature

(rGO)-incorporated nano-zinc oxide (n- ZnO) composites at 90 °C (Balasubramani et al. 2019). EIS has been utilized to design gas sensors due to its ultra-sensitivity

in identifying and measuring various toxic gases than conventional sensors. The integration with microheaters could be able to address issues such as identification of gases

Table 2 Characteristic features of various microheaters utilized for gas sensing

Sl. No	Substrate	Material	Thickness	Fabrication	Design	Application	Max. Temp	Max. Volt	Power Consumption	Response Time	Ref
1	Thermal oxide	Polysilicon	-	-	Meander	Gas sensors	706 °C	4 V	<50 mW	-	(Khanna et al. 2007)
2	Si	Au/Cr	200/10 nm	DC magnetron sputtering and lift-off	-	MEMS gas preconcentrator	300 °C	20 V	12.3 W	100 ms	(Yeom et al. 2008)
3	Si	Pt	5 µm	Electrochemical Deposition and lift off	U Dual meander	Gas sensors	500 °C	0.8 V	40mW	5s	(Hwang et al. 2011a)
4	Si ₃ N ₄	Ti/Pt	20/200 nm	DC sputtering and lift-off	Double spiral square	Gas sensors	400 °C	70 mA	1 W	-	(Velmathi et al. 2010)
5	SiO ₂	Alloy of Ni, Co, Fe	200 nm	E-beam deposition	Curved double spiral square	Gas sensors	200 °C	5 V	146 mW	-	(Roy et al. 2010)
6	AlN/SiC	SiC	1 µm	RF magnetron sputtering	Meander	NO sensor	500 °C	30 V	10.3 mW	100s	(Jae-Cheol and Gwyi-Sang 2010)
7	AlN/3CSiC	Pt	300 nm	Sputtering	Meander	Gas sensor	500 °C	14 V	312 mW	175.1 ms	(Chung and Jeong 2010)
8	Si ₃ N ₄	Pt	200 nm	Photoresist spray coating based lift-off process	Meander	Gas sensors	400 °C	-	30 mW	-	(Xu et al. 2011)
9	Silicon	Poly-Si-Heater, Pt-Contact pads	200 nm	LPCVD and sputtering	Optimized parallel meander structure	Gas sensors	460 °C	-	250 mW	< 20 ms	(Hwang et al. 2011b)
10	Si	Ni Alloy	200 nm	Bulk micromachining technique	Meander	Gas sensors	200 °C	5 V	~ 140 mW	~ 47s	(Roy et al. 2012)
11	SiO ₂	Au/Pt	100/100 nm	Surface and bulk micromachining technology	Meander	Gas sensors	200 °C	1.5 V	20 mW	-	(Gupta and Chaudhuri 2012)
12	Si ₃ N ₄	Pt/tantalum pentoxide (Ta ₂ O ₅)	200/30 nm	Sputtering	Meander	Gas sensors	149.42 °C	4 V	-	35s	(Yoon et al. 2012)
13	Si	Pt	-	Surface micromachining and lift-off	-	NO ₂ Gas Sensor	450 °C	-	20 mW	39s	(S. E. Moon et al. 2012)
14	Si	Pt/Ti	200/20 nm	Lift-off	Meander	Gas sensors	350 °C	-	~ 32 mW	~ 1s	(Dai et al. 2013)

Table 2 (continued)

Sl. No	Substrate	Material	Thickness	Fabrication	Design	Application	Max. Temp	Max. Volt	Power Consumption	Response Time	Ref
15		Pt	5 μm	-	Square gridded-type	Gas sensors	700 °C	60 mV	-	-	(Das and Kakoty 2015)
16	Polyethylene naphthalate (PEN)	Cu	100 nm	-	Rectangular mesh pattern	Gas sensor and biotechnological field	90 °C	-	80 mW	40s	(Botau et al. 2015)
17	SiO ₂	p-type polysilicon film	200 nm	Low-pressure chemical vapour deposition	Double spiral square	Gas sensors, flow meters, mass sensors, and PCR	200 °C	20 V	-	~35 ms	(Han and Meyyappan 2016)
18	SiO ₂	Pt	150 nm 100 nm	-	Meander	Semiconductor gas sensors	656 °C 448 °C	7 V	127 mW 84.66 mW	-	(Bedoui et al. 2016)
19	PCB	Cu	350 nm	Etching	Meander	Gas sensors	250 °C	-	~2 W	146s	(Megayanti et al. 2016)
20	Si	Ti-Heater, Al-Contact pads	150/300 nm	i-line lithography and reactive ion etching	Line	-	-	9 V	1.1 mW	~9 μs	(Kaushal and Das 2016)
21	SiO ₂	Cr/CrN/Pt/CrN/Cr	10/20/200/20/10 nm	Sputtering	Meander with rounded corners	Designing and fabricating micro-hot-plates	498 °C	25 V	2.35 W	-	(Chang and Hsihe 2016)
22	SiO ₂	Pt	1 μm	-	Meander	Gas sensor	915.12 °C	0.5 V	1.325 mW	-	(Hasan et al. 2016)
23	SiO ₂	Tungsten	10 μm	-	Plate	Gas sensors, micro-reactors, and infrared emitters	480.85 °C	0.5 V	20.10 mW	-	(Deo 2016)
24	Alumina ceramic film	Pt	-	Aerosol jet printing	Meander	Gas sensor	450 °C	-	~80 mW	3s	(Vasiliev et al. 2017)
25	Si ₃ N ₄	Silicon carbide (SiC)	130 nm	Low-pressure (170 mTorr) hot-wall reactor	-	Catalytic gas sensing	700 °C	-	28 mW	~1s	(Harley-Trochimczyk et al. 2017)
26	SiN _x	Pt	200 nm	-	Meander with rounded corners	Gas sensor	391 °C	-	39 mW	-	(Kang et al. 2017)
27	Glass	NiCr	10 μm	-	Dual meander	Gas sensor	348 °C	1.9 V	-	-	(Rajput et al. 2018)

Table 2 (continued)

Sl. No	Substrate	Material	Thickness	Fabrication	Design	Application	Max. Temp	Max. Volt	Power Consumption	Response Time	Ref
28	SiO ₂	Pt	200 nm	-	Meander	Gas sensor	1700 °C	1.5 V	75 mW	-	(Lekshmi et al. 2018)
29	Glass	Ti/Pt	20/200 nm	DC pulse sputtering system and lift-off	Double spiral square	Gas sensors	715 °C	19.5 V	1.3 W	2s	(Prajesh et al. 2019)
30	Si ₃ N ₄	Pt	300 nm	Reactive magnetron sputtering and ion etching	Double spiral square	Gas sensors, wearable devices, drug release, etc	498.1 °C	3 V	239.4 mW	2.5 ms	(Bai et al. 2019)
31	Si ₃ N ₄	In-situ doped polysilicon	100 nm	Evaporation and plasma etcher	Line	Gas sensors	~300 °C	5 V	6.8 mW	33 μs	(Zhou et al. 2015)
32	SiO ₂	Pt	100 nm	-	Double Spiral with an elliptical hole at the central region	Gas sensors	300 °C	-	13.4 mW	-	(Abdeslam et al. 2020)

at high temperatures, long-term reliability of the sensor, and operating in harsh environments (Balasubramani et al. 2020). The critical summary of physical, electrical, and thermal characteristics of different microheaters and their fabrication approaches in gas sensing are represented in Table 2.

7.2 Biological applications

A LOC device integrates multiple functioning abilities embedded in a compact platform for rapid output generation meets a tremendous demand. Some familiar functions rooted in the LOC are pumping, thermal cycling, mixing of fluids, dispensing, and separation (Miralles et al. 2013). The application of thermal cycling to control and regulate temperature plays a vital role in many biological, chemical, and physics applications (Chon and Li 2014). Some well-known examples that indulge accurate temperature requirements are PCR, Temperature Gradient Focusing for Electrophoresis (TGF), digital microfluidics, mixing, and protein crystallization. In the biomedical field, Ruiqi et al. integrated a compact ring-shaped low power Ti microheater on a silicon substrate as depicted in Fig. 18d to precisely mark the location of interests during the image diagnosis in capsule endoscopy (Ruiqi et al. 2011). Furthermore, Reverter et al. investigated the in-vitro thermal stimulation of single neurons using a high-resolution microheater array and analyzed the electro-thermal response, reliability issues, and lifetime of various microheater designs regarding self-heating and electromigration. The lower current density heater has a better median time to failure (Reverter et al. 2014). Si nanowires find their application in the biological and chemical fields due to their high sensitivity and fast responsivity. Thereby, Son et al. developed Si nanowire-heaters, as shown in Fig. 18e, with response time varied between 100–140 μs depending on the applied voltage and pulse duration. These heaters were most likely employed for local heating of single-cells and heat shock generation of bio-molecules (Son et al. 2017). The miniaturization of microbioreactor engenders applications such as biosensors, micro-fermentor arrays, and microbiological assay kits (Hegab et al. 2013). Hence, Utomo et al. fabricated microheaters, as shown in Fig. 18b, for dynamic-flow microbioreactor based on the specific requirements of microbioreactor such as shape, size, target working temperature, and heating rate profile (Utomo et al. 2019). However, no attempt has been made to control the performance of mono-disperse bio-polymer microcapsules for drug release. Therefore, Yeh et al. developed a microfluidic chip with an integrated microheater and flow-focusing device for generating uniform-sized gelatin microcapsules for vitamin C drug release (Yeh et al.

Microheaters for Biological Studies

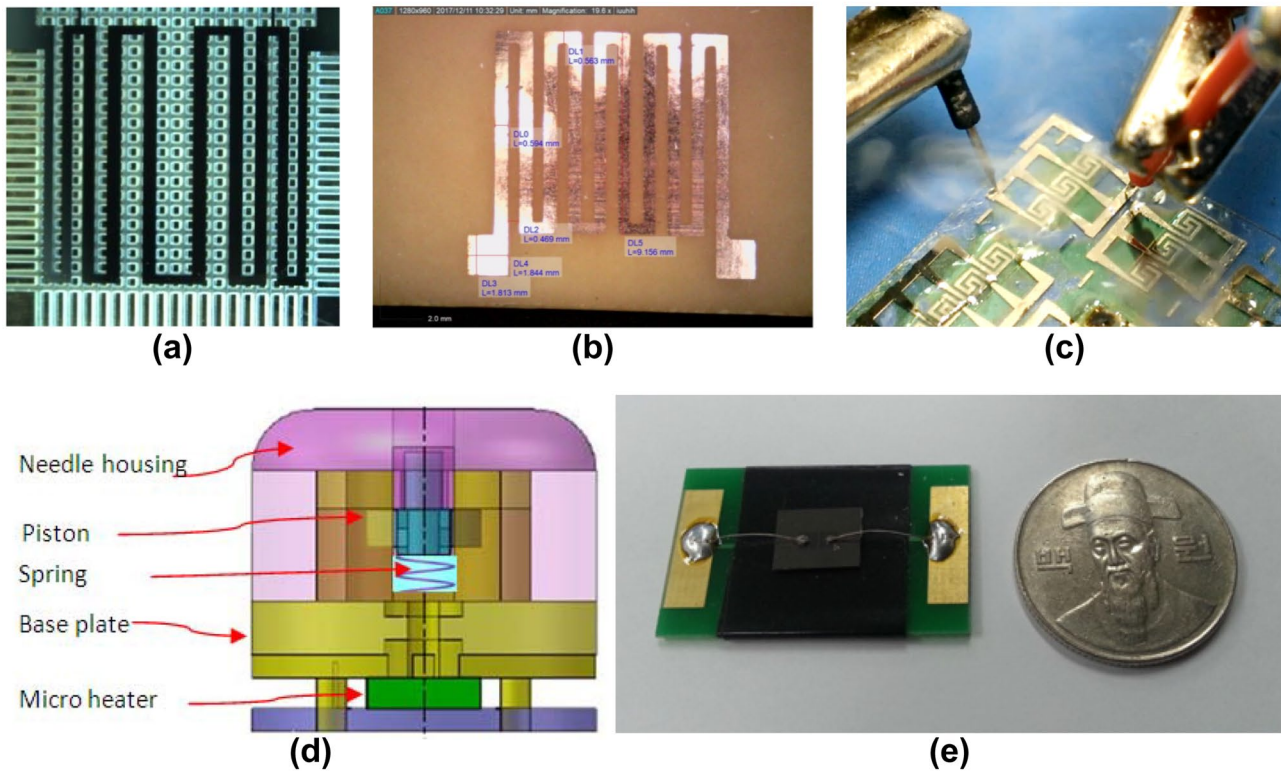


Fig. 18 Microheaters utilized in the biological sector. **(a)** Microheater with trench geometry on the glass substrate (Scorzoni et al. 2015) Reprinted with permission from Elsevier, **(b)** Copper microheater for dynamic microbio reactor (Utomo et al. 2019) Reprinted with permission from AIP, **(c)** A low cost microheater for aerosol generation (Liu

et al. 2014) Reprinted with permission from Elsevier, **(d)** Tagging module in capsule endoscope (Ruiqi et al. 2011) Reprinted with permission from IEEE, **(e)** Si nanowire-heater device (Son et al. 2017) Reprinted with permission from Springer Nature

2013). Moreover, a 3D-printed microheater was available with an integrated drug-encapsulated microneedle patch system for drug delivery in pain management (Yin et al. 2019). Similarly, Liu et al. fabricated a low-cost, fast-responding microheater as depicted in Fig. 18c for disposable aerosol dispensers. The investigations on double spiral-shaped and meander-shaped heaters shown similar results in an aerosol generation. The aerosol generation was accelerated when multiple parallel microheaters were used; however, the power consumption was raised by 50% (Liu et al. 2014). The design of a proper trench structure, as depicted in Fig. 18a, maximize the energy efficiency by improving the thermal resistance of microheaters and thermally isolate the heater from the glass substrate (Scorzoni et al. 2015) Nevertheless, Zheng et al. microfabricated a Ti heater to be compatible with *in situ* imaging in a scanning electron microscope (Zheng et al. 2017). In Table 3, the fabrication techniques, physical, electrical, and thermal characteristics of several microheaters employed in biological sector are summarised.

7.2.1 Cell culture

In cell culture, maintaining a specific temperature over an extended period of time is substantial for better replication of biological cells. Hence, Plessis et al. developed a high sensitivity and rapid test micro-incubator in environmental water quality screening tests. The incubation time can be adjustable between 30 min and 9h with a rise time of 15 min to reach the set-point temperature and can be autoclaved at 121 °C for reusability (du Plessis et al. 2017). Later, Christen et al. fabricated a CMOS integrated circuit for heating and sensing PDMS microfluidic channels and reservoirs for autonomous cell-culture and incubation microsystem (Christen and Andreou 2007). For microfluidic perfusion cell culture, Lin et al. developed a system that comprises a cell culture chip and an ITO glass microheater. The temperature variation of the microheater was found to be ± 0.3 °C during experimental evaluation (Lin et al. 2011). Silicon-based heaters have limited their applications in cell culture systems due to the complicated fabrication process. Hence, a glass substrate has

Table 3 Characteristic features of various microheaters used biological sector

Sl. No	Substrate	Material	Thickness	Fabrication	Design	Application	Max. Temp	Max. Volt	Power Consumption (Response Time)	Ref
1	Si	Ti- Heater, Au- Contact pads	250 nm	PVD	Ring-shaped	Capsule Endoscope	60–80 °C	-	85mW	(Ruiqi et al. 2011)
2	Glass	ITO	-	Chemical wet etching	Meander	Pharmaceutical applications	96 °C	16 V	-	(Yeh et al. 2013)
3	Si ₃ N ₄	Cr/Ni	10/20 nm	Metals deposition and wet etching process	Double spiral square and meander	Aerosol generator for drug delivery	350 °C	3 V	2.394 W	(Liu et al. 2014)
4		Al	480 nm	CMOS technology	Double spiral square	LOC thermal neural stimulation	60 °C	-	90 mW	(Reverter et al. 2014)
5	Glass	Cr/Al/Cr	30/200/30 nm	Vacuum evaporation and wet etching	Meander	LOC	94 °C	-	2.901 W	(Scorzoni et al. 2015)
6	SOI	Si nanowire doped by boron	15 μm	E-beam evaporation	Line	Heating of single-cells and heat shock generation of bio-molecules	88 °C	21 V	22.4 W (100 μs)	(Son et al. 2017)
			30 μm				79 °C	34 V	(140 μs)	
7	SiO ₂	Ti	400 nm	Electron beam evaporation and etching	Lines	Scanning electron microscope	100 °C	8 V	(~ 150s)	(Zheng et al. 2017)
8	PCB	Cu	-	Digital maskless photolithography using a commercial digital light projector	Meander Spiral square with large central region	Bioreactors	118 °C 138 °C	0.05 V	-	(Utomo et al. 2019)

Microheaters for Cell Culture

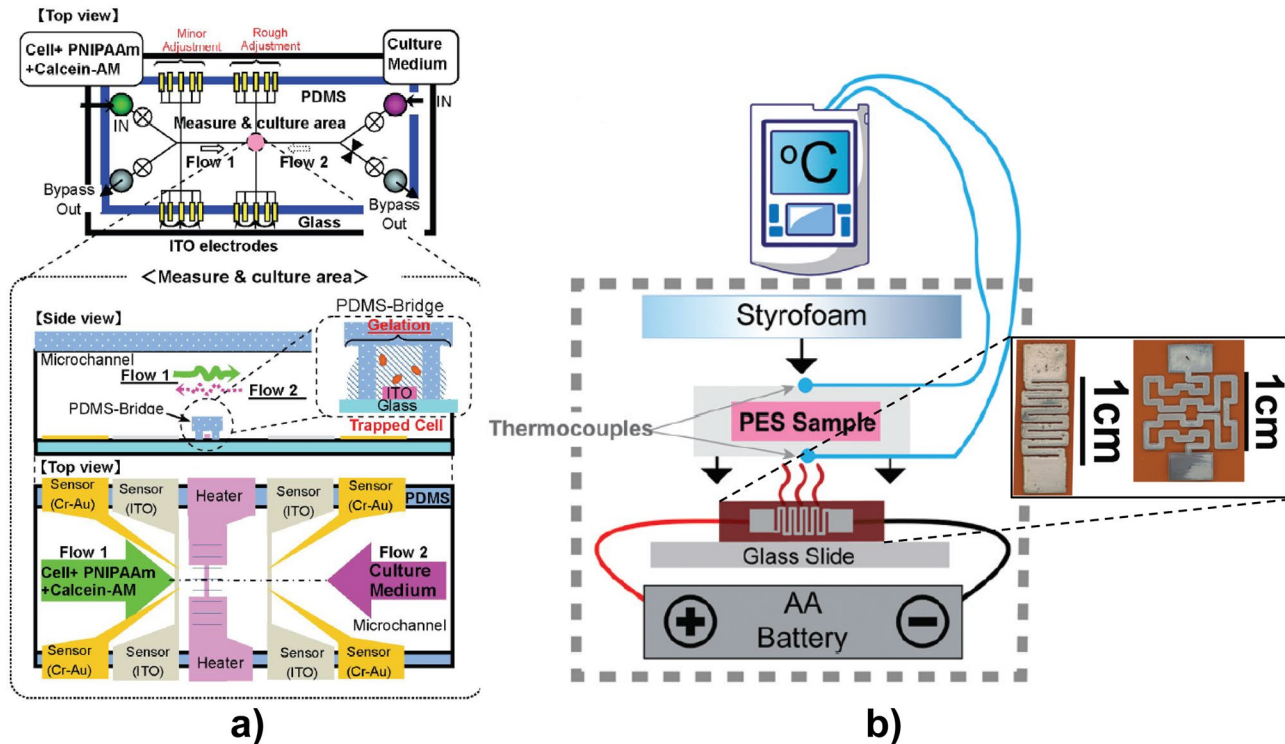


Fig. 19 Microheaters used in cell culturing and incubation. (a) Cell culturing temperature Controlled chip (Yamanishi et al. 2008) Reprinted with permission from IEEE, (b) Battery-powered incubation system with an enlarged view of two heater designs (Byers et al. 2019) Reprinted with permission from RSC

been adapted for faster thermal cycling (Huang et al. 2010). The temperature of the microfluidic chip can be controlled using thermo-sensitive hydrogel (PNIPAAm); however, due to the autofluorescence of the gel, thick hydrogel formation obstructs the observation of cell cultures. Hence, Yamanishi et al. controlled the height of gel by microbridge to make it thin and transparent, as illustrated in Fig. 19a (Yamanishi et al. 2008). Noguchi et al. evaluated the properties of heat localization of a local heating system with an integrated microfluidic channel and microheater for biological and biomedical fields. Thereby concluded, a water-filled microchannel provides effective local heating of 275.3 μJ absorbed heat in 180s heating (Noguchi and Kawai 2013). Subsequently, Tiwari et al. simulated and fabricated a screen-printed silver microheater for biomedical analysis. Screen printing offers high yield with low turnaround time, and it does not require a cleanroom facility or chemical etching process, and it can be fabricated with minimum facilities. The developed microheater can be operated at a maximum of 100 $^{\circ}\text{C}$. Similarly, Byers et al. uniquely designed and developed nanosilver ink printed microheaters via inkjet printing, as shown in Fig. 19b. These heaters are reusable, wettable, bendable, heating without hotspots, retain a stable resistance over 6 months, and can

be submerged in distilled water for 3 days without any physical deterioration (Byers et al. 2019). The physical, electrical, and thermal characteristics of various microheaters used for cell culture with their fabrication methods are recapitulated in Table 4.

be submerged in distilled water for 3 days without any physical deterioration (Byers et al. 2019). The physical, electrical, and thermal characteristics of various microheaters used for cell culture with their fabrication methods are recapitulated in Table 4.

7.2.2 DNA amplification

PCR is extensively employed in molecular biology for *in vitro* target DNA amplification (Bartlett and Stirling 2003). PCR is a non-isothermal amplification process that requires three temperature gradients. Initially, the denaturation step achieved at 94–96 $^{\circ}\text{C}$ results in single-stranded DNA molecule formation. Subsequently, an annealing step was performed at 50–65 $^{\circ}\text{C}$, which begins the DNA formation by attaching the polymerase to a single-strand. Finally, at 72 $^{\circ}\text{C}$, the elongation step engenders the formation of a new DNA strand complementary to the single-strand template in the presence of DNA polymerase (Miralles et al. 2013). The risk of cross-contamination and biohazard in PCR can be reduced by miniaturizing the PCR device into a single-use, self-contained, disposable microchip for

Table 4 Characteristic features of various microheaters used for cell culture

Sl. No	Substrate	Material	Thickness	Fabrication	Design	Application	Max. Temp	Max. Volt	Power Consumption (Response Time)	Temp. Difference	Ref
1	Silicon chip	Polysilicon	-	CMOS technology	-	Cell-culture and incubation microsystem	37 °C	-	-	-	(Christen and Andreou 2007)
2	Glass	ITO	350 nm	Sputtering	Line	Cell Immobilization	32 °C	-	-	-	(Lin et al. 2007)
3	Glass	ITO	300 nm	Sputtering	Line	Cell immobilization and culture system	35 °C	5 V	-	-	(Yamanishi et al. 2008)
4	ITO glass	Silver metal paste	10 µm	Screen printing	Plate	Cell culture	42 °C	-	(~ 60s)	± 0.2 °C	(Lin et al. 2010)
5	Glass	ITO- Heater, Ag-Contact pads	-	Screen printing	Plate	Cell culture system and real-time microscopic observation	37 °C	-	(375s)	± 0.3 °C	(Lin et al. 2011)
6	Glass	Pt	60 nm	Magnetron sputtering and lift-off process	Lines	Cell culture	350 °C	-	3.12 W (120s)	-	(Noguchi and Kawai 2013)
7	Photopaper	nano-silver ink	-	Printing	Double spiral	Biosensing and water quality screening tests	37 °C	12 V	(~ 750s)	± 3 °C	(du Plessis et al. 2017)
8	Polyethylene terephthalate (PET)	Silver-ink	2.75 µm	Screen printing	Meander	Cell culture and PCR applications	94 °C	2.7 V	(few ms)	-	(Tiwari et al. 2018a)
9	Kapton	Nanosilver Ink	1000 nm	Inkjet printing	Meander	LAMP	76.2 °C	1 V	220 mW (~40s) 174 mW (~40s)	-	(Byers et al. 2019)
10	Glass	Al	15 µm	-	Meander with rounded corners	Incubation LOC water monitoring devices	363.88 °C	5 V	-	0.13 °C	(Matvyukiv et al. 2018)

Microheaters for DNA amplification

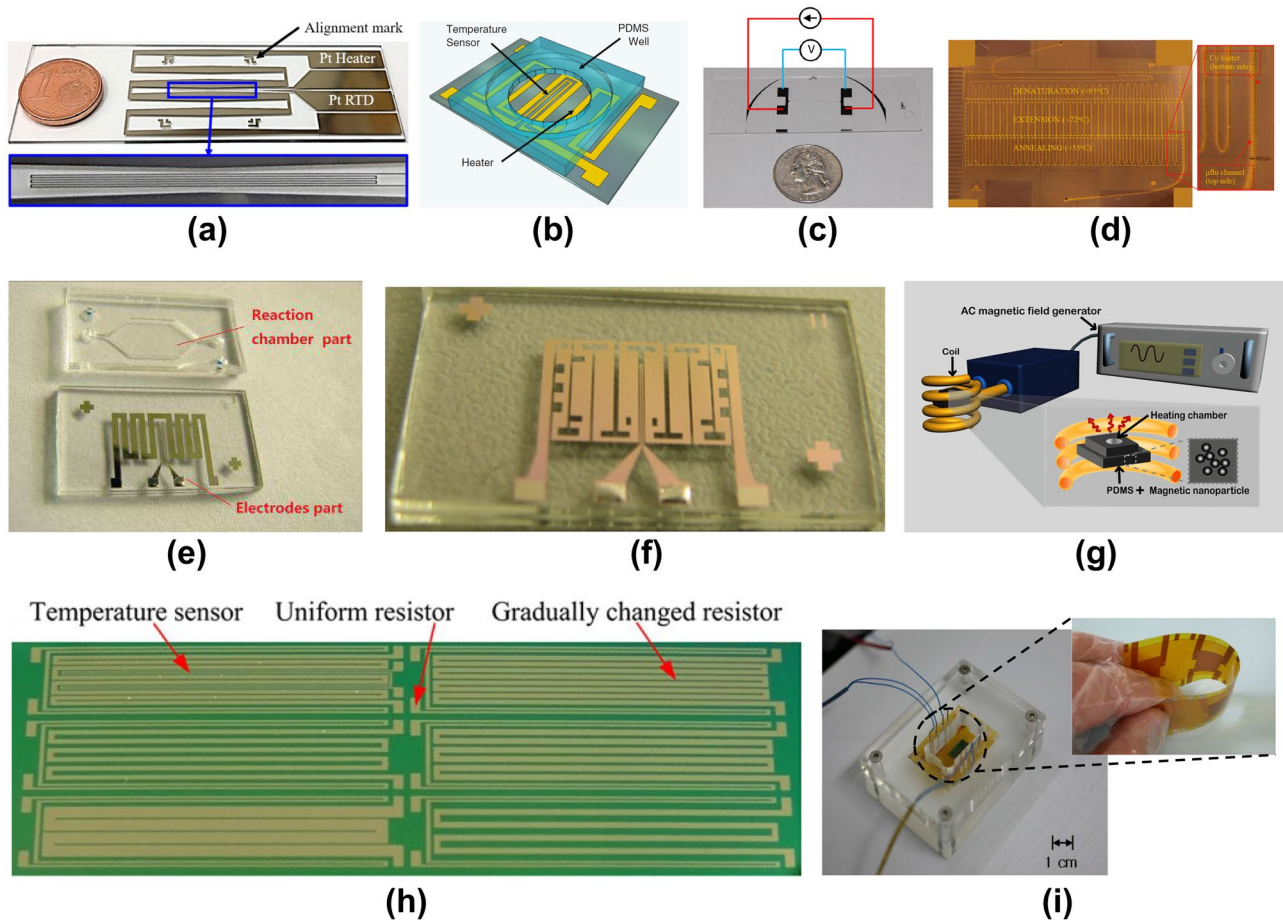


Fig. 20 Microheaters for DNA amplification. **(a)** Fabricated thin film heater/RTD PCR chip (Jeong et al. 2018), **(b)** Microheater and temperature sensor patterned glass slide (Hilton et al. 2012) Pictures reprinted with permission from Springer Nature, **(c)** External electrical circuit employed to drive the Ti microheater device (Javed et al. 2012) Reprinted with permission from AIP, **(d)** Photograph of a fabricated Cu heater in Cu-clad PI substrate (Moschou et al. 2014) Reprinted with permission from Elsevier, **(e)** PCR chip with reusable electrode part (Cao et al. 2015) Reprinted with permission from Trans Tech, **(f)**

Optimized meander electrode with holes (Cui et al. 2016) Reprinted with permission from Springer Nature, **(g)** Illustration of induction heating based on the magnetic nanoparticle-embedded PDMS (MNP-PDMS) chip (Kim et al. 2010) Reprinted with permission from APS, **(h)** Image of thin-film Au resistors (Nie et al. 2014) Reprinted with permission from Springer Nature, **(i)** Flexible PI film with integrated heater and a temperature sensor (Lee et al. 2008) Reprinted with permission from IEEE

infectious disease testing in which the microheater provides temperature stability of ± 2 °C over a time period of 25h (Veltkamp et al. 2020). Later, Liu et al. reduced the cross-contamination by integrating valves, mixer, pump, and microheater array in a microfluidic chip using PDMS and nano/micro-particle-based conducting composite. This is the first developed silver PDMS composite microheater array through the soft lithography technique (Liu et al. 2008). However, the complicated electrical connections may intervene in the testing, which can be circumvented via magnetic nanoparticles that generate heat under an AC magnetic field, as illustrated in Fig. 20g (Kim et al. 2010).

Furthermore, Luo et al. developed a portable PCR system where the temperature controller operated under a neural network for increased efficiency (Ching-Hsing Luo et al. 2005). In a portable, battery-powered microheater, two heat-spreading metal film layers mounted on either side of the heater module engenders uniform temperature distribution. (Lee et al. 2019; Mesforush et al. 2019). The rapid temperature ramping rate of 9–10 °C/s in microheater provides faster PCR amplification in centrifugal microfluidic system, whereas the traditional heater block generates only 1–2 °C/s (Amasia et al. 2012). Additionally, cost and performance were crucial considerations while choosing

substrate materials to fabricate the chip device (Park et al. 2011). Due to the transparency nature of the ITO microheater, cells can be visible, and the risk of metastatic cancer can be predicted; however, it lags the reusability (Jha et al. 2011). The DNA temperature sensitivity and its interactions with surfaces were not much reported. Hence, Javed et al. microfabricated microdevices with integrated microheater as shown in Fig. 20c to enable the detachment of DNA only from the desired locations in a glass-based DNA analysis chip. Thereby engenders new capabilities of detection and separation in DNA analysis (Javed et al. 2012). The development of a bead-based microfluidic system and the integration of microheater with thermal sensors, as depicted in Fig. 20b enhances simpler, more efficient amplification, detection, and rapid control of the thermal cycle (Hilton et al. 2012). Similarly, Lin et al. fabricated a low-cost microheater and a thermo-sensor directly inside the microchannel for accurate temperature sensing and control (Lin et al. 2007).

Moreover, Nie et al. fabricated a gradually changed resistor, as shown in Fig. 20h, to maintain temperature for denaturation, annealing, and extension for DNA amplification, where the heating power was regulated to control the temperature gradient of the microfluidic chip (Nie et al. 2014). Later, Ugsornrat et al. developed an array of three microheaters with thermal sensors and optimized the voltages. Even though it successfully amplified DNA, it comprises complex multiple fabrication steps and lags reusability (Kessararat Ugsornrat et al. 2010). Hence, the microfluidic chip is expensive for PCR. Therefore, Cao et al. designed a PCR chip with reusable separable electrodes part and disposable reaction chamber part, as shown in Fig. 20e, with the view of reducing the fabrication cost with good temperature uniformity and repeatability (Cao et al. 2015). Thereby, optimized the microheater by providing some openings and holes in the heater structure, as depicted in Fig. 20f, to achieve better spatial temperature uniformity. The different resistance distribution engenders non-uniform heat generation, which balances the non-uniform heat conduction to the chamber (Cui et al. 2016). Similarly, Jeong et al. developed a reusable dual Pt microheater, as shown in Fig. 20a. The dual arrangement of the heater on either side of the glass engenders improved thermal uniformity of the PCR chip with lower power consumption than that of the Peltier element (Jeong et al. 2018).

For LOC application, Lee et al. demonstrated a flexible polyimide film-based micro PCR chip, as depicted in Fig. 20i, where the fast heating and cooling were achieved through a high thermal conductivity silicon chamber and reduced thermal mass of polyimide film (Lee et al. 2008). According to the electrical and thermal characterization, the Cu micro resistors fabricated on a polymeric flexible PI substrate can be utilized both as heater and temperature sensors (Mavraki et al. 2011). Later, Moschou et al.

designed, fabricated, and evaluated a low-cost, low-power, and continuous-flow microfluidic device on a Cu-clad PI substrate, as depicted in Fig. 20d. In addition, a homemade temperature-control system was developed to control the integrated heating elements and temperature sensors to enhance the home-based DNA amplification (Moschou et al. 2014). Further, Mirasoli et al. developed a LOC device for loop-mediated isothermal amplification (LAMP) coupled with Bioluminescent Assay in Real-Time (BART) and integrated a resistive thin-film heater and thin-film amorphous silicon diodes which act as temperature and radiation sensors for detecting BL signal (Mirasoli et al. 2018). Since the LAMP is an isothermal amplification technique, it requires a single temperature. Recently, Lee et al. developed a POC biosensor for rapid detection of SARS-CoV-2 RNA. The biosensor was compact, standalone CRISPR Optical Detection of Anisotropy (CODA) device with optoelectronics, an embedded heater, and a microcontroller for data processing. The developed device detects the SARS-CoV-2 RNA within 20 min of sample loading with the detection limit of 3 copy/ μL (Lee et al. 2021). Hence, the microheater implementation will be simple. The critical summary of physical, electrical, and thermal characteristics of several microheaters utilized for DNA amplification and their fabrication approaches are reported in Table 5.

7.2.3 Biochemical research

Low power consumption and large active area are the crucial requirement of high-performance microheater in biosensing/chemical-sensing applications. The sensitivity of biosensors/chemical sensors decreases when using a small active area (Xu et al. 2011). Hence, Yu et al. developed an Au microheater on a low thermal conductivity polyimide thin film, as shown in Fig. 21b, facilitating high-temperature reach with low power consumption and fast response time (Yu et al. 2015). The chemical sample detection at low volume and low concentration is the core functionality of miniaturized bioanalytical devices. For biochemical research, Guan et al. developed a double spiral geometry microheater as depicted in Fig. 21a that can precisely control the temperature below 100 °C and consumes few nano Watts to achieve 60 °C (Guan and Puers 2010). The cross-contamination in parallel elution of specifically bound aptamers can be circumvented by integrating microheater, microfluidic chamber, and pneumatic valves together into a single chip, as shown in Fig. 21c (Lee et al. 2013). In temperature gradient focusing (TGF), an appropriate buffer and temperature differential create a gradient in the microchannel. Thereby, the ionic species either concentrated by balancing the electrophoretic velocity against the bulk flow or separated according to their individual electrophoretic mobilities (Miralles et al. 2013). Later, Horade et al. optimized the design and materials of

Table 5 Characteristic features of various microheaters used for DNA amplification

Sl. No	Substrate	Material	Thickness	Fabrication	Design	Application	Max. Temp	Max. Volt	Power Consumption	Response Time (Heating Rate)	Difference	Ref
1	Polyimide film	Cu	-	Flexible printed circuit (FPC) technology	Meander	PCR	95 °C	12 V	0.096 W	(8 °C/s)	±0.3 °C	(Shen et al. 2005)
2		Pt	-	-	-	PCR	95 °C	9 V	1.18 W	300 μs	-	(Liao et al. 2005)
3	PCB	Ni	28 μm	Nickel sulfate bath	Meander	Microfluidic devices	350 °C	10 V	250 mW	(90 °C/s)	-	(Nicolau et al. 2005)
4	Glass	Pt/Ti	100 nm/12 nm	E-beam evaporation process	-	PCR	94 °C	9 V	1.4 W	0.5s	-	(Ching-Hsing Luo et al. 2005)
5	Polyimide	Sn/Cu-Heater, Ni/Au-Contact pads	100 nm/8 μm, 100 nm/0.5 μm	Sputtering & electroplating	Meander	Genomic DNA Amplification	95 °C	-	< 1 W	320s (6 K/s)	-	(Lee et al. 2008)
6	PDMS	Silver-PDMS composite	72 μm	Soft lithography	Meander	PCR	96 °C	-	-	-	-	(Liu et al. 2008)
7	PDMS	Silver paint	50 μm	Injection molding	Meander with rounded corners	DNA amplification	100 °C	2.05 V	-	~3s (20 °C/s)	-	(Wu et al. 2009)
8	Glass	Ti/Pt	10 nm/60 nm	Sputtering	Inverted U	PCR-CE microfluidic DNA analysis system	95 °C	12 V	-	(14 °C/s)	-	(Zhong et al. 2009)
9	Glass	Cr/Au	30 nm/70 nm	Sputtering	Meander with rounded corners	PCR	91.25 °C	1.08 V	-	-	<0.5 °C	(Kessarat Ugsornrat et al. 2010)
10	PDMS	Superparamagnetic iron oxide (Fe ₃ O ₄)	-	Soft lithography technique	Plate	PCR	95 °C	-	-	10s (4.08 °C/s)	-	(Kim et al. 2010)
11	Silicon	Cr/Pt	20/200 nm	Electron-beam evaporation	Meander	PCR	170 °C	20 V	-	~70s (6 °C/s)	0.4 °C	(Sripumkhai et al. 2010)
12	Pyralux (double-sided Cu-clad polyimide)	Cu	18 μm	photolithography and etching	Meander	DNA amplification	95 °C	-	1320 mW	-	-	(Mavraki et al. 2011)

Table 5 (continued)

Sl. No	Substrate	Material	Thickness	Fabrication	Design	Application	Max. Temp	Max. Volt	Power Consumption	Response Time (Heating Rate)	Difference	Ref
13	Glass	ITO- Heater, Au-Contact pads	-	Thermal evaporator and etching	-	PCR	95 °C	5 V	-	-	-	(Jha et al. 2011)
14	Glass	Cr/Au	20/200 nm	Thermal deposition and etching	Meander	PCR	95 °C	-	-	~1.4s	±0.5 °C	(Hilton et al. 2012)
15	Glass	Ti	200 nm	Metal deposition	Line	DNA analysis	100 °C	12 mA	-	35s	0.01 °C	(Javed et al. 2012)
16	Glass	ITO	-	Photolithography and wet etch process	Meander	PCR	92 °C	18 V	3 W	~250s	-	(Han et al. 2013)
17	Cu-clad PI substrate	Cu	18 µm	Photolithography and Cu wet etching	Meander	PCR	95 °C	-	2.4 W	~2s (12.5 °C/s)	±0.2 °C	(Moschou et al. 2014)
18	PDMS or silicon	EGaIn	90 µm	Liquid metal injection	C shaped	PCR, thermophoresis, and incubation	100 °C	9 V	4 W	~500s	-	(Jinsol and Jungchul 2014)
19	Si ₃ N ₄	Cr/Au	120 nm	Metal deposition and lift off	Meander	PCR	90 °C	-	3.5 W	-	4 °C	(Nie et al. 2014)
20	Glass	Cr/Pt	200 nm	Sputtering and etching	Meander	PCR	95 °C	7 V	-	120s	1.7 °C	(Cao et al. 2015)
21	LiNbO ₃	Au/Cr	100/30 nm	E-beam evaporation and lift-off process	Lines	DNA amplification	95 °C	-	Below 6 W	-	±1 °C	(Ha et al. 2015)
22	Glass	ITO- Heater, Cr/Al/ Cr-Contact pads	1100 nm, 30/150/30 nm	Vacuum evaporation, sputtering, and lift-off	Circular	Isothermal PCR	65 °C	4 V	-	-	2.5 °C	(Petrucci et al. 2015)
23	Borosilicate glass	Cr/Pt	20/200 nm	Magnetron sputtering and ion beam etching	Meander with holes	PCR	100 °C	8.7 V	-	160s	1 °C	(Cui et al. 2016)

Table 5 (continued)

Sl. No	Substrate	Material	Thickness	Fabrication	Design	Application	Max. Temp	Max. Volt	Power Consumption	Response Time (Heating Rate)	Difference	Ref
24		PTC polymer	-	-	Plate	Disposable LoC NAAT	63 °C	3 V	-	5 min	±1.5 °C	(Pardy et al. 2017)
25	Soda-lime glass	Al	16.1 nm	Physical vapor deposition (PVD) and laser ablation	Wing	PCR and cell culture	120 °C	30 V	1.8 W	3s	1 °C	(Nieto et al. 2017)
26	Si	Al	300 nm	Deposition and etching	Meander with rounded corners	DNA amplification	95 °C	-	1.4 W	150s	<0.1 °C	(Barman et al. 2018)
27	Glass	NiCr	200 nm	-	Lines	PCR	98 °C	9 V	113 mW	<200s	1 °C	(Tiwari et al. 2018b)
28	Glass	Cr/Al/Cr	100/600/100 nm	Vacuum evaporation	Double concentric spiral geometry	LAMP	65 °C	2.9 V	-	-	±1 °C	(Mirasoli et al. 2018)
29	Glass	Ti/Pt	30 nm	RF and DC mode sputtering and lift off	Meander	PCR	94 °C	12 V	-	34s	±1.5 °C	(Jeong et al. 2018)
30	Polyimide	Cu	12 µm	FPCB and etching	Meander	PCR	96 °C	-	0.6 W	-	-	(Lee et al. 2019)
31	FR-4 substrate	Cu alloy	18 µm	-	Meander	PCR	94 °C	1.32 V	-	-	1 °C	(Mesforush et al. 2019)
32	Cyclic olefin copolymer (COC)	Au	100 nm	DC magnetron sputtering or e-beam physical vapour deposition	Meander	DNA amplification	106.3 °C	-	129.4 mW	-	±0.3 °C	(Veltkamp et al. 2020)

Microheaters for Biochemical Research

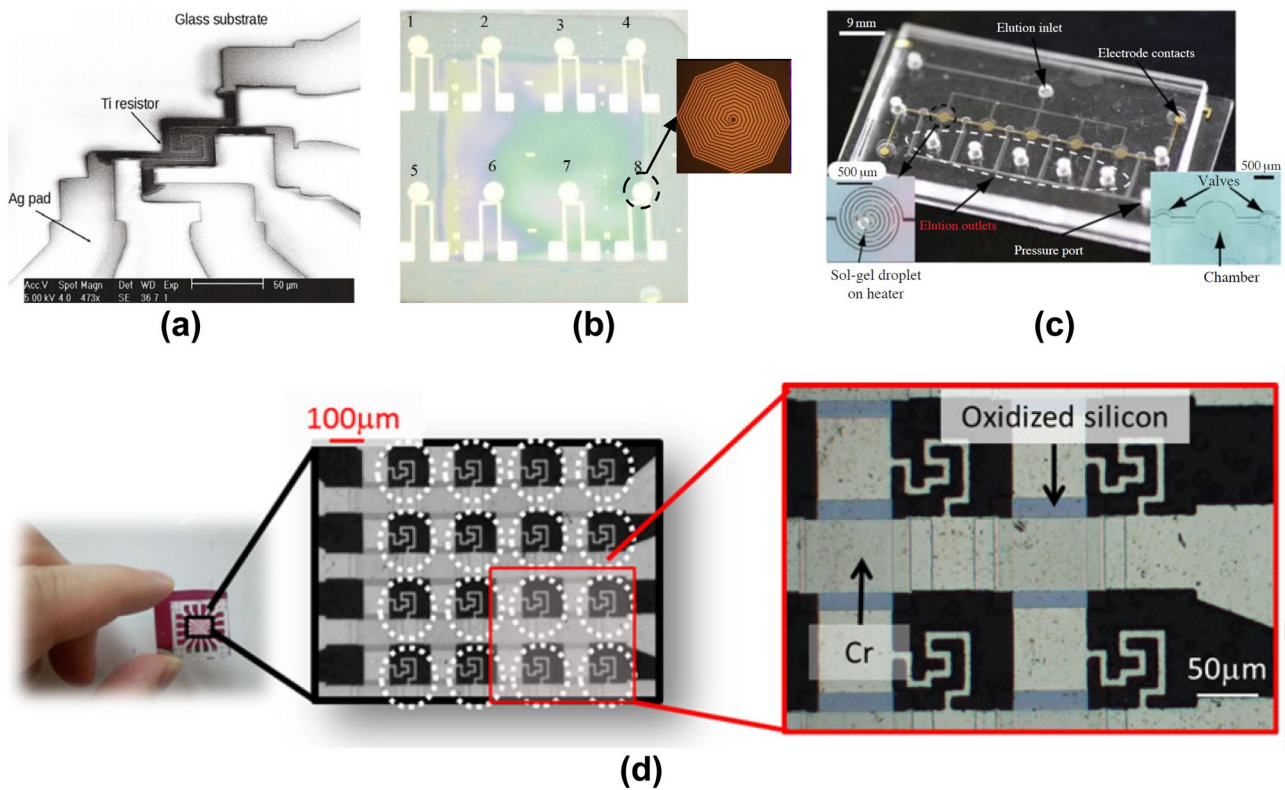


Fig. 21 Microheaters implemented in biochemical research. **(a)** SEM image of the Ag/Ti microheater (Guan and Puers 2010) Reprinted with permission from Elsevier, **(b)** Octogen gold heater on polyimide thin film substrate (Yu et al. 2015) Reprinted with permission from ASME, **(c)** Au/Cr microheater on the glass substrate for cross-

contamination free parallel elution of specifically bound aptamers (Lee et al. 2013) Reprinted with permission from Springer Nature, **(d)** 4-by-4 matrix microheater array device (Horade et al. 2016) Reprinted with permission from CCSE

a microheater array and verified using a thermo-responsive gel. The microheater array, as depicted in Fig. 21d, can be heated with regional selectivity; hence it was capable of generating temperature gradients (Horade et al. 2016). Table 6 summarises the physical, electrical, and thermal properties of several microheaters and their fabrication methods in biochemical research.

7.2.4 Wearable devices

In wearable technologies, the use of liquid metal-based flexible microheaters becomes a hot research frontier. As depicted in Fig. 22a, the liquid metal-based soft and flexible microheater circumvents complicated vapouring, sputtering, or deposition processes and not vulnerable to mechanical deformations, as metal heaters may easily crack or be detached upon mechanical stress. It can also be applied to medical instruments such as heating soles, implantable heating probes, and PCR (Zhang et al. 2020). Later, the scientists prompted a new technology, viable and scalable, to monitor

the air quality to save lives and make people aware through a semiconducting metal oxide wearable gas sensor. The developed sensors were more efficient in monitoring the air and food quality as well as cost-effective in a long-term perspective (Lahlalia et al. 2018). In addition, Kim et al. developed a full-colour display pixel via M13 phage-based temperature-dependent biomimetic colour-generation platform as shown in Fig. 22b for implantable, wearable, and flexible devices. The temperature of the microheater was precisely and reversibly regulated to provide a wide spectrum of RGB colours with low power consumption and possess cycling and chemical stability (Kim et al. 2015). Thermal therapy is the most popular for treating joint injuries via physiotherapies. Conventional heat packs and wraps cause discomfort due to bulkiness. Hence, Choi et al. developed a soft, thin, and stretchable heater for long-term wearable continuous articular thermotherapy by integrating a nanocomposite of silver nanowires with a styrene-butadiene-styrene (SBS), a thermoplastic elastomer. (Choi et al. 2015). Later, Jang et al. integrated microheater with Bluetooth smart devices, as

Table 6 Characteristic features of various microheaters used in biochemical research

Sl. No	Substrate	Material	Thickness	Fabrication	Design	Application	Max. Temp	Max. Volt	Power Consumption (Response Time)	Ref
1	Silica glass	Ti- Heater. Ag- Contact pads	110 nm/190 nm	Sputtering	Double spiral square	Biochemical research	60 °C	5 μ A	210 nW	(Guan and Puers 2010)
2	Polyimide	Cr/Au	10/200 nm	Deposition and lift-off	Octagon	Bio-molecular study	100 °C		18 mW	(Yu et al. 2015)
3	Sapphire	Au	100 nm	E-beam evaporation	Line	Chemical and biological applications	70 °C	2 V	-	(Son et al. 2015)
4	Glass	Cr	100 nm	Sputtering and Cr etching	Hook shaped	Biochemical and sensor applications	32 °C	-	-	(Horade et al. 2016)
5	Alumina	SnO ₂	500 nm	Ultrasonic spray pyrolysis system	Sheet or film or plate	Chemical sensors	350 °C	8 V	-	(Ghahresi and Ansari 2016)
6	Glass	Cr/Au	-	Metal deposition and etching	Double spiral	Multiplex systematic evolution of ligands by exponential enrichment	100 °C	20 V	(30s)	(Lee et al. 2013)

Microheaters for Wearable Systems

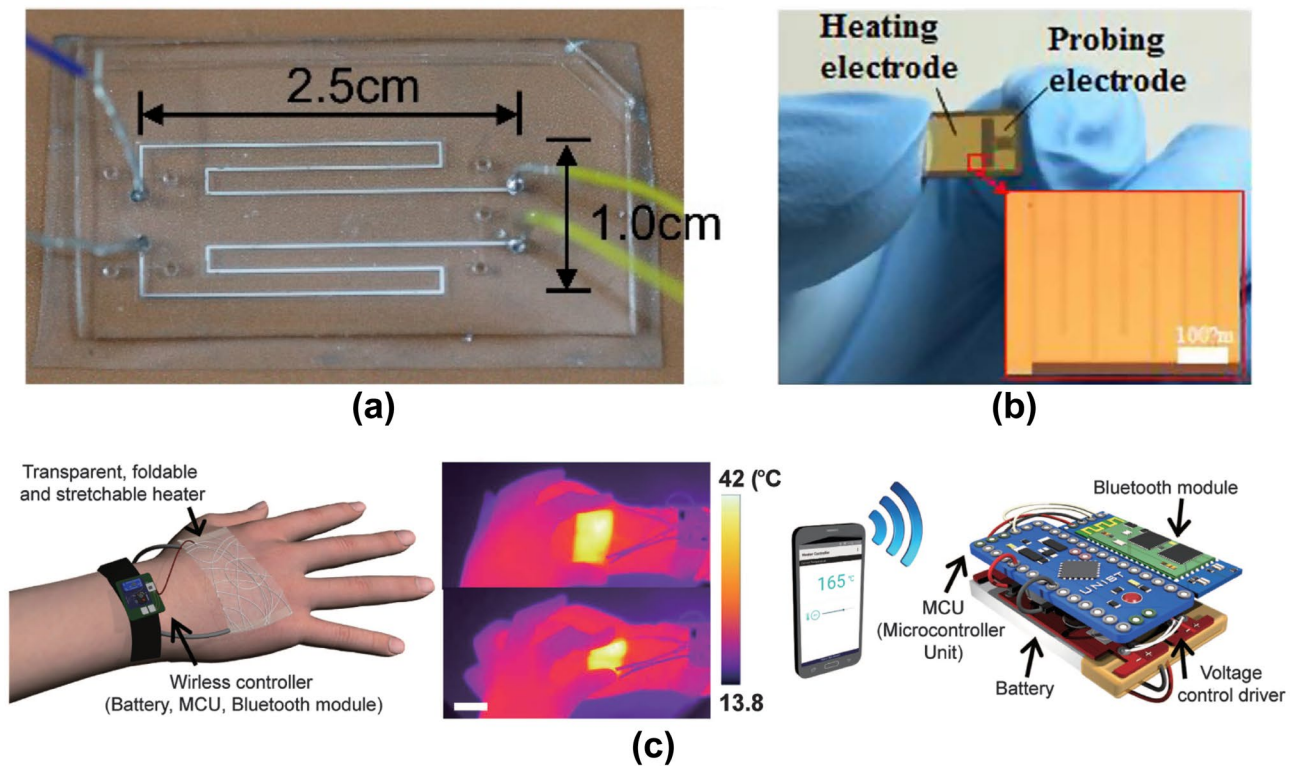


Fig. 22 (a) EGaIn liquid metal-based microheater (Zhang et al. 2020) Reprinted with permission from MDPI, (b) Temperature-controllable microheater chip for colour display devices (Kim et al. 2015), (c)

Bluetooth-integrated temperature-controlled wearable heater (Jang et al. 2017) Pictures reprinted with permission from Springer Nature

illustrated in Fig. 22c, to wirelessly control the temperature of the heating film (Jang et al. 2017). The physical, electrical, and thermal characteristics of several microheaters utilized in wearable systems with their fabrication approaches are tabulated in Table 7.

7.3 Electrical and mechanical applications

Microheater array powder sintering is an alternative to laser sintering and photonic curing due to its fine resolution, lower power consumption, and scalability. Holt et al. replaced the laser beam with the array of microheaters as depicted in Fig. 23a as an energy source to sinter the powder particles. It has the potential to significantly increase the printing speed while reducing the power consumption and can attain the target temperature of 600 °C within milliseconds. The simulated microheater array can effectively transfer the heat over the air gap to sinter the powder particles (Holt et al. 2018). Carbon nanotube microheaters find their application in gas sensors, thermochromic displays, and flexible electronics. Liu et al. were the first to develop a CNT-based microheater array on PET, as shown in Fig. 23b (Liu et al. 2011). To

further shorten the thermal response of the microheater, the substrate thickness and coverage of CNT film on PET were decreased. Moreover, it also worked normally in a curved state. The CNT microheater fabricated using an inkjet printer as depicted in engenders cost-effective large-scale fabrication and can generate above 70 °C with a power consumption of 150mW (Falco et al. 2020). For short-temperature pulse applications in harsh environments, Zhang et al. developed an Au/Ti microheater. The performance was analyzed using FEA-based electrothermal modeling and validate through experimental measurements (Zhang et al. 2007). For phase change switch applications, the heater should be capable of heating above 1000 K and cool back in less than 1 μ s. To meet these requirements, Xu et al. fabricated a thin film tungsten heating element capable of reaching temperatures above 1600 K and a fall time of less than 40 ns (Xu et al. 2016).

Microheater can also be applied as actuators for bending. The high temperature of the resistive heater produces a large mismatch in the thermal expansion of the two structural layers (i.e.) polyimide (PI) film and a PDMS, which engenders the bending effect, as shown in

Table 7 Characteristic features of various microheaters employed in wearable systems

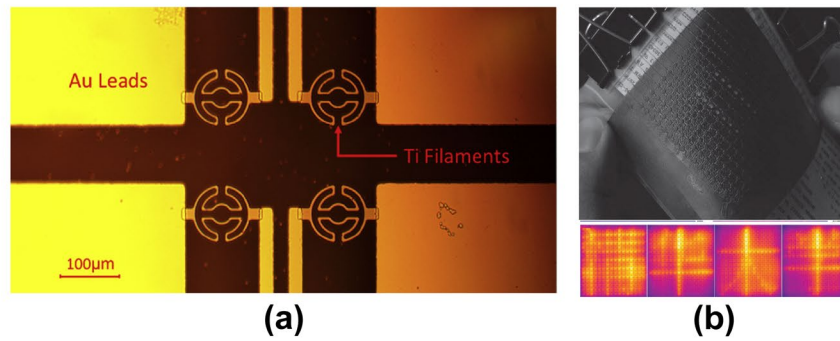
Sl. No	Substrate	Material	Thickness	Fabrication	Design	Application	Max. Temp	Max. Volt	Power Consumption (Response Time)	Ref
1	SiO ₂	Au/Cr	200/10 nm	E-beam evaporation and liftoff	Meander	Implantable, wearable, and flexible devices	~91 °C	5 V	-	(Kim et al. 2015)
2	PDMS	EGaIn	2100 μm	Injection	Meander	Wearable and medical instruments	223.4 °C	2 V	1.89 W (> 30 min)	(Zhang et al. 2020)
3	Si	Pt	180 μm	-	Circle	Wearable gas sensors	300 °C	20 V	7.3 mW (20 ms)	(Lahlalia et al. 2018)
4	SBS	Ag NWs	-	PDMS molding technique	Meander	Wearable Articular Thermotherapy	~40 °C	1 V	(~60s)	(Choi et al. 2015)
5	Polyimide	Ag nanofibers	-	Electrospinning	Network structure	Wireless wearable heaters	250 °C	4.5 V	0.65 W cm ⁻²	(Jang et al. 2017)

Fig. 23c (Cao and Dong 2019). Similarly, during high-pressure loading, thin-film heating elements undergo only tiny plastic deformation; hence, they can be utilized for high-pressure and high-temperature experiments on metals. So, Weir et al. modified diamond anvils with eight thin-film tungsten electrodes and encased them in a diamond film layer, as illustrated in Fig. 23d (Weir et al. 2009). The fabrication and high level of integration of Al/CuO-based nano energetic materials with Au/Pt/Cr thin-film microheater on Pyrex 7740 glass, Kaili et al. developed a nano initiator, as depicted in Fig. 23e, with a 98% ignition success rate (Kaili et al. 2008). Later, Jiang et al. integrated micro-scale solid oxide fuel cells (μ -SOFCs) with temperature testing Pt thermistors module, as depicted in Fig. 23f, to evaluate the thermal balance by providing thermal insulation, controlled heating, temperature control, and gas exchange. Moreover, they examined the heating performance and the crucial issue of the ramping-up phase in the μ -SOFC operation of the thermistor (Jiang et al. 2012). The development of a multilayer thin-film Al/Ti microheater on a Pyrex 7740, as shown in Fig. 23g, for the micro thruster liquid propellant vaporizing and gas heating increases the specific impulse and revealed that the heat loss of the microheater was relatively lower than normal heaters (Li et al. 2017). Solution-based inkjet printing of metal oxide semiconductor necessitates a heat treatment step. Hence, Tran et al. fabricated microheater on the same thermal resistive substrate with the printed precursor pattern, as shown in Fig. 23h, to facilitate the formation of a zinc oxide (ZnO) semiconductor. The increasing input heating power enhances the electrical properties that lead to a better ZnO formation (Tran et al. 2020). The critical summary of physical, electrical, and thermal characteristics and the fabrication approaches of different microheater in the electrical and mechanical fields are reported in Table 8.

8 Discussion

The development of microheaters forgoes conventional bulk heaters, improves portability, reduces cost, and enhances the integration with MEMS devices. Initially, the microheater is widely implemented in the field of gas sensing. Later, microheaters are broadly utilized in mining, biological, chemical, electrical, wearable systems, and even space. However, the evolution of micro and nanoscale device in several sectors made the microheater inevitable. Thermal engineering plays a role in the improvement of current microdevices and the evolution of new systems. A better understanding of heat transfer and temperature manipulation of the microdevices will lead to improved performance. Thermal effects

Microheaters for Electrical Applications



Microheaters for Mechanical Applications

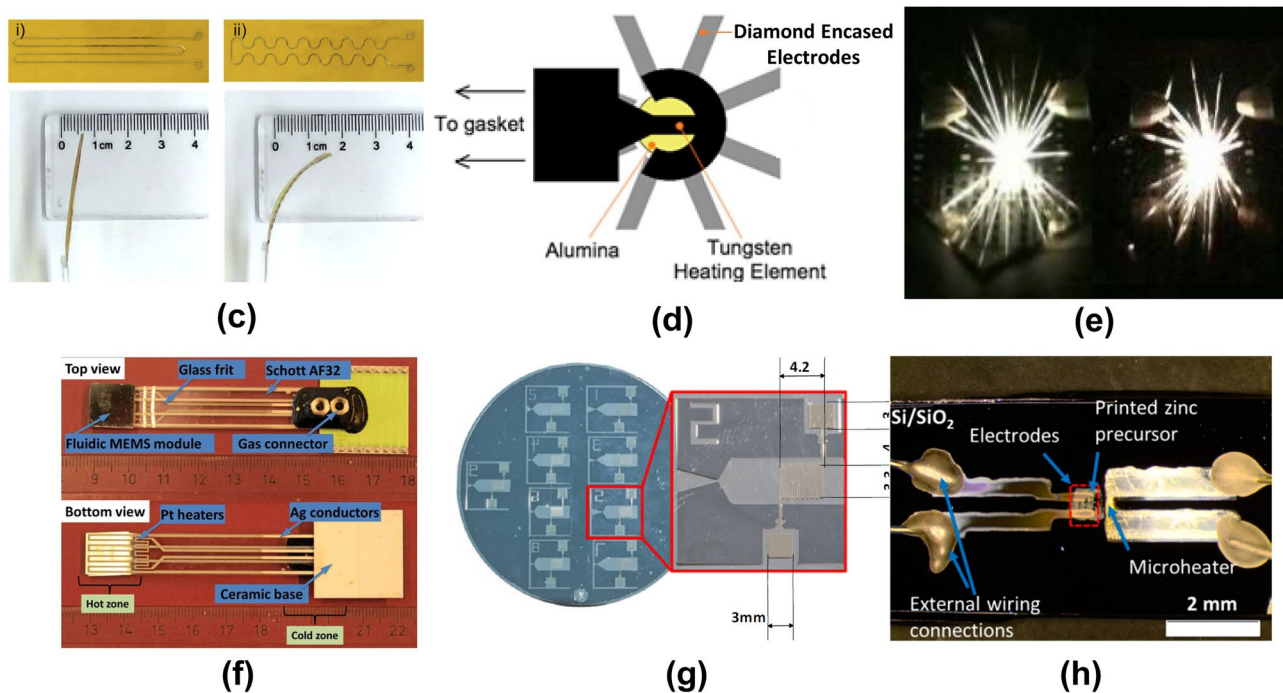


Fig. 23 (a) Microheater array for powder sintering (Holt et al. 2018) Reprinted with permission from Elsevier, (b) Curved CNT-film microheater array on PET for thermochromic displays (Liu et al. 2011) Reprinted with permission from Wiley, (c) Bending performance of actuators with different heater patterns at similar temperature (Cao and Dong 2019) Reprinted with permission from Elsevier, (d) Illustration of a Tungsten microheater designer anvil showing the eight diamond encased electrodes (Weir et al. 2009) Reprinted with permission from AIP, (e) Optic images of combustion flame in the

nano initiator (Kaili et al. 2008) Reprinted with permission from IEEE, (f) Microheater integrated fluid channels for testing micro-solid oxide fuel cell components (Jiang et al. 2012) Reprinted with permission from Elsevier, (g) Al/Ti microheater in the micro thruster (Li et al. 2017) Reprinted with permission from Springer Nature, (h) Printed Joule heating device with electrodes section, printed zinc salt film, and microheater (Tran et al. 2020) Reprinted with permission from MDPI

are crucial in determining the behaviour of the biological microsystems. The growth of miniaturization devices for cell culture and DNA amplification leads to the rapid diagnosis of viruses and improves the POCTs. Moreover, it engenders the access and availability of pathogen detection techniques and equipment in resource-limited clinical settings of underdeveloped and developing countries. The progress and optimization of microdevices play a vital part in shaping

the nature of basic biological research and the medical care industry (Jain and Goodson 2011; Z. E. Jeroish et al. 2020).

During the continuous operation for an extended period, a mismatch of thermal coefficient expansion is the main reason for microheater failure. The continuous operation of Pt-based microheater at 250 °C provided a resistance change of only 1 Ω during a 1-month operation period (Prajesh et al. 2019). In CNT microheaters, the larger number of CNT

Table 8 Characteristic features of various microheaters used in the electrical and mechanical sector

Sl. No	Substrate	Material	Thickness	Fabrication	Design	Application	Max. Temp	Max. Volt	Power Consumption	Response Time (Heating Rate)	Ref
1	Polyimide (PI)	Bi58/Sn42 paste	100 µm	Electrohydrodynamic (EHD) printing	Dual meander with curved edges	Low-voltage soft electrothermal actuator	60 °C	3 V	-	~60s	(Cao and Dong 2019)
2	PET	CNT	-	Screen printing and laser-cutting technology	Lines	Thermochromic displays	50 °C	4.5 V	2.5 W for 16×16 pixel	2s	(Liu et al. 2011)
3	Al ₂ O ₃	Pt	1 µm	Micro-pen and laser sintering	Meander	Microelectronic applications	400 °C	-	3.55 W	<35s	(Cai et al. 2011)
4	Glass	Pt/Ti	400 nm	Sputtering	Meander	Surface-thermometry	80 °C	-	-	17s	(Jung et al. 2011)
5	Quartz crystal	Au	100 nm	Evaporation	Double spiral	Thermal desorption spectroscopy	100 °C	13 V	0.6 W	-	(Sakai et al. 2013)
6	Sapphire	Tungsten	55 nm	DC sputtering and reactive ion etching (RIE)	Line	Calorimetry and phase-change switches	1391 °C	5 V	-	200 ns (1.67×10 ¹⁰ K/s)	(Xu et al. 2016)
7	Glass	Al	45 nm	Thermal evaporation and etching	Dual meander	Low-temperature electronic devices	140 °C	-	1000 mW	6s	(Phatthanakun et al. 2012)
8	Polyimide	Au/Ti	100/10 nm	E-beam deposition and lift off	Octagon	Programmable heating such as impulse and step driving	53.7 °C	-	6.28 mW	50s	(Yu et al. 2017)
9	Glass	Silver nanoparticle paste	-	Screen printing	Meander with rounded corners	Time-of-Flight sensing in microchannels	27 °C	2 V	0.25 W	125s	(Offenzeller et al. 2018)
10	Colourless PI	Silver nanowires (AgNWs)	-	Roll coater	Plate	Defogging or defrosting	118.4 °C	6 V	-	20s (23.9 °C/s)	(Shi et al. 2018)
11	PI	AZO/Ag-SnO _x /AZO	40/10/40 nm	Magnetron sputtering	Plate	Harsh environments and high-temperature conditions	438.8 °C	16 V	-	~2.5s	(Wang et al. 2020b)

Table 8 (continued)

Sl. No	Substrate	Material	Thickness	Fabrication	Design	Application	Max. Temp	Max. Volt	Power Consumption	Response Time (Heating Rate)	Ref
12	Si	Pt	2 μm	-	Meander	Volatile organic compounds sensing	46.05 °C	5 V	10 mW	-	(Sri Surya Srikanth et al. 2019)
13	SiO ₂	Ti/Pt	20/200 nm	DC sputtering method and a lift-off process	Meander	Vaporizer unit	145 °C	-	6 W	95s	(Resnik et al. 2011)
14	Alumina	Tungsten	500 nm	Sputtering	-	Diamond anvil cell experiments	1646.85 °C	1 A	1 W	-	(Weir et al. 2009)
15	Schott's AF 32 eco glass wafer	Pt/Ti	150/10 nm	E-beam evaporation and lift-off process	Dual C	Microheater Array Powder Sintering (MAPS)	400 °C	10 V	0.4 W	~ 1 ms	(Holt et al. 2017)
16	Ultra-thin glass	Ti- Heater, Au- Contact pads	200/200 nm	E-beam evaporation and lift-off process	Dual C	Microheater	600 °C	-	1.2 W	1 ms	(Holt et al. 2018)
17	Pyrex-7740 glass	Au/Ti	77 nm/206 nm	E-beam evaporation	Meander	Microthruster ignition, micro explosive boiling, and microsensor	~275 °C	8 V	-	3s	(Zhang et al. 2007)
18	Pyrex 7740 glass	Au/Pt/Cr	20/120/800 nm	E-beam evaporation	Meander	Nano Initiator	~1000 °C	~22 V	1.16±0.13 W	0.1–0.6 ms	(Kaili et al. 2008)
19	Glass	Pt- Heater, Ag- Contact pads	2.5 ± 0.4/ 40.0 ± 5.0 μm	Screen-printed	Meander	Micro-scale solid oxide fuel cells or hydrogen generation technology	600 °C	22 V	5 W	720s	(Jiang et al. 2012)
20	Glass	Al/Ti	200/80 nm	Magnetron sputtering	Meander with rounded corners	Microthruster liquid propellant vaporizing and gas heating	366 °C	36 V	5.05 W	-	(Li et al. 2017)
21	Si wafer	Silver nanoparticle ink	200 nm	Inkjet printing	-	Additive manufacturing, UV photodetector	267 °C	5 V	5 W	5 min	(Tran et al. 2020)

layers reduces the voltage to attain the transition temperature; however, the resistance after the recovery was increased once it reached the transition temperature. Thus, the voltage consumption is increased. Hence the burn-in procedure was exploited to stabilize the temperature coefficient (Falco et al. 2020). The inkjet-printed nano-silver ink microheaters maintain a stable resistance over 6 months and are reusable, wettable, durable to bending, and heating without hotspots (Byers et al. 2019). But the development of reusable microheater put forth cross-contamination, which leads to false-positive results. Hence, proper decontamination or insulation is crucial while dealing with infectious biological samples. The meander geometry provides uniform temperature distribution all over the chip whereas, the optimized meander pattern with some openings and holes increases the resistance of peripheral meanders, engenders more heat generation in the peripheral region than the central region, thus provides more uniform temperature distribution throughout the heater (Cui et al. 2016). The use of expensive microheaters for low thermal applications is unworthy since low-cost microheaters can even provide sufficient temperature. So, suitable material should be selected for the substrate and heating element. For large scale disposable applications, sputtering or PVD fabrication techniques is time-consuming and increases the workforce. In that case, a screen-printing fabrication procedure is preferred however, the metal inks for all heater materials are not available. Some of the key considerations to be followed while designing and fabricating a microheater are:

- **Lifetime and reusability:** Materials such as SiO₂ should be deposited above the heater to minimize the oxidation of the heating element via encapsulating the entire structure from the environment, which elevates the long-term reliability and reusability of the device (Bai et al. 2019).
- **Uniform heating:** The heater should produce identical heating all over the active area and no hotspots. The design plays a crucial role in managing the thermal distribution by varying the resistance. The high thermal conductive layer above the heater influences better thermal distribution in the gaps of the heater filament.
- **Mechanical stability:** The substrate should be capable of working at ambient temperature and withstand maximum temperature for desired applications. The decrease in stress and displacement will improve the mechanical strength of the microheater. The deformation gradient and thermal expansion of the microheater must also be lower to achieve efficient results. Nevertheless, the microheater material and its structure influence the stability (Sri Surya Srikanth et al. 2019).
- **Response time:** The short response time drastically reduces the time requirement and the power consumption.

Several temperature control systems and algorithms are available to integrate with the microheater.

- **Power consumption:** The optimal design, thickness, substrate, and thermal conductive layer influence better power consumption. The cavity in the insulating substrate can also improve power consumption effectively. In addition, the increase in resistance declines the overall power usage, which enhances battery-operated devices for portability and easy use.

Numerous efforts were made to improve the performance of the microheater in terms of temperature uniformity in the active region, thermal response time, power consumption, and mechanical stability by analyzing the suitable design regarding heater geometry or membrane structuring and/or by microheater element choice (Bhattacharyya 2014). The deposition of an additional layer on the heater should not improve a single parameter (i.e.) lifetime alone; however, it has to enhance at least two or three considerations. For instance, the deposition of SiO₂ boosts long-term reliability, mechanical support, and considerable involvement in thermal distribution and insulation. Microheaters with PDMS substrate consume minimum power to reach the same maximum temperature as Si wafer, but Si wafer provides better thermal uniformity than the PDMS sheet (Jinsol and Jungchul 2014).

The implementation of thermal control systems improves thermal management, sensing, user accessibility, and rapid thermal response. In thermal control algorithms, the on/off as well as the PID controllers have high control accuracy and do not require any adjustments whenever the set-point values were modified. Nevertheless, OLCLS PI quicker response than the PID controller and similar disturbance handling capability as PI. However, the PID algorithm is mostly preferred since it circumvents the ripple formation, decreases the peak overshoot, and introduces damping (Singh et al. 2018; Zainal Alam et al. 2014). The short response time allows the heaters to run at ultra-short pulsing mode, decreasing the average power consumption to the μ W range. The heat conduction of the supporting substrate engenders heat loss and high power consumption. The "suspended beam" construction diminished the thermal contact between the heater and substrate, promoting ultra-low power requirement and fast responding microheater (Zhou et al. 2015). However, the suspended beam adoption degrades the mechanical stability of the microheater chip.

The use of IR camera as a thermal sensor decreases the portability and compactness but still gives accurate temperature on the surface of the chip. However, the insertion of the Pt sensor inside the microfluidic channel provides more promising results. Whereas engenders cross-contamination and requires more attention. The development of a microthermal

sensor integrated microheater or 4-wire microheater extracts the microheater temperature in the active area by analyzing the heating power and electrical resistance. Accurate calibration of the microthermal sensor reduces the inaccuracies and effective sensing of the desired area. In the biological sector, the integration of neural network algorithms and Internet-of-Things (IoT) enhances the tele-access and improves accuracy (Narayanamurthy et al. 2020a). The integration of microheater in LAMP-based nucleic acid amplification test lags mainly due to the inadequate research in the LAMP assay and POCT kits. The research in this field brings a huge change in bedside or POC rapid detection of viral pathogens effectively. The study of thermal engineering and the interaction of thermal effects in the biological sector will improve the BioMEMS applications. This involves the collaborative researchers of doctors, biomedical engineers, thermal engineers, and physicians to imply innovative techniques and methodologies to develop biocompatible microdevices (Jain and Goodson 2011; Narayanamurthy et al. 2020b).

8.1 Role of microheaters in pandemic [COVID-19 (SARS-COV-2)]

The outbreak of a certain infectious disease over a whole country or the world leads to a pandemic situation. The gold standard for the biomolecular research and diagnosis of viral infections is viral culturing. However, it is a time-consuming procedure that can only be carried out in a laboratory with a high biosafety rating that is specially designed to handle biohazardous pathogens. Serological-based lateral flow immunoassays (LFA) detect anti-SARS-CoV-2 antibodies simultaneously for the diagnosis of COVID-19 without the requirement of any thermal cycles (Whitman et al. 2020). Nevertheless, antibody detection suffers from a window period and can be detected even during inactive infections (Narayanamurthy et al. 2021). The LFA is simple to use, inexpensive, and easy to mass-produce, which has a lot of potential for fast in-field detection of SARS-CoV-2 RNA with high sensitivity when combined with microfluidics or nucleic acid isothermal exponential amplification (Reboud et al. 2019). The gold standard for COVID-19 diagnosis is now RT-PCR. Since RT-PCR can detect a single RNA molecule in a single reaction, it is extremely effective and sensitive in detecting viral genomes (Song et al. 2021). For any nucleic acid amplification, the heater is crucial to maintain the required temperature. In laboratories, PCR was performed using desktop-sized thermo-cyclers, thus limiting its function in resource-limited settings. When battling an epidemic, testing must be performed both rapidly and accurately to forbid a positive patient from being discharged prematurely and placing others at risk (Suleman et al. 2021). Thus, the integration of miniaturized heaters is necessary

to develop straightforward and affordable testing kits that engender home-based diagnosis. The advancement of diagnostic kits with single-use microheater has a significant demand in POC devices to enable on-site viral detection and limiting the further spread of infection.

In a LOC, sample preparation, micro-PCR, and detection will all be integrated in a compact portable device for rapid sample-in and result-out. The reaction chamber and the heating/cooling system make up the microreactor in a micro-PCR system. The heating/cooling system comprises a single microheater or microheater array. Similarly, Tang et al. developed a semi-automated, fully disposable, and integrated paper-based biosensor that contains a paper-based valve and a sponge-based reservoir for extracting nucleic acids from crude samples with a portable battery and a heater (Tang et al. 2017). They are very compact and add little thermal mass to the system resulting in a significantly faster heat-cool cycle and enabling rapid results in minutes. The heating ramp times in microheater is shorter than external heaters; however, for device compactness, cooling happens only through natural convection, which results in longer cooling times (Barman et al. 2018). The necessity of different temperatures at different reaction cycles in PCR, making it difficult to develop the POC and home-based diagnostic kits since it requires specific temperature control algorithms (Suleman et al. 2021).

LAMP is another nucleic acid amplification technology that does not involve thermal cycling and can probe multiple targets of COVID-19 RNA in a single reaction which was quicker, easier to use, and more cost-effective than qRT-PCR assays (Notomi et al. 2000). The LAMP assay occurs at a temperature of about 60–65 °C. Li et al. developed a reduced graphene oxide hybridized multi-walled carbon nanotubes nano-circuit electrothermal heater and integrated it with a paper-based analytical device for the detection of SARS-CoV-2 N gene using coloured LAMP reaction. The modules such as the sealing glass, heater, electrode plate, and battery can be reusable to reduce the cost and medical waste. (Li et al. 2021). In terms of sensitivity, precision, and specificity for SARS-CoV-2 detection, several research studies have shown that LAMP outperforms RT-PCR. Additionally, Park et al. reported that the SARS-CoV-2 specific LAMP kit has no cross-reactivity with other respiratory pathogens, including human coronavirus strains HCoV-OC43 and HCoV-229E (Park et al. 2020). This reveals that LAMP based COVID-19 diagnostic kit is effective than PCR due to the integrated microheater with simple electronic systems that makes it economical and handheld. Furthermore, the biosensors with integrated microheater and electronic system are simple and user-friendly, which can detect COVID-19 nucleic acids in patient samples and

enables smartphone interface results. This aid homebased test in identifying the infected individuals and inhibit the widespread of disease.

9 Conclusion and future perspectives

Microheaters find their application in various fields, such as science, engineering, mining, and space. This review summarizes the technological developments in designing and fabricating a microheater for general and specific applications. Though there are multiple technologies available, the study had focused on providing an overview of knowledge and considerations for manufacturing microheaters. Additionally, the importance of selecting suitable heating elements is briefly explained so that future researchers can look up to this article for a glimpse of information. Moreover, we furnished the details about computational modeling and designing in suitable simulation software to arrive at the best heating element design for practical applications. It is witnessed that most of the research and development has been focused on metal microheaters through which significant improvements were made to develop an optimized microheater. This review will be a valuable reference for the researchers who work and needs further knowledge in the field of microheaters. Further, computational modeling should be performed for the analysis of various microheater designs that will be crucial for predicting and enhancing the thermal uniformity for specific applications. Moreover, the development of reusable and low-cost microheaters using inexpensive substrates and heater materials will be considered as future work. In the current situation, there is an immense demand for the development of an integrated microheater with the LAMP-based COVID-19 home-based test kits to enable on-site viral detection and limiting the further spread of infection. Finally, specific research should be implemented to expand the application of paper-based microheaters for disposable low-temperature microdevices to circumvent cross-contamination and biohazard.

Acknowledgements The authors would like to thank the support from University Malaysia Pahang, Universiti Teknikal Malaysia Melaka, Ministry of Higher Education Malaysia, and acknowledge the research grants RDU1803183 and PGRS2003188.

References

2008. Refractive index database. <https://refractiveindex.info/>
2020. Nickel-alloys.net. The Alloys Network. <https://nickel-alloys.net/article/nichrome-nickel-chrome-alloys.html>
- A.A. Abdeslam, K. Fouad, A. Khalifa, Digest. J. Nanomater. Biostruct. **5**, 1 (2020)
- A.P. Mammanna, M.H.M.O. Hamanakab, T.E.A. Santosb, L.P. Cardoso, D. den Engelsena, C.I.Z. Mammanaa, Resistance behavior of thin SnO₂ films at high temperature, (LatinDisplay & IDRC 2012, 2012), pp.
- M.J. Alam, D.C. Cameron, Thin. Solid. Films. **377–378** (2000)
- M. Amasia, M. Cozzens, M.J. Madou, Sens. Actuators. B. Chem. **161**, 1 (2012)
- S.V. Angus, S. Cho, D.K. Harshman, J.Y. Song, J.Y. Yoon, Biosens Bioelectron. **74**, (2015)
- Aperam, 2012. Dilver P1. In: Imphy, A.A. (Ed.), Cold Rolled Strip.
- C. Augello, H. Liu, in Surface Modification of Magnesium and its Alloys for Biomedical Applications, (2015), p. 335–353
- Avigyan Datta Gupta, Chirashree Roy Chaudhuri. Int. J. Sci. Eng. Res. **3**, 6 (2012)
- AZoM, Indium Tin Oxide (ITO) - Properties and Applications. AZO Materials. (2004a)
- AZoM, Silicon Carbide (SiC) Properties and Applications. AZO Materials. (2004b)
- AZoM, Gallium Arsenide (GaAs) Semiconductors. AZO Materials. (2013a)
- AZoM, Tin Dioxide (SnO₂) Semiconductors. AZO Materials. (2013b)
- Y. Bai, J. Tian, Z. Lin, M. You, J. Liu, X. Wang, Microsyst. Technol. **26**, 3 (2019)
- V. Balasubramani, S. Chandraleka, T.S. Rao, R. Sasikumar, M.R. Kuppusamy, T.M. Sridhar, J. Electrochem. Soc. **167**, 3 (2020)
- V. Balasubramani, S. Sureshkumar, T.S. Rao, T.M. Sridhar, ACS Omega **4**, 6 (2019)
- A. Baptista, F. Silva, J. Porteiro, J. Míguez, G. Pinto, Coatings **8**, 11 (2018)
- U. Barman, R.S. Wiederkehr, P. Fiorini, L. Lagae, B. Jones, J. Micro-mech. Microeng. **28**, 8 (2018)
- J.M. Bartlett, D. Stirling, Methods. Mol. Biol. **226** (2003)
- M. Batzill, U. Diebold, Prog. Surf. Sci. **79**, 2–4 (2005)
- P. Becker, P. Scyfried, H. Siebert, Zeitschrift. Für. Physik. b. Condens. Matter. **48**, 1 (1982)
- S. Bedoui, S. Gomri, H. Samet, A. Kachouri, Design and electro-thermal analysis of a platinum micro heater for gas sensors, (2016 13th International Multi-Conference on Systems, Signals & Devices (SSD), IEEE, 2016), pp. 558–561
- P. Bhattacharyya, IEEE Trans. Device Mater. Reliab. **14**, 2 (2014)
- A. Botau, D. Bonfert, C. Negrea, P. Svasta, C. Ionescu, Electro-thermal analysis of flexible micro-heater, (2015 38th International Spring Seminar on Electronics Technology (ISSE), IEEE, 2015), pp. 358–363
- K.M. Byers, L.K. Lin, T.J. Moehling, L. Stanciu, J.C. Linnes, Analyst. **145**, 1 (2019)
- Z.X. Cai, X.Y. Zeng, J. Duan, Thin Solid Films **519**, 11 (2011)
- J.T. Cao, F. Cui, W. Chen, Z.X. Guo, W.Y. Chen, X.S. Wu, W. Liu, W.P. Zhang, Appl. Mech. Mater. **742** (2015)
- Y. Cao, J. Dong, Sens. Actuators. A. Phys. **297** (2019)
- W.-Y. Chang, Y.-S. Hsihe, Microelectron. Eng. **149** (2016)
- M. Chen, R.C. Haddon, R. Yan, E. Bekyarova, Mater. Horiz. **4**, 6 (2017)
- C.-H. Luo, T.-M. Hsieh, C.-S. Liao, G.-B. Lee, F.-C. Huang, J. Med. Biol. Eng. **26**, 1 (2005)
- S. Choi, J. Park, W. Hyun, J. Kim, J. Kim, Y.B. Lee, C. Song, H.J. Hwang, J.H. Kim, T. Hyeon, D.H. Kim, ACS Nano **9**, 6 (2015)
- C.H. Chon, D. Li, in Encyclopedia of Microfluidics and Nanofluidics, (2014), p. 1–6
- J.B. Christen, A.G. Andreou, IEEE. Trans. Biomed. Circuits. Syst. **1**, 1 (2007)
- G.-S. Chung, J.-M. Jeong, Microelectron. Eng. **87**, 11 (2010)
- P.G. Collins, P. Avouris, Sci. Am. **283**, 6 (2000)
- F. Cui, W. Chen, X. Wu, Z. Guo, W. Liu, W. Zhang, W. Chen, Microsyst. Technol. **23**, 8 (2016)
- M. Dai, W. Guo, X. Liu, M. Zhang, Y. Wang, L.F. Wei, G.C. Hilton, J. Hubmayr, J. Ullom, J. Gao, M.R. Vissers, J. Low. Temp. Phys. **194**, 5–6 (2018)

- Z. Dai, L. Xu, G. Duan, T. Li, H. Zhang, Y. Li, Y. Wang, Y. Wang, W. Cai, *Sci. Rep.* **3** (2013)
- K. Das, P. Kakoty, in *Advances in Communication and Computing*, (2015), p. 221–229
- A.J. de Mello, M. Habgood, N.L. Lancaster, T. Welton, R.C. Wootton, *Lab. Chip.* **4**, 5 (2004)
- E. Deligoz, K. Colakoglu, Y.O. Ciftci, *J. Phys. Chem. Solids.* **69**, 4 (2008)
- J. Deng, L. Zhang, L. Hui, X. Jin, B. Ma, *Sensors (basel)*. **20**, 5 (2020)
- P.B. Deo, *J. Technol. Adv. Sci. Res.* **2**, 1 (2016)
- M.D. Dickey, R.C. Chiechi, R.J. Larsen, E.A. Weiss, D.A. Weitz, G.M. Whitesides, *Adv. Funct. Mater.* **18**, 7 (2008)
- L.A. Dobrzański, D. Pakuła, *J. Mater. Process. Technol.* **164–165** (2005)
- M. du Plessis, E. Clasen, K. Land, T.-H. Joubert, *Micro-incubator for bacterial biosensing applications*, (Fourth Conference on Sensors, MEMS, and Electro-Optic Systems, 2017), pp.
- A. Elements, 2020. Iron Nickel Cobalt Alloy.
- J. Engel, J. Chen, C. Liu, J. Micromech. Microeng. **13**, 3 (2003)
- A. Falco, F.J. Romero, F.C. Loghin, A. Lyuleeva, M. Becherer, P. Lugli, D.P. Morales, N. Rodriguez, J.F. Salmeron, A. Rivadeneyra, *Nanomaterials (basel)*. **10**, 9 (2020)
- B. Fasolt, M. Hodgins, G. Rizzello, S. Seelecke, *Sens. Actuators. A. Phys.* **265** (2017)
- M. Fox, in *Oxford Master Series in Physics*, (Oxford University Press, 2010), p. 283
- M. Gassner, M. Rebelo de Figueiredo, N. Schalk, R. Franz, C. Weiß, H. Rudigier, H. Holzschuh, W. Bürgin, M. Pohler, C. Czettel, C. Mitterer, *Surf. Coat. Technol.* **299** (2016)
- M. Gayake, D. Bodas, S. Gangal, *Simulations of Polymer based Micro-heater Operated at Low Voltage*, (2011 COMSOL Conference, 2011), pp.
- M. Gharezi, M. Ansari, *IOP Conf. Ser. Mater. Sci. Eng.* **108** (2016)
- D. Giancoli, *In Physics for Scientists and Engineers with Modern Physics* (Prentice Hall, Upper Saddle River, New Jersey, 2009), p. 658
- D.J. Griffiths, *In Electrodynamics* (Prentice Hall, Upper Saddle River, New Jersey, 1999), p. 286
- T. Guan, R. Puers, *Proc. Eng.* **5** (2010)
- R.M. Guijt, A. Dodge, G.W. van Dedem, N.F. de Rooij, E. Verpoorte, *Lab Chip.* **3**, 1 (2003)
- B.H. Ha, K.S. Lee, G. Destgeer, J. Park, J.S. Choung, J.H. Jung, J.H. Shin, H.J. Sung, *Sci. Rep.* **5** (2015)
- D. Han, Y.-C. Jang, S.-N. Oh, R. Chand, K.-T. Lim, K.-I. Kim, Y.-S. Kim, *Microsyst. Technol.* **20**, 3 (2013)
- H. Han, D. Adams, J.W. Mayer, T.L. Alford, *J. Appl. Phys.* **98**, 8 (2005)
- J.-W. Han, M. Meyyappan, *IEEE. Sens. J.* **16**, 14 (2016)
- A. Harley-Trochimczyk, A. Rao, H. Long, A. Zettl, C. Carraro, R. Maboudian, *J. Micromech. Microeng.* **27**, 4 (2017)
- M.N. Hasan, D. Acharjee, D. Kumar, A. Kumar, S. Maity, *Proc. Comput. Sci.* **92** (2016)
- H.M. Hegab, A. Elmekawy, T. Stakenborg, *Biomicrofluidics* **7**, 2 (2013)
- J.P. Hilton, T. Nguyen, M. Barbu, R. Pei, M. Stojanovic, Q. Lin, *Microfluidics. Nanofluidics.* **13**, 5 (2012)
- N. Holt, L.G. Marques, A. Van Horn, M. Montazeri, W. Zhou, *Int. J. Adv. Manuf. Technol.* **95**, 1–4 (2017)
- N. Holt, A. Van Horn, M. Montazeri, W. Zhou, *J. Manuf. Process.* **31** (2018)
- J. Hone, M.C. Llaguno, M.J. Biercuk, A.T. Johnson, B. Batlogg, Z. Benes, J.E. Fischer, *Appl. Phys. a. Mater. Sci. Process.* **74**, 3 (2002)
- M. Horade, M. Kojima, K. Kamiyama, Y. Mae, T. Arai, *Mech. Eng. Res.* **6**, 1 (2016)
- C.-T. Hsieh, J.-M. Wei, H.-T. Hsiao, W.-Y. Chen, *Electrochim. Acta.* **64** (2012)
- M. Huang, S. Fan, W. Xing, C. Liu, *Math. Comput. Model.* **52**, 11–12 (2010)
- S.-W. Huang, C.-C. Yeh, Y.-J. Yang, *Sens. Actuators. A. Phys.* **315** (2020)
- I.-S. Hwang, E.-B. Lee, S.-J. Kim, J.-K. Choi, J.-H. Cha, H.-J. Lee, B.-K. Ju, J.-H. Lee, *Sens. Actuators. b. Chem.* **154**, 2 (2011a)
- J.-S. Hwang, S.-Y. Kim, Y.-S. Kim, H.-J. Song, C.-Y. Park, J.-D. Kim, *Int. J. Control. Autom.* **8**, 2 (2015)
- W.J. Hwang, K.S. Shin, J.H. Roh, D.S. Lee, S.H. Choa, *Sensors (basel)*. **11**, 3 (2011b)
- Y. Igasaki, H. Mitsushashi, K. Azuma, T. Muto, *Jpn. J. Appl. Phys.* **17**, 1 (1978)
- S. Jae-Cheol, C. Gwiy-Sang, *Fabrication and characteristics of Pt/ZnO NO sensor integrated SiC micro heater*, (2010 IEEE Sensors, 2010), pp. 350–353
- A. Jain, K.E. Goodson, *J. Therm. Biol.* **36**, 4 (2011)
- J. Jang, B.G. Hyun, S. Ji, E. Cho, B.W. An, W.H. Cheong, J.-U. Park, *NPG. Asia. Mater.* **9**, 9 (2017)
- A. Javed, S.M. Iqbal, A. Jain, *Appl. Phys. Lett.* **101**, 9 (2012)
- S. Jeong, J. Lim, M.Y. Kim, J. Yeom, H. Cho, H. Lee, Y.B. Shin, J.H. Lee, *Biomed. Microdevices.* **20**, 1 (2018)
- Z.E. Jeroish, K.S. Bhuvaneshwari, V. Narayanamurthy, R. Premkumar, F. Samsuri, *J. Eng. Sci. Technol.* **15**, 3 (2020)
- S.K. Jha, G.-S. Joo, G.-S. Ra, H.H. Lee, Y.-S. Kim, *IEEE. Sens. J.* **11**, 9 (2011)
- B. Jiang, P. Muralt, P. Heeb, A.J. Santis-Alvarez, M. Nabavi, D. Poulikakos, P. Niedermann, T. Maeder, *Sens. Actuators. B. Chem.* **175** (2012)
- J. Jinsol, L. Jungchul, *J. Microelectromech. Syst.* **23**, 5 (2014)
- J.P. Joule, London. Edinburgh. Dublin. Philos. Mag. J. Sci. **19**, 124 (1841)
- S. Joy, J.K. Antony, *Design and Simulation of a Micro Hotplate Using COMSOL Multiphysics for MEMS Based Gas Sensor*, (2015 Fifth International Conference on Advances in Computing and Communications (ICACC), 2015), pp. 465–468
- W. Jung, Y.W. Kim, D. Yim, J.Y. Yoo, *Sens. Actuators. a. Phys.* **171**, 2 (2011)
- Z. Kaili, C. Rossi, M. Petrantoni, N. Mauran, *J. Microelectromech. Syst.* **17**, 4 (2008)
- K. Kakaei, M.D. Esrafil, A. Ehsani, in *Graphene Surfaces - Particles and Catalysts*, (2019), p. 253–301
- A.I. Kalachev, D.N. Nikogosyan, G. Brambilla, *J. Light. Technol.* **23**, 8 (2005)
- J.-G. Kang, J.-S. Park, K.-B. Park, J. Shin, E.-A. Lee, S. Noh, H.-J. Lee, *Micro. Nano. Syst. Lett.* **5**, 1 (2017)
- K.S.C. Karnati, S.R. Nagireddy, R.B. Mishra, A.M. Hussain, *Design of Micro-heaters Inspired by Space Filling Fractal Curves*, (2019 IEEE Region 10 Symposium (TENSYP), 2019), pp. 231–236
- S. Kaushal, B.K. Das, *Appl. Opt.* **55**, 11 (2016)
- Kenneth Holmberg, Allan Matthews, 2 edn. (Elsevier, Netherland, 2009), pp. 576
- K. Ugsornrat, N.V. Afzulpurkar, A. Wisitsoraat, A. Tuantranont, *Sens. Mater.* **22**, 6 (2010)
- V.K. Khanna, M. Prasad, V.K. Dwivedi, C. Shekhar, A.C. Pankaj, J. Basu, *Indian. J. Pure. Appl. Phys.* **45** (2007)
- J.A. Kim, S.H. Lee, H. Park, J.H. Kim, T.H. Park, *Nanotechnology* **21**, 16 (2010)
- W.G. Kim, K. Kim, S.H. Ha, H. Song, H.W. Yu, C. Kim, J.M. Kim, J.W. Oh, *Sci Rep.* **5**, (2015)
- Kiyotaka Wasa, Makoto Kitabatake, Hideaki Adachi, (William Andrew, Netherland, 2004), pp.
- A. Lahlalia, L. Filipovic, S. Selberherr, *IEEE. Sens. J.* **18**, 5 (2018)

- C.D. Landon, R.H.T. Wilke, M.T. Brumbach, G.L. Brennecke, M. Blea-Kirby, J.F. Ihlefeld, M.J. Marinella, T.E. Beechem, *Appl. Phys. Lett.* **107**, 2 (2015)
- C.Y. Lee, I. Degani, J. Cheong, J.H. Lee, H.J. Choi, J. Cheon, H. Lee, *Biosens. Bioelectron.* **178** (2021)
- D.-S. Lee, O.R. Choi, Y. Seo, *Micro. Nano. Syst. Lett.* **7**, 1 (2019)
- D.-S. Lee, S.H. Park, K.H. Chung, H.-B. Pyo, *IEEE. Sens. J.* **8**, 5 (2008)
- S. Lee, J. Kang, S. Ren, T. Laurell, S. Kim, O.C. Jeong, *BioChip. J.* **7**, 1 (2013)
- M.S. Lekshmi, R. Pamula, A. Kartik, K.J. Suja, Performance analysis of micro hotplate based metal oxide nanowire gas sensor, (2018 7th International Symposium on Next Generation Electronics (ISNE), IEEE, 2018), pp. 1–4
- S. Li, S. Huang, Y. Ke, H. Chen, J. Dang, C. Huang, W. Liu, D. Cui, J. Wang, X. Zhi, X. Ding, *Adv. Funct. Mater.* (2021)
- Li T., Xu L., W. Y., (Springer, Singapore, 2018), pp. 717–752
- X. Li, Y. Huang, X. Chen, X. Xu, D. Xiao, *Microsyst. Technol.* **24**, 5 (2017)
- C.S. Liao, G.B. Lee, H.S. Liu, T.M. Hsieh, C.H. Luo, *Nucleic. Acids. Res.* **33**, 18 (2005)
- J.L. Lin, M.H. Wu, C.Y. Kuo, K.D. Lee, Y.L. Shen, *Biomed. Microdevices.* **12**, 3 (2010)
- L. Lin Jr., S.S. Wang, M.H. Wu, C.C. Oh-Yang, *Sensors (basel).* **11**, 9 (2011)
- Y.-C. Lin, Y. Yamanishi, F. Arai, On-chip Temperature Sensing and Control for Cell Immobilization, (2007 2nd IEEE International Conference on Nano/Micro Engineered and Molecular Systems, 2007), pp. 659–663
- G. Liu, D.A. Lowy, A. Kahrim, C. Wang, Z. Dilli, N. Kratzmeier, W. Zhao, M. Peckerar, *Microelectron. Eng.* **129** (2014)
- G. Liu, Q. Sheng, D. Dam, J. Hua, W. Hou, M. Han, *Opt. Lett.* **42**, 7 (2017)
- L. Liu, W. Cao, J. Wu, W. Wen, D.C. Chang, P. Sheng, *Biomicrofluidics* **2**, 3 (2008)
- L. Liu, S. Peng, X. Niu, W. Wen, *Appl. Phys. Lett.* **89**, 22 (2006)
- P. Liu, L. Liu, K. Jiang, S. Fan, *Small* **7**, 6 (2011)
- S. Liu, J. Wang, J. Zeng, J. Ou, Z. Li, X. Liu, S. Yang, *J. Power Sources* **195**, 15 (2010)
- H. Long, A. Harley-Trochimczyk, T. He, T. Pham, Z. Tang, T. Shi, A. Zettl, W. Mickelson, C. Carraro, R. Maboudian, *ACS. Sens.* **1**, 4 (2016)
- N. Lovecchio, G. Petrucci, D. Caputo, S. Alameddine, M. Carpentiero, L. Martini, E. Parisi, G. de Cesare, A. Nascetti, Thermal control system based on thin film heaters and amorphous silicon diodes, (2015 6th International Workshop on Advances in Sensors and Interfaces (IWASI), 2015), pp. 277–282
- Marian K. Kazimierzczuk, in *Pulse-Width Modulated DC–DC Power Converters*, (John Wiley & Sons, Ltd, 2016), p.
- D.M. Mattox, 2 edn. (Elsevier, Netherland, 2010), pp. 792
- R.A. Matula, *J. Phys. Chem. Ref. Data.* **8**, 4 (1979)
- O. Matviyukiv, T. Klymkovych, N. Bokla, Modeling and analysis of integrated precise joule micro-heater for lab-chip diagnostic devices, (2018 XIV-th International Conference on Perspective Technologies and Methods in MEMS Design (MEMSTECH), 2018), pp. 155–160
- E. Mavraki, D. Moschou, G. Kokkoris, N. Vourdas, S. Chatzandroulis, A. Tserepi, *Proc. Eng.* **25** (2011)
- M. Megayanti, C. Panatarani, I.M. Joni, Development of microheaters for gas sensor with an AT-Mega 8535 temperature controller using a PWM (pulse width modulation) method, (2016), pp.
- S. Mesforush, A. Jahanshahi, M.K. Zadeh, Finite element simulation of isothermal regions in serpentine shaped PCB electrodes of a micro-PCR device, (2019 27th Iranian Conference on Electrical Engineering (ICEE), IEEE, 2019), pp. 280–284
- V. Miralles, A. Huerre, F. Malloggi, M.C. Jullien, *Diagnostics (basel).* **3**, 1 (2013)
- M. Mirasoli, F. Bonvicini, N. Lovecchio, G. Petrucci, M. Zangheri, D. Calabria, F. Costantini, A. Roda, G. Gallinella, D. Caputo, G. de Cesare, A. Nascetti, *Sens. Actuators. B. Chem.* **262** (2018)
- S.E. Moon, H.K. Lee, N.J. Choi, J. Lee, C.A. Choi, W.S. Yang, J. Kim, J.J. Jong, D.J. Yoo, *Sens. Actuators. B. Chem.* **187** (2013)
- C.E. Morosanu, (Elsevier, New York, Tokyo, 1990), pp.
- D. Moschou, N. Vourdas, G. Kokkoris, G. Papadakis, J. Parthenios, S. Chatzandroulis, A. Tserepi, *Sens. Actuators. B. Chem.* **199** (2014)
- V. Narayanamurthy, K.S. Bhuvaneshwari, Z.E. Jeroish, F. Samsuri, *J. Phys. Conf. Series.* **1502** (2020)
- V. Narayanamurthy, Z.E. Jeroish, K.S. Bhuvaneshwari, P. Bayat, R. Premkumar, F. Samsuri, M.M. Yusoff, *RSC. Adv.* **10**, 20 (2020)
- V. Narayanamurthy, Z.E. Jeroish, K.S. Bhuvaneshwari, F. Samsuri, *Anal. Methods.* **13**, 6 (2021)
- D.V. Nicolau, Y. Zhu, A. Bui, H. Jin, S. Nahavandi, E.C. Harvey, I.D. Sutalo, Thermal modeling of a microheater in a microchannel chip, (BioMEMS and Nanotechnology II, 2005), pp.
- J. Nie, Y. Zhao, N. Peng, *Microsyst. Technol.* **21**, 1 (2014)
- D. Nieto, P. McGlynn, M. de la Fuente, R. Lopez-Lopez, M. O'Connor G, *Colloids. Surf. B. Biointerfaces.* **154** (2017)
- Y. Noguchi, A. Kawai, *J. Photopolym. Sci. Technol.* **26**, 6 (2013)
- T. Notomi, H. Okayama, H. Masubuchi, T. Yonekawa, K. Watanabe, N. Amino, T. Hase, *Nucleic. Acids. Res.* **28**, 12 (2000)
- R. Nowak, M. Pessa, M. Saganuma, M. Leszczynski, I. Grzegory, S. Porowski, F. Yoshida, *Appl. Phys. Lett.* **75**, 14 (1999)
- C. Offenzeller, M. Knoll, T. Voglhuber-Brunnmaier, M.A. Hintermuller, B. Jakoby, W. Hilber, *IEEE. Sen. J.* **18**, 21 (2018)
- T. Pardy, I. Tulp, C. Kremer, T. Rang, R. Stewart, *PLoS ONE* **12**, 12 (2017)
- G.S. Park, K. Ku, S.H. Baek, S.J. Kim, S.I. Kim, B.T. Kim, J.S. Maeng, *J. Mol. Diagn.* **22**, 6 (2020)
- S. Park, Y. Zhang, S. Lin, T.H. Wang, S. Yang, *Biotechnol. Adv.* **29**, 6 (2011)
- B. Peng, M. Locascio, P. Zapol, S. Li, S.L. Mielke, G.C. Schatz, H.D. Espinosa, *Nat. Nanotechnol.* **3**, 10 (2008)
- R.S. Pessoa, M.A. Fraga, L.V. Santos, N.K.A.M. Galvão, H.S. Maciel, M. Massi, in *Anti-Abrasive Nanocoatings*, (2015), p. 455–479
- G. Petrucci, D. Caputo, A. Nascetti, N. Lovecchio, E. Parisi, S. Alameddine, G. de Cesare, A. Zahra, Thermal characterization of thin film heater for lab-on-chip application, (2015 XVIII AISEM Annual Conference, IEEE, 2015), pp. 1–4
- J. Pflüger, J. Fink, W. Weber, K.P. Bohnen, G. Crecelius, *Phys. Rev. B.* **30**, 3 (1984)
- R. Phatthanakun, P. Deekla, W. Pummara, C. Sriphung, C. Pantong, N. Chomnawang, Design and fabrication of thin-film aluminum microheater and nickel temperature sensor, (2012 7th IEEE International Conference on Nano/Micro Engineered and Molecular Systems (NEMS), IEEE, 2012), pp. 112–115
- R. Prajesh, V. Goyal, V. Saini, J. Bhargava, A. Sharma, A. Agarwal, *Microsyst Technol.* **25**, 9 (2019)
- S. Rahemi Ardekani, A. Sabour Rouh Aghdam, M. Nazari, A. Bayat, E. Yazdani, E. Saievar-Iranizad, *J. Anal. Appl. Pyrolysis.* **141** (2019)
- Rajput G.Y., Gofane M.S., Dhobale S, (Springer, Singapore, 2018), pp.
- J. Ramousse, O. Lottin, S. Didierjean, D. Maillet, *J. Power. Sources.* **192**, 2 (2009)
- K. Rapolu, S. Dugan, M. Manelis, J. Weldon, R. Wessel, Kapton RS Flexible Heaters – Design and Applications, (2018 17th IEEE Intersociety Conference on Thermal and Thermomechanical Phenomena in Electronic Systems (ITherm), IEEE, 2018), pp. 19–25
- J. Reboud, G. Xu, A. Garrett, M. Adriko, Z. Yang, E.M. Tukahebwa, C. Rowell, J.M. Cooper, *Proc. Natl. Acad. Sci. u. s. a.* **116**, 11 (2019)

- A. Reina, X. Jia, J. Ho, D. Nezich, H. Son, V. Bulovic, M.S. Dresselhaus, J. Kong, *Nano. Lett.* **9**, 1 (2009)
- D. Resnik, D. Vrtačnik, M. Možek, B. Pečar, S. Amon, J. Micromech. Microeng. **21**, 2 (2011)
- F. Reverter, T. Prodromakis, Y. Liu, P. Georgiou, K. Nikolic, T. Constandinou, Design considerations for a CMOS Lab-on-Chip microheater array to facilitate the *in vitro* thermal stimulation of neurons, (2014 IEEE International Symposium on Circuits and Systems (ISCAS), IEEE, 2014), pp. 630–633
- C.A.D. Rodriguez, G. Tremiliosi-Filho, in *Encyclopedia of Tribology*, (2013), p. 918–922
- A. Roy, M. Azadmehr, B.Q. Ta, P. Hafliker, K.E. Aasmundtveit, *Sensors (basel)*. **19**, 19 (2019)
- S. Roy, T. Majhi, S. Sinha, C.K. Sarkar, H. Saha, Electro thermal analysis and fabrication of low cost microheater using a nickel alloy for low temperature MEMS based gas sensor application, (2010 International Conference on Industrial Electronics, Control and Robotics, 2010), pp. 59–64
- S. Roy, C.K. Sarkar, P. Bhattacharyya, *Solid. State. Electron.* **76** (2012)
- L. Ruiqi, J. Chandrappan, K. Vaidyanathan, S.S. Win, Silicon micro heater based tagging module and the biocompatible packaging for capsule endoscope, (2011 IEEE 61st Electronic Components and Technology Conference (ECTC), 2011), pp. 1300–1307
- V. Russo, G.C. Righini, S. Sottini, S. Trigari, *Appl. Opt.* **23**, 19 (1984)
- S.E. Moon, H.K. Lee, N.J. Choi, J. Lee, W.S. Yang, J. Kim, J.J. Jong, D.J. Yoo, *J. Nanosci. Nanotechnol.* **12**, 7 (2012)
- J. Sakai, N. Iida, M. Sohga, T. Abe, Design and evaluation of microheater combined QCM array for thermal desorption spectroscopy, (2013 Transducers & Eurosensors XXVII: The 17th International Conference on Solid-State Sensors, Actuators and Microsystems (TRANSDUCERS & EUROSENSORS XXVII), IEEE, 2013), pp. 234–237
- D. Sánchez-Portal, E. Artacho, J.M. Soler, A. Rubio, P. Ordejón, *Phys. Rev. b*. **59**, 19 (1999)
- A. Scorzoni, D. Caputo, G. Petrucci, P. Placidi, S. Zampolli, G. de Cesare, M. Tavernelli, A. Nascetti, *Sens. Actuators. A. Phys.* **229** (2015)
- A. Scorzoni, M. Tavernelli, P. Placidi, P. Valigi, A. Nascetti, Accurate analog temperature control of a thin film microheater on glass substrate for lab-on-chip applications, (IEEE SENSORS 2014 Proceedings, IEEE, 2014), pp. 1216–1219
- R.A. Serway, in *Principles of Physics*, (Fort Worth : Saunders College Pub., Texas; London, 1998), p. 602
- K. Shen, X. Chen, M. Guo, J. Cheng, *Sens. Actuators. b. Chem.* **105**, 2 (2005)
- X. Shi, W. Xu, W. Shen, G. Wang, R. Wang, X. Li, W. Song, *J. Mater. Sci. Mater. Electron.* **30**, 3 (2018)
- F.J.G. Silva, A.P.M. Baptista, E. Pereira, V. Teixeira, Q.H. Fan, A.J.S. Fernandes, F.M. Costa, *Diam. Relat. Mater.* **11**, 9 (2002)
- S. Singh, D.K. Sharma, K. Kishore, B.A. Botre, S.A. Akbar, *IEEE Sens. J.* **18**, 20 (2018)
- J.M. Son, C. Lee, S.K. Hong, J.J. Kang, Y.H. Cho, *Int. J. Precis. Eng. Manuf. Green. Technol.* **4**, 1 (2017)
- J.M. Son, J.H. Lee, J. Kim, Y.H. Cho, *Int. J. Precis. Eng. Manuf.* **16**, 2 (2015)
- Q. Song, X. Sun, Z. Dai, Y. Gao, X. Gong, B. Zhou, J. Wu, W. Wen, *Lab. Chip.* **21**, 9 (2021)
- R.G. Spruit, J.T. van Omme, M.K. Ghatkesar, H.H.P. Garza, *J. Microelectromech. Syst.* **26**, 6 (2017)
- Sri Surya Srikanth, S. Rajesh Kumar, B. Suresh, V. Jyothi, V. Int. J. Innov. Technol. Explor. Eng. **9**, 2S3 (2019)
- R. Srinivasan, I.M. Hsing, P.E. Berger, K.F. Jensen, S.L. Firebaugh, M.A. Schmidt, M.P. Harold, J.J. Lerou, J.F. Ryley, *AIChE. J.* **43**, 11 (1997)
- W. Sripumkhai, A. Lekwichai, W. Bunjongpru, S. Porntheeraphat, B. Tunhoo, E. Ratanaudomphisut, T. Kamsri, C. Hruanun, A. Poyai, J. Nukeaw, *Adv. Mater. Res.* **93–94** (2010)
- S. Suleman, S.K. Shukla, N. Malhotra, S.D. Bukkittgar, N.P. Shetti, R. Pilloton, J. Narang, Y. Nee Tan, T.M. Aminabhavi, *Chem. Eng. J.* **414** (2021)
- Y. Taki, M. Kitiwan, H. Katsui, T. Goto, *J. Asian. Ceram. Soc.* **6**, 1 (2018)
- R. Tang, H. Yang, Y. Gong, M. You, Z. Liu, J.R. Choi, T. Wen, Z. Qu, Q. Mei, F. Xu, *Lab. Chip.* **17**, 7 (2017)
- J. Thewlis, A.R. Davey, *Nature* **174**, 4439 (1954)
- D. Thuau, I. Koymen, R. Cheung, *Microelectron. Eng.* **88**, 8 (2011)
- S.K. Tiwari, S. Bhat, K.K. Mahato, *Microsyst. Technol.* **24**, 8 (2018a)
- S.K. Tiwari, S. Bhat, K.K. Mahato, B.B. Manjunath, *Front. Heat. Mass. Transf.* **10** (2018b)
- V.T. Tran, Y. Wei, H. Du, *Micromachines (basel)*. **11**, 5 (2020)
- P.V. Trinh, N.V. Luan, D.D. Phuong, P.N. Minh, A. Weibel, D. Mesguich, C. Laurent, *Compos. Pt. A. Appl. Sci. Manuf.* **105** (2018)
- A. Tserepi, D. Moschou, N. Vourdas, M.K. Filippidou, V. Tsouti, G. Kokkoris, G. Tsekenis, I. Zergioti, S. Chatzandroulis, A. Tserepi, M. Delgado-Restituto, E. Makarona, Integrated biochip for PCR-based DNA amplification and detection on capacitive biosensors, (Bio-MEMS and Medical Microdevices, 2013), pp.
- T. Tsuchiya, T. Hemmi, J.-Y. Suzuki, Y. Hirai, O. Tabata, *Appl. Sci.* **8**, 6 (2018)
- P. Turkes, C. Pluntke, R. Helbig, *J. Phys. c. Solid. State. Phys.* **13**, 26 (1980)
- K. Ueno, T. Fudetani, Y. Arakawa, A. Kobayashi, J. Ohta, H. Fujioka, *APL. Mater.* **5**, 12 (2017)
- M.S. Utomo, Y. Whulanza, G. Kiswanto, Maskless visible-light photolithography of copper microheater for dynamic microbioreactor, (THE 4TH BIOMEDICAL ENGINEERING'S RECENT PROGRESS IN BIOMATERIALS, DRUGS DEVELOPMENT, HEALTH, AND MEDICAL DEVICES: Proceedings of the International Symposium of Biomedical Engineering (ISBE) 2019, 2019), pp.
- A. VanHorn, W. Zhou, *Int. J. Adv. Manuf. Technol.* **86**, 9–12 (2016)
- A.A. Vasiliev, A.V. Nisan, N.N. Samotaev, *Proceedings.* **1**, 4 (2017)
- G. Velmathi, N. Ramshanker, S. Mohan, Design, Electro-Thermal simulation and geometrical optimization of double spiral shaped microheater on a suspended membrane for gas sensing, (IECON 2010 - 36th Annual Conference on IEEE Industrial Electronics Society, 2010), pp. 1258–1262
- H.W. Veltkamp, F. Akegawa Monteiro, R. Sanders, R. Wiegink, J. Lotters, *Micromachines (Basel)*. **11**, 3 (2020)
- C.-P. Wang, M.-H. Hsiao, G.-H. Lee, T.-L. Chang, Y.-W. Lee, *Microelectron Eng.* **228** (2020)
- L. Wang, J. Wen, C. Yang, B. Xiong, *Sci. Technol. Adv. Mater.* **19**, 1 (2018)
- Y. Wang, G.J. Weng, in *Micromechanics and Nanomechanics of Composite Solids*, (2018), p. 123–156
- Y. Wang, C. Zhang, J. Li, G. Ding, L. Duan, *Vacuum.* **140** (2017)
- Z. Wang, J. Li, J. Xu, J. Huang, Y. Yang, R. Tan, G. Chen, X. Fang, Y. Zhao, W. Song, *J. Mater. Sci. Technol.* **48** (2020)
- S.T. Weir, D.D. Jackson, S. Falabella, G. Samudrala, Y.K. Vohra, *Rev. Sci. Instrum.* **80**, 1 (2009)
- J.D. Whitman, J. Hiatt, C.T. Mowery, B.R. Shy, R. Yu, T.N. Yamamoto, U. Rathore, G.M. Goldgof, C. Whitty, J.M. Woo, A.E. Gallman, T.E. Miller, A.G. Levine, D.N. Nguyen, S.P. Bapat, J. Balcerak, S.A. Bylsma, A.M. Lyons, S. Li, A.W. Wong, E.M. Gillis-Buck, Z.B. Steinhart, Y. Lee, R. Apathy, M.J. Lipke, J.A. Smith, T. Zheng, I.C. Boothby, E. Isaza, J. Chan, D.D.

- Acenas, 2nd, J. Lee, T.A. Macrae, T.S. Kyaw, D. Wu, D.L. Ng, W. Gu, V.A. York, H.A. Eskandarian, P.C. Callaway, L. Warriar, M.E. Moreno, J. Levan, L. Torres, L.A. Farrington, R. Loudermilk, K. Koshal, K.C. Zorn, W.F. Garcia-Beltran, D. Yang, M.G. Astudillo, B.E. Bernstein, J.A. Gelfand, E.T. Ryan, R.C. Charles, A.J. Iafrate, J.K. Lennerz, S. Miller, C.Y. Chiu, S.L. Stramer, M.R. Wilson, A. Manglik, C.J. Ye, N.J. Krogan, M.S. Anderson, J.G. Cyster, J.D. Ernst, A.H.B. Wu, K.L. Lynch, C. Bern, P.D. Hsu, A. Marson, medRxiv. (2020)
- J. Wu, W. Cao, W. Wen, D.C. Chang, P. Sheng, *Biomicrofluidics* **3**, 1 (2009)
- L. Xu, T. Li, X. Gao, Y. Wang, *IEEE. Electron. Device. Lett.* **33**, 2 (2012)
- L. Xu, T. Li, Y. Wang, *IEEE. Electron. Device. Lett.* **32**, 9 (2011)
- M. Xu, G. Slovin, J. Paramesh, T.E. Schlesinger, J.A. Bain, *Rev Sci Instrum.* **87**, 2 (2016)
- Y. Yamanishi, E. Chow, J. Teramoto, Y. Magariyama, A. Ishihama, T. Fukuda, F. Arai, On-Chip Temperature Sensing and Control for Cell Immobilization and Culture System, (2008 International Symposium on Micro-NanoMechatronics and Human Science, 2008), pp. 295–300
- C.-C. Yeh, Y.-J. Yang, An RF-Powered Wireless Micro-Heater Integrated with Acrylate-Composite-Based Temperature Regulator for Hyperthermia Treatment, (2020 IEEE 33rd International Conference on Micro Electro Mechanical Systems (MEMS), 2020), pp. 357–360
- C.-H. Yeh, K.-R. Chen, Y.-C. Lin, *Microfluidics Nanofluidics.* **15**, 6 (2013)
- J. Yeom, C.R. Field, B. Bae, R.I. Masel, M.A. Shannon, *J. Micromech. Microeng.* **18**, 12 (2008)
- M. Yin, L. Xiao, Q. Liu, S.Y. Kwon, Y. Zhang, P.R. Sharma, L. Jin, X. Li, B. Xu, *Adv. Healthc. Mater.* **8**, 23 (2019)
- J.-H. Yoon, B.-J. Kim, J.-S. Kim, *Mater. Chem. Phys.* **133**, 2–3 (2012)
- I.F. Yu, Y.H. Yu, L.Y. Chen, S.K. Fan, H.Y. Chou, J.T. Yang, *Lab. Chip.* **14**, 18 (2014)
- M.F. Yu, O. Lourie, M.J. Dyer, K. Moloni, T.F. Kelly, R.S. Ruoff, *Science* **287**, 5453 (2000)
- S. Yu, M. Kaviani, *J. Chem. Phys.* **140**, 6 (2014)
- S. Yu, S. Wang, M. Lu, L. Zuo, A Novel Micro Heater Integrated on Flexible Polyimide Substrate With Fast Response and Uniform Temperature Distribution Volume 4: 20th Design for Manufacturing and the Life Cycle Conference; 9th International Conference on Micro- and Nanosystems, 2015), pp.
- S. Yu, S. Wang, M. Lu, L. Zuo, *Sens. Actuators. A. Phys.* **257** (2017)
- M.N.H. Zainal Alam, A.A.A. Moghadam, A. Kouzani, *Microsyst. Technol.* **21**, 2 (2014)
- D. Zhang, Q. Xiang, X. Fan, X. Li, *Chem. Eng. J.* **301** (2016)
- K. Zhang, Y. Yang, E.Y. Pun, R. Shen, *Nanotechnology* **21**, 23 (2010)
- K.L. Zhang, S.K. Chou, S.S. Ang, *Int. J. Therm. Sci.* **46**, 6 (2007)
- L. Zhang, P. Zhang, R. Wang, R. Zhang, Z. Li, W. Liu, Q. Wang, M. Gao, L. Gui, *Micromachines (basel)*. **11**, 2 (2020)
- C. Zheng, G.P.S. Balasubramanian, Y. Tan, A.M. Maniatty, R. Hull, J.T. Wen, *IEEE/ASME. Trans. Mechatron.* **22**, 4 (2017)
- R. Zhong, X. Pan, L. Jiang, Z. Dai, J. Qin, B. Lin, *Electrophoresis* **30**, 8 (2009)
- Q. Zhou, A. Sussman, J. Chang, J. Dong, A. Zettl, W. Mickelson, *Sens. Actuators. A. Phys.* **223** (2015)

Publisher's Note Springer Nature remains neutral with regard to jurisdictional claims in published maps and institutional affiliations.